

Syracuse University

SURFACE

Earth Sciences - Theses

College of Arts and Sciences

8-2012

Geochemical and $^{40}\text{Ar}/^{39}\text{Ar}$ constraints on the evolution of volcanism in the Woodlark Rift, Papua New Guinea

Joseph Paul Catalano

Follow this and additional works at: https://surface.syr.edu/ear_thesis



Part of the Geology Commons

Recommended Citation

Catalano, Joseph Paul, "Geochemical and $^{40}\text{Ar}/^{39}\text{Ar}$ constraints on the evolution of volcanism in the Woodlark Rift, Papua New Guinea" (2012). *Earth Sciences - Theses*. 1.
https://surface.syr.edu/ear_thesis/1

This Thesis is brought to you for free and open access by the College of Arts and Sciences at SURFACE. It has been accepted for inclusion in Earth Sciences - Theses by an authorized administrator of SURFACE. For more information, please contact surface@syr.edu.

Abstract

The tectonic mechanisms producing Pliocene to active volcanism in eastern Papua New Guinea (PNG) have been debated for decades . In order to assess mechanisms that produce volcanism in the Woodlark Rift, we evaluate the evolution of volcanism in eastern PNG using $^{40}\text{Ar}/^{39}\text{Ar}$ thermochronology and whole rock geochemistry.

Active volcanism in southeastern Papua New Guinea occurs on the Papuan Peninsula (Mt. Lamington, Mt. Victory and Waiwa), in the Woodlark Rift (Dobu Island, SE Goodenough Island, and Western Fergusson Island), and in the Woodlark Basin . In the Woodlark Basin, seafloor spreading is active and decompression melting of the upper mantle is producing basaltic magmatism. However, the cause of Pliocene and younger volcanism in the Woodlark Rift is controversial. Two hypotheses for the tectonic setting have been proposed to explain Pliocene and younger volcanism in the Woodlark Rift: 1) southward subduction of Solomon Sea lithosphere beneath eastern PNG at the Trobriand Trough and 2) decompression melting of mantle, previously modified by subduction , as the lithosphere undergoes extension associated with the opening of the Woodlark Basin .

A comparison of $^{40}\text{Ar}/^{39}\text{Ar}$ ages with high field strength element (HFSE) concentrations in primary magmas indicates that HFSE concentrations correlate with age in the Woodlark rift. These data support the hypothesis that Pliocene to active volcanism in the Woodlark Rise and D'Entrecasteaux Islands results from decompression melting of a relict mantle wedge. The subduction zone geochemical signatures (negative HFSE anomalies) in Woodlark Rift lavas younger than 4 m.y. are a relict from older subduction beneath eastern Papua, likely in the middle Miocene . As the lithosphere is extended ahead of the tip of the westward propagating seafloor spreading center in the Woodlark Basin, the composition of volcanism is inherited from

prior arc magmatism (via flux melting) and through time evolves toward magmatism associated with a rifting (via decompression melting).

GEOCHEMICAL AND $^{40}\text{Ar}/^{39}\text{Ar}$ CONSTRAINTS ON THE EVOLUTION OF VOLCANISM
IN THE WOODLARK RIFT, PAPUA NEW GUINEA

By

Joseph P. Catalano
B.S., Union College, Schenectady, New York, 2009

THESIS

Submitted in partial fulfillment of the requirements for the degree of Master of
Science in Geology in the Graduate School of Syracuse University

August 2012

Copyright 2012 Joseph Paul Catalano
All rights Reserved

Acknowledgements

I would like to acknowledge the Syracuse University Noble Gas Research laboratory Syracuse University, the ICP-MS laboratory at Union College, and the National Science Foundation Continental Dynamics Project (grant #EAR0709054) for funding the majority of this research. Brian Horton is thanked for providing samples from the Papuan Peninsula used in this study. I would also like to recognize my primary advisor, Suzanne Baldwin, for her guidance and support throughout this research project.

To Joe Kula and Jim Metcalf: thank you for your help maintaining the noble gas lab, guidance reducing analytical data, and support during tough times. I couldn't have received better advice on every aspect of being a graduate student during my time at SU.

I would particularly like to thank my family for their support, but especially my mother and father, who helped guide me through numerous post-graduate life curveballs with a positive attitude.

TABLE OF CONTENTS

1.1 Introduction.....	pg. 1
Crustal structure of Eastern Papua New Guinea.....	pg. 2
1.2 Methods.....	pg. 3
Electron microprobe analysis.....	pg. 4
$^{40}\text{Ar}^{39}\text{Ar}$ analysis.....	pg. 4
ICPMS and ICPOES analysis.....	pg. 5
2.1 History of the generation and obduction of oceanic lithosphere in the Solomon Sea Region.....	pg. 7
Ophiolite in eastern Papua New Guinea.....	pg. 7
Ocean crust surrounding eastern Papua New Guinea.....	pg. 8
2.2 The age and composition of basalts in the Woodlark Rift.....	pg. 8
Shadowa Complex.....	pg. 8
Dabi Volcanics.....	pg. 9
Loluai Volcanics.....	pg. 11
Panapompom Island.....	pg. 12
D'Entrecasteaux Islands.....	pg. 13
2.3 Summary.....	pg. 15
3.1 Miocene Magmatism.....	pg. 15
Papuan Peninsula.....	pg. 16
Panapompom Island.....	pg. 17
Louisiade Archipelago.....	pg. 18
Woodlark Island.....	pg. 19
3.2 Summary	pg. 20

4.1 Pliocene – Active Volcanism.....	pg. 21
Papuan Peninsula.....	pg. 22
Egum Atoll.....	pg. 23
Lusancay Islands.....	pg. 24
Amphlett Islands.....	pg. 26
Nuamata and Normanby Islands.....	pg. 27
Goodenough Island.....	pg. 28
Sanaroa, Fergusson, and Dobu Islands.....	pg. 30
4.2 Summary.....	pg. 31
5.1 Conclusions.....	pg. 32
Figures.....	pg. 35
Tables.....	pg. 66
Appendix 1: Sample and Petrographic Descriptions.....	pg. 68
Appendix 2 $^{40}\text{Ar}/^{39}\text{Ar}$ Data Tables.....	pg. 92
Appendix 2.1 <3.5 Ma igneous rocks.....	pg. 92
Appendix 2.2 Miocene igneous rocks.....	pg. 95
Appendix 2.3 early Miocene – Eocene igneous rocks	pg. 96
Appendix 3 Geochemistry Data Tables	pg 97

Appendix 3.1 ICPMS and ICPOES data tables	pg. 97
Appendix 3.2 Electron microprobe data tables	pg. 110
References.....	pg. 115
Vita.....	pg. 125

LIST OF FIGURES

- Figure 1.** Geologic and tectonic map of southeastern Papua New Guinea.....pg. 44
- Figure 2.** Sample location map.....pg. 45
- Figure 3.** Map of oceanic lithosphere in eastern Papua New Guineapg. 46
- Figure 4.** Photomicrographs of samples interpreted to represent oceanic lithosphere....pg. 47
- Figure 5.** K₂O vs. SiO₂ classification diagram for samples interpreted to represent oceanic lithospherepg. 48
- Figure 6.** N-MORB normalized multi-element diagrams for samples interpreted to represent oceanic lithosphere.....pg. 48
- Figure 7.** ⁴⁰Ar/³⁹Ar age spectra for samples interpreted to represent oceanic lithospherepg. 49
- Figure 8.** Inverse isochron plots for oceanic lithosphere samplespg. 50
- Figure 9.** Map of Miocene igneous rocks in eastern Papuapg. 51
- Figure 10.** Photomicrographs of Miocene igneous rocks.....pg. 52
- Figure 11.** K₂O vs. SiO₂ classification diagram for Miocene igneous rocks.....pg. 53
- Figure 12.** N-MORB normalized multi-element diagrams from samples from Miocene igneous rocks.....pg. 53
- Figure 13.** ⁴⁰Ar/³⁹Ar composite age spectra for Miocene igneous rocks.....pg. 54
- Figure 14.** Inverse isochron plots for Miocene igneous rocks.....pg. 55
- Figure 15.** ⁴⁰Ar/³⁹Ar age spectrum and inverse isochron plot for sample 08P010pg. 56
- Figure 16.** K₂O vs. SiO₂ classification diagram for <4 Ma lavas in the Woodlark Rift...pg. 56
- Figure 17.** Photomicrographs of samples from the Woodlark Rift.....pg. 57
- Figure 18.** N-MORB normalized multi-element diagram for samples from the Lusancay Island group.....pg. 59
- Figure 19.** N-MORB normalized multi-element diagram for samples from the Amphlett Island group.....pg. 59

- Figure 20.** $^{40}\text{Ar}/^{39}\text{Ar}$ composite age spectra and inverse isochron plots for the Amphlett Island group.....pg. 60
- Figure 21.** $^{40}\text{Ar}/^{39}\text{Ar}$ age spectra and inverse isochron plots for Goodenough Island.....pg. 61
- Figure 22.** N-MORB normalized multi-element diagram for samples from the Normanby and Nuamata Islands.....pg. 62
- Figure 23.** N-MORB normalized multi-element diagram for samples from the Goodenough Island.....pg. 62
- Figure 24.** $^{40}\text{Ar}/^{39}\text{Ar}$ age spectra and inverse isochron plots for sanidine from samples from the Dawson Strait area.....pg. 63
- Figure 25.** N-MORB normalized multi-element diagram for samples from the Dawson Strait volcanics.....pg. 64
- Figure 26.** Plot of Nb*/Nb vs. $^{40}\text{Ar}/^{39}\text{Ar}$ age.....pg. 65
- Figure 27.** Plot of Ta*/Ta vs. $^{40}\text{Ar}/^{39}\text{Ar}$ age.....pg. 65

LIST OF TABLES

Table 1.	Summary of standards, analytical precisions, and detection limits for ICP-OES and ICP-MS analyses.....	pg. 66
Table 2.	Summary of $^{40}\text{Ar}/^{39}\text{Ar}$ total fusion analyses and previous published geochronologic ages for <4 Ma lavas in the Woodlark Rift.....	pg. 67

LIST OF APPENDICES

Appendix 1 Hand sample descriptions, sample locations, and mineral assemblages observed in thin section.....	pg. 68
Appendix 2.1 $^{40}\text{Ar}/^{39}\text{Ar}$ analyses for < 3.5 Ma samples in the Woodlark Rift.....	pg. 92
Appendix 2.2 $^{40}\text{Ar}/^{39}\text{Ar}$ analyses for Miocene samples in the Woodlark Rift.....	pg. 95
Appendix 2.3 $^{40}\text{Ar}/^{39}\text{Ar}$ analyses for samples interpreted to represent oceanic lithosphere in the Woodlark Rift.....	pg. 96
Appendix 3.1 Whole rock geochemistry of igneous samples in the Woodlark Rift.....	pg. 97
Appendix 3.2 Electron Microprobe analyses of xenolith samples in volcanic rocks in the Woodlark Rift.....	pg. 110

1.1 Introduction

Papua New Guinea lies within the obliquely convergent Australian and Pacific Plate boundary zone (Johnson and Molnar, 1972). Oblique convergence has resulted in the generation of numerous microplates along this boundary (Baldwin et al., 2012; Figure 1). Southeastern Papua New Guinea straddles the Australian and Woodlark microplate boundary (Figure 1). The Woodlark microplate is rotating in a counterclockwise direction, driven by slab pull from subduction at the New Britain Trench, which in turn is thought to cause extension in the Woodlark Rift System and sea-floor spreading in the Woodlark Basin (Wallace et al., 2004; Webb et al., 2008; Weissel and Watts, 1979; Figure 1). In the eastern end of the Woodlark Rift System, sea-floor spreading is active. The western part of the rift system is characterized by crustal extension of a hybrid lithosphere (a combination of oceanic and continental crust), where (U)HP rocks, including coesite-eclogite in the D'Entrecasteaux Islands, have been exhumed since ~8 Ma. (Baldwin et al., 2008).

The oldest igneous rocks in the Woodlark Rift System form the Papuan Ultramafic Belt (PUB; Figures 1, 3), an ophiolite on the Papuan Peninsula (Davies and Jaques, 1984). The PUB is comprised of Late Cretaceous to Paleocene gabbro, basalt, and sea-floor sediments located on the Papuan Peninsula and might extend as far east as the Moresby seamount (Francis et al., 1991; Monteleone et al., 2001). There is evidence that it continues as far north as the Trobriand Trough (Catalano et al., 2011) and as far south as the Louisiade Archipelago (Figure 1) (Webb et al., 2009). On the Papuan Peninsula, PUB rocks are intruded by Paleocene diorites, (Rogerson, 1991) synchronous with Paleocene volcanism (Walker and McDougall, 1982). After a complex tectonic evolution involving arc volcanism and ophiolite obduction in the Paleocene, the basaltic basement to the Woodlark Rise and the New Britain Arc formed in the Oligocene (Honza et al.,

1987; Trail, 1967). In the Miocene, subduction-related magmatism intruded the Oligocene basement (Ashley and Flood, 1981; Smith, 1972; Trail, 1967). Sub aerial, Pliocene and younger volcanism occurs on the islands in the Woodlark Basin and range in age from 3.5 Ma to historically active volcanism on Dobu and Fergusson Islands (Smith et al., 1977), Mt. Victory and Mt. Lamington (Johnson et al., 1971), and the Managalase Plateau Volcanic Field (Ruxton, 1999; Figure 1).

The objective of this thesis is to apply whole rock geochemistry (major, minor, trace, and rare earth elements) and $^{40}\text{Ar}/^{39}\text{Ar}$ thermochronology to evaluate the spatial and temporal evolution of volcanism in eastern Papua New Guinea. While some workers have studied the Miocene magmatic rocks (Ashley and Flood, 1981; Page, 1976; Smith, 1972) and Pliocene volcanic rocks (Hegner and Smith, 1992; Smith et al., 1977; Stoltz et al., 1992), the evolution of magmatism/volcanism from the Miocene to present and their eruption on top of, and intrusion into the PUB has not been evaluated. This research shows that Miocene arc magmas were intruded into and erupted on top of Oligocene basalts on the Papuan Peninsula and the islands in the Woodlark Rift System (Figure 9). This is followed by a hiatus in volcanism from the late Miocene until the Pliocene, when magmatism associated with extension erupted in the Woodlark Rift System (Figures 1, 2) .

Crustal Structure in Eastern Papua New Guinea

The structure of the crust in Eastern Papua New Guinea is such that relatively dense ophiolite associated with the PUB (Webb et al., 2008) overlies less dense, subducted and metamorphosed continental crust. The origin of the subducted continental material is likely sediment derived from NE Australia, formed prior to the opening of the Coral Sea (Zirakparvar, 2012).

The PUB upper plate was uplifted and thrust over continental crust from 66 – 58 Ma (Lus et al., 2004; Zirakparvar et al., 2011) along the Papuan Peninsula and in the islands of the Woodlark Rift System (Davies, 1971; Figure 3). The PUB is a continuous section of pillow basalt, sheeted dykes, gabbro, and upper mantle that is ~ 13 to 18 km thick (Davies, 1971). The crystallization age of the PUB gabbro is 117 Ma, based on a single K/Ar pyroxene age (Davies, 1980). The PUB was obducted onto the northern margin of AUS/PNG in the early Paleocene (Lus et al., 2004; Zirakparvar et al., 2011), forming the majority of the ‘upper plate’ of eastern Papua. The upper plate is also comprised of the Coral Sea floor, Woodlark Basin sea floor, and Solomon Sea floor but these are less voluminous than the PUB.

The lower plate is comprised of metamorphic rocks on Misima Island (De Keyser, 1961), the Papuan Peninsula (Worthing, 1988), and in the D’Entrecasteaux Islands (Davies and Ives, 1965) (Figure 3). The protolith of the metamorphic rocks is most likely volcaniclastic sediment derived from NE Australia prior to the opening of the Coral Sea (Zirakparvar, 2012). These rocks range in metamorphic grade from lower greenschist facies in the Louisiade Archipelago (Webb et al., 2009; Zirakparvar, 2012) to (U)HP eclogites in the D’Entrecasteaux Islands (Baldwin et al., 2008) (Figure 1). The lower plate was exhumed from (U)HP conditions since ~8 Ma. (Baldwin et al., 2008; Zirakparvar et al., 2011).

The structure of the crust is critical for modeling the exhumation of (U)HP rocks in the D’Entrecasteaux Islands (Ellis et al., 2011; Little et al., 2011). Key constraints on the regional extent of the upper and lower plates can be assessed by investigations into xenoliths along the Woodlark Rise. This thesis contains some preliminary data on xenoliths along the Woodlark Rise but this area requires further investigation.

1.2 Methods

Samples were collected during field work in the Woodlark Rift System in 2003 - 2004, 2006, 2008, 2009, and 2010 from locations shown in figure 2. Sample size ranged from 0.5 to 5 kg, depending on homogeneity and grain size. Only fresh, representative, relatively homogeneous material was sampled in the field.

Electron microprobe analysis

Thin sections were prepared and subsequently analyzed in the electron microprobe laboratory at Rensselaer Polytechnic Institute. Minerals were analyzed for the elements Na, Mg, Si, Al, K, Ca, Mn, Fe, Cl, Ti, V, Ni, and Cr using standards of jadeite, forsterite, obsidian, kyanite, orthoclase, plagioclase, spessartine, hematite, chlorite, titanite, V₂O₃ (synthetic), NiO (synthetic), and chromite respectively to determine mineral compositions. Beam conditions were 15 keV accelerating voltage, 10 nA current, and a 10 µm spot size.

⁴⁰Ar/³⁹Ar analysis

Pure mineral separates (> 99%) and crystal-poor pieces of aphanitic basalt were analyzed in the Syracuse University Noble Gas Isotope Research Laboratory (SUNGIRL). Prior to analysis, samples were irradiated for 0.5 hours in the Cadmium-Lined In-Core Irradiation Tube (CLICIT) of the 1 MW TRIGA type reactor at the Oregon State University Radiation Center. Included with the mineral separates were CaF₂, K-glass, 77-600 amphibole, Alder Creek sanidine, and GA-1550 biotite to monitor interfering reactions on Ca and K, and the fast neutron flux (i.e. to determine J-factors). Analyses of CaF₂ and K-glass yielded Ca correction factors of (³⁶Ar/³⁷Ar)_{Ca} = 1.08 x 10⁻⁴ ± 434% and (³⁹Ar/³⁷Ar)_{Ca} = 1.93 x 10⁻⁴ ± 13.35% and a measured (⁴⁰Ar/³⁹Ar)_K value of 1.2335 x 10⁻² ± 13.18%. J factors were determined by laser fusion analyses of ~1 mg of GA-1550 biotite, 77-600 amphibole, and Alder Creek sanidine. These flux monitors

were stacked with samples in vacuum-sealed Suprasil® quartz tubes, J-values for samples were determined by interpolating between standards in the tube by assuming a linear fit.

Mass discrimination corrections of $0.971 \pm 0.92\%$ (4 AMU) were determined by repeated analysis from a pipette attached to a tank of high-purity atmospheric argon . Samples were step-heated in a custom-built double vacuum resistance furnace with an inner crucible temperature calibration determined from dual-thermocouple experiments prior to the analyses. Reactive gases were removed using two SAES ST-707 getters (1 at 400°C , 1 at $\sim 20^{\circ}\text{C}$) prior to admittance by expansion to a Micromass 5400 gas source mass spectrometer. Isotopes ^{36}Ar , ^{37}Ar , ^{38}Ar , ^{39}Ar , ^{40}Ar and ^{35}Cl were measured using an ion-counting electron multiplier by peak-hopping through 11 cycles for linear regression back to the time the sample gas was admitted. Plateau ages were defined as three or more consecutive steps of the gas released with ages overlapping at the 2σ level of uncertainty (McDougall and Harrison, 1988). Inverse isochrons were assessed using the MSWD criteria of Wendt and Carl (1991).

ICPMS and ICP-OES analysis

In the laboratory at Union College (Schenectady, NY), samples were mechanically disaggregated and altered pieces were removed with a hydraulic splitter or 5 lb. sledge hammer. Fragments were crushed with a hydraulic press between 12 cm tungsten carbide faces, to pass through a 6 mm stainless steel sieve. No wear was seen on the tungsten carbide faces after >400 samples, and Co concentrations as low as 0.9 ppm in granitoid samples suggest negligible contamination from the tungsten carbide. Splits of ~100 g were crushed to a fine powder by 5 minute agitations in a Spex 15 cm aluminum oxide puck mill. This mill also showed no significant wear, and contamination from it is assumed to be negligible.

For major elements, 5 g aliquots were dried at 110°C overnight and analyzed by inductively coupled plasma optical emission spectroscopy (ICP-OES) at ACME Labs, Vancouver, Canada, including loss-on-ignition by weight percent. Several trace elements were also analyzed, but these were only used to assess the quality of ICP-MS analyses.

Trace elements were analyzed at the Union College Geology Department. Acids were purified in-house using Teflon sub-boiling stills, water was purified to 18.3 MΩ by ion exchange, and plastic test tubes were pre-cleaned with 1 percent HNO₃ to remove minor copper and zinc contamination. All powdered samples and the standards BIR-1, NIST-688, BCR-2 (all basalts), and NIST-278 (obsidian) were dried at 110°C overnight. Two hundred milligram aliquots of the unknowns and standards were weighed and placed into digestion vessels, and two empty vessels were left for the determination of blank signal.

Digestions were done in a PicoTrace (Bovenden, Germany) Teflon bomb system using the following sequence. Five milliliters of 50% HF was added to the samples and the vessels were sealed and heated to 180°C for four days. The long reaction time ensured complete dissolution of possible zircon. The vessels were evaporated to dryness overnight at ~100°C under flowing, filtered air. Fifteen milliliters of 70% HNO₃ was added and the vessels were evaporated to dryness again. One hundred twenty five milliliters of HNO₃, twenty five milliliters of 37% HCl, one milliliter of HF, and three tenths of a milliliter of 1000 ng/g Rh, In, Re, and Bi internal standard solutions (Inorganic Ventures, Lakewood, New Jersey) were combined and diluted to five hundred milliliters, and fifteen milliliters of this mixture was added to each sample. The vessels were again sealed and heated to 150°C overnight. Immediately upon cooling two tenths of a milliliter of each sample solution was transferred into twelve milliliter polypropylene test tubes, and ten milliliters of 1% HNO₃ (by volume) was added.

Samples were analyzed immediately with a PerkinElmer Elan 6100 DRC ICP-MS instrument in three sets: V and Cr in DRC mode with 0.4 ml/minute NH₃ gas flowing to the DRC chamber to reduce polyatomic ion interferences. All other elements were analyzed in normal mode. Li and Be were analyzed in a separate run. Zn and Cu were corrected for TiO⁺ and Ba²⁺ interferences, and the lanthanides, Hf, and Ta were corrected for a variety of Ba and lanthanide oxide, hydroxide, and isobaric interferences. Standard concentrations, detection limits, and analytical precision of sample replicates are shown in table 1. Digestion vessels were carefully checked for residual solids after analysis was complete (e.g. zircon), but none were found.

2.1 History of the generation and obduction oceanic lithosphere in the Solomon Sea Region

Oceanic lithosphere is widespread onshore and offshore in eastern Papua (Figure 3). The oldest known oceanic lithosphere in the Papua New Guinea region is the PUB. The Mesozoic crystallization age of the PUB correlates with the age of the Pacific Plate in New Guinea Region (Figure 3) (Beiersdorf et al., 1995; Taylor, 2006). Oceanic lithosphere of various ages and origins surround eastern Papua New Guinea (Figure 3) and some samples have been identified in the Woodlark Rift System.

Ophiolite in eastern Papua

The oldest subaerially exposed oceanic lithosphere in eastern Papua is Mesozoic (143 - 117 Ma.) oceanic crust and upper mantle of the Papuan Ultramafic Belt (Davies, 1971; Rogerson, 1991), Marum Ophiolite, and April Ultramafics) (Davies, 1971; Figure 3). These ophiolites were emplaced on the Papuan margin in the Paleocene (66 – 58 Ma.) (Lus et al., 2004; Zirakparvar et al., 2011; Figure 3). The opening of the Coral Sea (61-53 Ma.) and Dabi

Volcanism (64 – 53 Ma.) were synchronous with PUB ophiolite obduction along the Papuan peninsula (Gaina et al., 1999; Walker and McDougall, 1982; Figure 3).

Oceanic crust surrounding eastern Papua

The ages of the oceanic lithosphere in the Solomon Sea and Caroline Sea are approximately 35 – 25 Ma. (Hill and Hall, 2003; Joshima et al., 1986; Figure 3). Oceanic crust of this age is also found on New Britain and New Ireland where these rocks comprise the basement upon which younger oceanic island arcs were built (Figure 3). The Torrecelli Intrusive Complex in central Papua New Guinea represents a small piece of Caroline Sea Floor that was obducted onto the leading edge of the Papua New Guinea margin during the Miocene based on K-Ar dating of deformed metasediments that occur with basalts (Weiland, 1999; Figure 3).

The youngest oceanic crust occurs in the Bismarck Sea (Yan and Kroenke, 1993) and the Woodlark basin (Taylor et al., 1995; Figure 3). The Bismarck Sea has been inferred to result from sea floor spreading in the back arc of the New Britain arc from 3.5 Ma to present (Cloos, 2005; Hill and Hall, 2003; Figure 3). Sea floor spreading in the Woodlark Basin originated at 6 Ma in the eastern part of the basin, and is still active and propagating westwards (Taylor et al., 1995; Figure 3).

2.2 The age and composition of oceanic basalts in the Woodlark Rift System

The Shadowa Complex

The Shadowa Complex is comprised of the Shadowa Gabbro and the Kutu Volcanics and occurs along the southern coast of the Papuan Peninsula (Francis et al., 1991; Figure 3). The age of the Shadowa Complex is constrained by K-Ar dating of hornblende (55.7 – 56.3 Ma.)

from the gabbro but the age of the Kutu Volcanics has not been investigated (Rogerson and Hilyard, 1989).

The mineral assemblage in the Shadowa Gabbro is plagioclase + orthopyroxene + olivine + Fe-oxides ± chlorite ± epidote (Figure 4A). Samples collected from the Kutu Volcanics are highly weathered and slightly altered and the primary mineralogy is not clear. The Shadowa gabbro is compositionally a low-K basalt (Figure 5) and contains rare earth element abundances similar to N-MORB, with excess Rb, Ba, Sr, and Th (Figure 6), consistent with alteration during eruption and cooling on the seafloor, or during obduction.

Although there are no radiometric ages for the Kutu Volcanics, these units are interbedded with ocean floor sediments that contain Eocene hemipelagic micrite (Smith, 1976a). The Kutu Volcanics are cross-cut by Miocene dikes and plutons (Rogerson and Hilyard, 1989) and may represent a slice of Coral Sea lithosphere obducted during the Miocene, related to subduction during that time.

Dabi Volcanism

The Dabi Volcanics are a volumetrically small unit in the Cape Vogel Peninsula (blue star; Figure 3). The timing of Dabi Volcanism is constrained by three $^{40}\text{Ar}/^{39}\text{Ar}$ whole rock analyses and six K/Ar analyses (Walker and McDougall, 1982). The three $^{40}\text{Ar}/^{39}\text{Ar}$ whole rock analyses yielded two plateau ages (53.8 Ma and 58.9 Ma.) (Walker and McDougall, 1982). The sample that yielded a 53.8 m.y. plateau, however the sample has been partially reset and the initial steps show what is interpreted to be a loss profile. Therefore it is concluded that 53.8 Ma is a *minimum* age. The K/Ar analyses yielded ages ranging from 63.9 – 27.2 Ma. Walker and McDougall (1982) concluded that Cape Vogel Volcanics cooled through Ar closure between

63.9 – 58.9 Ma. The exact timing of Dabi volcanism has important implications for obduction of the PUB, as discussed below.

The phenocrysts in the Dabi Volcanics are plagioclase + orthopyroxene + clinopyroxene + olivine + Fe-oxides ± chlorite ± clinoenstatite (Figure 4F). The initial discovery of clinoenstatite in these rocks was made by Dallwitz et al. (1966) who interpreted its crystallization to unusual magma compositions. Experimental work on clinoenstatite indicate a low temperature variety associated with shock metamorphism during asteroid impact (Mason and Nelen, 1968; Tomioka and Fujino, 1997) and a high temperature variety that has been identified in island arc magmas (Komatsu, 1980; Shiraki et al., 1980). There is no direct evidence at this time confirming which type of clinoenstatite is in the Dabi Volcanics. However, it is more likely that clinoenstatite in the Dabi Volcanics is the high temperature variety because there have been no identified asteroid impacts proximal to the sample location and also the major element composition of the volcanics are consistent with an island arc, where high temperature clinoenstatite is known to have previously occurred.

The composition of the Dabi Volcanics is calc-alkaline basalt to basaltic andesite (Figure 5). They contain trace and rare earth element abundances less than N-MORB with the exception of Rb, Ba, Sr, and Th (Figure 6), which is likely due to slight alteration and metasomatism. These samples have negative Nb and Ta anomalies and are therefore interpreted to have originated in a tholeiitic island arc.

In the early Paleocene the exact sequence of tectonic events is unclear, but data suggest the PUB was obducted ca. 66 – 58 Ma (Lus et al., 2004), Dabi Island Arc volcanism terminated 64 – 54 Ma (Walker and McDougall, 1982), and the Coral Sea Basin opened 63 – 52 Ma (Gaina et al., 1999; Weissel and Watts, 1979). After the Coral Sea formed, the Solomon Sea was

formed in the Oligocene (Joshima et al., 1986), and the Woodlark Basin formed in the Pliocene (Taylor et al., 1995; Figure 3). Small slices of obducted seafloor are present throughout eastern New Guinea on Woodlark Island (Trail, 1967), the D'Entrecasteaux Islands (Davies and Ives, 1965), and on the ‘southern rifted margin of Australia’ (De Keyser, 1961; Figure 1) (Panapompom Island, Misima Island, Louisiade Archipelago, and Rossel Island). The first thermochronologic ages for some of these obducted slices of seafloor are presented below.

Loluai Volcanics

The Loluai volcanics are pillow basalt and dolerite that all occur with interbedded pelagic sediments; these units comprise the crystalline basement of Woodlark Island (Trail, 1967; Figures 1 - 3). The Loluai Volcanics are overlain by middle Miocene volcanic rocks and intruded by Miocene granite, capped by late Miocene limestone (Trail, 1967). The phenocrysts in the pillow basalt are orthopyroxene + clinopyroxene + plagioclase ± serpentine ± chlorite ± Fe-oxides (Figure 4B). The Loluai Volcanics are compositionally low-K basalt (Figure 5) with rare earth element abundances similar to N-MORB but with slight LREE enrichment and excess Rb, Ba, Sr, and Th (Figure 6). The whole rock compositions of the Loluai Volcanics are consistent with a petrogenetic interpretation involving metasomatism during magma eruption and cooling on the sea floor, or metasomatism occurring during uplift and intrusion by younger, Miocene magmas.

$^{40}\text{Ar}/^{39}\text{Ar}$ whole rock analysis of PNG10-017 pillow basalt from Suloga Point on Woodlark Island yielded an age spectrum characterized by an age gradient from 11.5 to 32.2 Ma (Figure 7B). The inverse isochron for PNG10-017 pillow lava yields an age of 28 ± 2 Ma., (MSWD = 31). The regression is based on 5 out of 10 data points with steps corresponding to

the youngest apparent ages omitted (figure 8B). The $^{40}\text{Ar}/^{36}\text{Ar}$ intercept is 290 ± 34 , concordant with atmospheric values (Figure 8B).

Given the pronounced age gradient for PNG10-017, we interpret of the interpretation of the whole rock age spectra is that the minimum age of crystallization of the pillow basalt to be 32.2 Ma, as indicated by the maximum $^{40}\text{Ar}/^{39}\text{Ar}$ apparent ages. The lower intercept of the age spectrum is ~ 11.5 Ma and is interpreted as the approximate time of reheating by the Miocene magmatism that crosscuts the basalt. The minimum crystallization age of the basalt is concordant with ages of the Solomon Sea, indicating the basement of Woodlark Island is likely to be Solomon Sea floor that was intruded by younger Miocene magmas.

Panapompom Island

Basement rocks on Panapompom Island are comprised of gabbro and basalt (Figures 1, 2, 3). The basement rocks are cross-cut by Miocene microdiorite, which is a possible correlative to the Boiou microdiorite on Misima Island (Adshead and Appleby, 1996). The Panapompom Island gabbro is comprised of orthopyroxene + plagioclase \pm epidote \pm chlorite \pm Fe-oxides (Figure 4A). The Panapompom Island igneous rocks are compositionally low-K basalts (Figure 5) with rare earth element abundances slightly above N-MORB with excess Rb, Ba, Sr (Figure 6). This composition is consistent with a petrogenetic interpretation involving metasomatism during magma eruption and cooling on the sea floor, or during obduction.

$^{40}\text{Ar}/^{39}\text{Ar}$ whole rock analysis of PNG03-188 gabbro yielded an age spectrum with an age gradient from 10 to 29 Ma (Figure 7C). The inverse isochron for PNG03-0188 gabbro yields an age of 27 ± 2 Ma, regressed through 3 of 9 data points, omitting partially reset steps (figure 8C). The $^{40}\text{Ar}/^{36}\text{Ar}$ intercept is 287 ± 33 , concordant with atmospheric values (figure 8C).

The interpretation of the minimum age of crystallization of the gabbro is 29 Ma, as indicated by oldest apparent $^{40}\text{Ar}/^{39}\text{Ar}$ ages for this sample. As with sample PNG10-017 from Woodlark Island, the gabbro was reheated by the Miocene magmas that crosscuts the gabbro at ~10.5 Ma, as indicated by the youngest $^{40}\text{Ar}/^{39}\text{Ar}$ apparent ages. The minimum crystallization age of the gabbro is concordant with ages of the Solomon Sea, and the gabbro may be a sliver of Solomon Sea floor that was intruded by younger Miocene magmas.

D'Entrecasteaux Islands

Oceanic lithosphere comprising the upper plate of the D'Entrecasteaux Islands core complexes is found on Normanby, Fergusson, and Goodenough Islands (Figures 1, 3). Due to similarities in rock types and structural relationships between the PUB and the upper plate of the D'Entrecasteaux Islands, they have been considered to be correlative (Catalano et al., 2011; Webb et al., 2008; Zirakparvar et al., 2011). In addition to field relationships, zircon in gabbro drilled during ODP leg 180 on Moresby Seamount gives a U/Pb zircon age of 66 Ma (Monteleone et al., 2001). This age is similar to $^{40}\text{Ar}/^{39}\text{Ar}$ amphibole ages from the metamorphic sole of the PUB (Lus et al., 2004), and within error of 68 Ma Lu/Hf garnet age from the shear zone of Goodenough Island (Zirakparvar et al., 2011). The similar ages reinforce the idea that the upper plate of the D'Entrecasteaux Islands is at least in part, equivalent to the PUB.

Basalt sample PNG03-117 from the upper plate on southern Goodenough Island is comprised of clinopyroxene + orthopyroxene + plagioclase + olivine (Figure 4C). Olivine and pyroxene from this sample have weathered rims that are comprised of Fe-rich olivine and pyroxene. The composition of the Goodenough Island volcanic is high-K, high-Al, calc-alkalic

to alkaline, basalt to basaltic andesites (Figure 5). The N-MORB normalized multi-element pattern for PNG03-117 shows incompatible trace and LREE enrichment with respect to heavy rare earth elements, negative Nb and Ta anomalies, and positive Sr anomalies (Figure 6).

$^{40}\text{Ar}/^{39}\text{Ar}$ analysis of PNG03-117 K-feldspar yielded an age spectrum with an age gradient from 1.8 to 31 Ma. (Figure 7A) The inverse isochron for PNG03-117 pillow lava yields an age of 25 ± 2 Ma., (MSWD = 78), regressed through 4 of 10 data points, omitting partially reset steps (Figure 8A). $^{40}\text{Ar}/^{36}\text{Ar}$ intercept is 295 ± 67 , concordant with atmospheric values (Figure 8A).

PNG03-117 basalt has a composition similar to other young volcanics (PNG08-004, PNG08-005b, PNG10-064b) that intrude and are extruded onto the upper plate on Wagifa and Goodenough Islands (Figure 2), but the feldspar $^{40}\text{Ar}/^{39}\text{Ar}$ apparent ages are significantly older than the young (<1 Ma), mafic volcanics from Goodenough Island. It is likely that the basalt has incorporated xenocrysts from the upper plate during eruption as indicated by feldspar $^{40}\text{Ar}/^{39}\text{Ar}$ apparent ages. The minimum age of upper plate xenocrysts is 25 Ma, which is slightly younger than the age of the Solomon Sea, 28 Ma (Joshima et al., 1986). It is likely that the lower intercept of 1.5 Ma records the timing of eruption (Figure 8A). The 25 Ma upper intercept may represent a mixed age of reset Solomon Sea or PUB age xenocrysts with young 1.5 Ma phenocrysts, and is geologically meaningless.

Serpentinite sample PNG03-058 from the upper plate of Normanby Island (Figures 1, 3) is comprised of serpentine + chlorite + Fe-oxide + plagioclase \pm calcite (Figure 4D). The composition of this Normanby Island mafic rock is low-K basalt (Figure 5) with slight light rare

earth element enrichment and excess Rb, Ba, Sr (Figure 6). This composition likely results from metasomatism during eruption and cooling on the sea floor, or during obduction.

2.3 Summary

The crystallization age of the PUB is constrained as Mesozoic, indicating it is correlative with basalts of Pacific plate affinity. Obduction of oceanic crust of Pacific plate affinity at ~ 65 Ma could explain the origin of the PUB. Eocene/Oligocene sea floor spreading following PUB obduction may have created the Solomon Sea, which comprises at least part of the upper plate in the Woodlark Rift System (e.g. Woodlark Island and Panapompom Island). This interpretation is further supported by 45 – 30 Ma. geochronologic ages from the upper plate in eastern Papua New Guinea (Dallwitz et al., 1966; Rogerson, 1991; Rogerson and Hilyard, 1989; Stolz et al., 1992; Weiland, 1999; Worthing, 1988; Worthing and Crawford, 1996). $^{40}\text{Ar}/^{39}\text{Ar}$ results from this study suggest that in the Miocene, the Coral Sea oceanic lithosphere (future Shadowa Complex) and the Solomon Sea oceanic lithosphere were obducted onto Woodlark and Panapompom Islands, respectively, prior to intrusion of the middle Miocene magmatism, (Maramuni Arc magmatism) which crosscuts it (Smith, 1976a). The exact timing of emplacement of the various slices of oceanic lithosphere is unknown, but is loosely constrained between the Paleocene (when the seafloor formed) and the middle Miocene (when magmas cross cut it). Overall, the origin of ocean lithosphere in eastern Papua is an area in need of further investigation because there are very few published analyses that record the origin and tectonic evolution of these rocks.

3.1 Miocene magmatism: Papuan Peninsula, Louisiade Archipelago, Panapompom Island, Woodlark Island

Miocene igneous rocks occur in an E-W trending belt that is widely distributed across the entire length of Papua New Guinea (Figure 9). This belt of Miocene magmatism is known as the ‘Marimuni Arc’ (e.g. Hill and Raza, 1999; Weiland, 1999). Miocene magmatism is voluminous in central Papua New Guinea (Page, 1976; Figure 9), but its extent in the eastern Papua New Guinea is not well constrained. In eastern Papua New Guinea, Miocene igneous rocks occur on Misima Island (Adshead and Appleby, 1996), the Papuan Peninsula (Smith, 1972), Louisiade Archipelago, Panapompom Island, and Woodlark Island (Ashley and Flood, 1981; Figures 1, 2, 9).

Papuan Peninsula

On the northern coast of the Papuan Peninsula, volcanic rocks unconformably overlie ophiolitic rocks associated with the upper plate of the Dayman Dome core complex (Figure 2). In turn, Miocene igneous rocks are overlain by late Miocene limestone (Davies, 1971). Because these subaerially erupted volcanic rocks were eroded to base level by the late Miocene when limestone was deposited, it is likely that middle Miocene magmatism was relatively short lived (~ 10 m.y.) on the northern coast of the Papuan Peninsula.

Miocene dacite (sample 08P006) on the northern coast of Papuan Peninsula contains phenocrysts of amphibole + Fe-oxides in a fine-grained crystal-rich groundmass of quartz + feldspar (Figure 10A). Sample 08P-006 is a high-Al₂O₃, high-K₂O dacite (Figure 11) with high concentrations of LILE and LREE enrichment, HFSE and HREE depletion, and La_N/Yb_N = 18.27 (Figure 12). The pattern has negative Ti, Nb, and Ta anomalies and positive Li, Sr, and Ba anomalies (Figure 12). This composition and pattern is consistent with a petrogenetic interpretation of partial melting of metasomatized subduction zone mantle wedge (e.g. Grove et al., 2012).

08P006 amphibole yielded a $^{40}\text{Ar}/^{39}\text{Ar}$ plateau age of 17.03 ± 0.94 Ma based on 99.2 % of the ^{39}Ar released (Figure 13). The inverse isochron for 08P006 amphibole yielded a concordant age of 16.5 ± 1.5 Ma. (MSWD = 7.5), regressed through all data points (Figure 14A). $^{40}\text{Ar}/^{36}\text{Ar}$ intercept is 316 ± 15 , slightly higher than atmospheric values (Figure 14A). 08P006 amphibole was cooled through Ar closure after eruption between ~ 17 Ma.

Panapompom Island

Panapompom Island is a small island ~ 25 km southwest of Misima Island (Figures 1, 2). It is part of an inactive remnant of a larger, eroded volcanic structure that correlates temporally with igneous intrusions on Misima Island. The Panapompom Island basement is comprised of altered oceanic basalt that is intruded by microdiorite. The assemblage of the Panapompom microdiorite is amphibole + biotite + Fe-oxides in a finely crystalline groundmass of quartz + feldspar (Figure 10E).

Sample PNG03-199 from Panapompom Island is a high K_2O diorite (Figure 11) with high concentrations of LILE and LREE enrichment, HFSE and HREE depletion, and $\text{La}_{\text{N}}/\text{Yb}_{\text{N}} = 23.21$ (Figure 12). The N-MORB normalized multi-element pattern has negative Nb and Ta anomalies and positive Li, Sr, and Ba anomalies (Figure 12). This composition and pattern is consistent with a petrogenetic interpretation of partial melting of metasomatized subduction zone mantle wedge (e.g. Grove et al., 2012)

$^{40}\text{Ar}/^{39}\text{Ar}$ whole rock analysis of PNG03-199 yielded a plateau age of 8.07 ± 0.32 Ma that comprises 81.6% of the ^{39}Ar released (Figure 13). The inverse isochron for PNG03-199 whole rock yielded an age of 8.4 ± 1.4 Ma. (MSWD = 28), regressed through 8 of 9 data points (Figure 14C). $^{40}\text{Ar}/^{36}\text{Ar}$ intercept is 285 ± 20 , concordant with atmospheric values (Figure 14C).

The timing of magmatism on Panapompom Island is synchronous with magmatism on Misima Island (based on a U/Pb zircon age of 8.1 Ma) reported by Adshead and Appleby (1996), and with (U)HP metamorphism in the D'Entrecasteaux Islands (Baldwin et al., 2004; Zirakparvar et al., 2011). The Panapompom Island microdiorite is the youngest known pluton associated with the Maramuni Arc in the Woodlark Rift System and is potentially one of the last intrusions derived from the subducted slab at ~8 Ma before subduction ceased and (U)HP rocks were exhumed.

Louisiade Archipelago

The Louisiade Archipelago are comprised of low grade metamorphic rocks whose protolith were derived from the rifted margin of Australia (Zirakparvar, 2012); it now forms the southern conjugate margin to the Woodlark Rise (Figure 1). The lower plate of the Louisiade Archipelago is primarily comprised of low grade metasediments structurally overlain by an upper plate comprised of sea floor basalt that has been shallowly intruded by intermediate igneous rocks (Webb et al., 2009) (Figure 2). The Louisiade Archipelago diorite sill contains amphibole + Fe-oxides in a finely crystalline groundmass of quartz + feldspar (Figure 10B).

Sample PNG09-005 from Rossel Island in the Louisiade Archipelago is from a calc-alkaline diorite (Figure 11) with high concentrations of LILE and LREE enrichment, HFSE and HREE depletion, and $\text{La}_\text{N}/\text{Yb}_\text{N} = 23.21$ (Figure 12). The pattern has negative Nb and Ta anomalies and positive Sr and Ba anomalies (Figure 12). This composition and pattern is consistent with the interpretation of partial melting of metasomatized subduction zone mantle wedge (e.g. Grove et al., 2012).

PNG09-005 amphibole yielded a plateau age of 11.84 ± 0.16 Ma that comprises 79.2% of the ^{39}Ar released (Figure 13). The inverse isochron for PNG09-005 amphibole yields an age of

11.48 ± 0.33 Ma. (MSWD = 2.1), regressed through 7 of 9 data points (Figure 14B). The $^{40}\text{Ar}/^{36}\text{Ar}$ intercept is 301.9 ± 8.0 , concordant with atmospheric values (Figure 14B).

The initial, low-temperature steps yielded the youngest $^{40}\text{Ar}/^{39}\text{Ar}$ ages and the form of the age spectrum is interpreted as a loss profile, possibly due to reheating at ~5-6 Ma. The most likely cause for reheating was onset of Woodlark seafloor spreading, which began at ~6 Ma (Taylor et al., 1995). PNG09-005 diorite sill was emplaced shallowly in the crust, cooled below the closure temperature for Ar in hornblende (Harrison, 1982) by ~11.5 Ma, and was reheated at 5-6 Ma.

Woodlark Island

Woodlark Island is comprised of altered oceanic basalt that has been intruded by granite and capped by Miocene volcanic rocks and limestone (Figures 1, 2) (Trail, 1967). The mineral assemblage in volcanic rocks is amphibole + K-feldspar + Fe-oxides \pm clinopyroxene \pm apatite \pm zircon (Figure 10C). The granite consists of amphibole + biotite + K-feldspar + Fe-oxides \pm clinopyroxene \pm apatite \pm zircon (Figure 10D).

The trace element concentrations of Woodlark Island granite and volcanic rocks are similar (Figure 12), suggesting that they are intrusive and extrusive correlatives. The alkaline granite (PNG10-014a) and high-K dacite (PNG10-005b) (Figure 11) have high concentrations of LILE and LREE enrichment, HFSE and HREE depletion, and $\text{La}_\text{N}/\text{Yb}_\text{N} = 10.36 - 21.31$ (Figure 12). These patterns have negative Nb and Ta anomalies and positive Sr and Ba anomalies (Figure 12). This composition and pattern is consistent with an interpretation that the magmas were derived from partial melting of metasomatized subduction zone mantle wedge (e.g. Grove et al., 2012).

PNG10-005b amphibole from Woodlark Island yielded a plateau age of 13.42 ± 1.01 Ma that comprises 84.5 % of the ^{39}Ar released (Figure 13). The inverse isochron yields an age of 12.9 ± 1.4 Ma. (MSWD = 0.55), regressed through 8 of 11 data points (Figure 14E). The $^{40}\text{Ar}/^{36}\text{Ar}$ intercept is 301.8 ± 9.5 , concordant with atmospheric values (Figure 14E). The dacite was erupted at 12.9 Ma. The initial, low temperature steps suggest some $^{40}\text{Ar}^*$ was lost but the spectra are complex and the timing of reheating is uncertain.

PNG10-014b amphibole from Woodlark Island yielded a plateau age that comprises 95.8 % of the ^{39}Ar released and plateau age of 12.42 ± 0.37 Ma (Figure 13). The inverse isochron for PNG10-014b amphibole yields an age of 12.6 ± 0.97 Ma (MSWD = 7.6), regressed through all data points (Figure 14D). $^{40}\text{Ar}/^{36}\text{Ar}$ intercept is 271 ± 16 , slightly lower than atmospheric values (Figure 14D). PNG10-014b granite is interpreted to have been emplaced in the crust and cooled through the Ar closure temperature in hornblende (Harrison, 1982) at ~ 12.5 Ma, and reheated at ~ 5 Ma.

3.1 Summary

Geochemical data from Miocene igneous rocks in the eastern Papua New Guinea are high-K, high-Al melts that are similar to igneous rocks associated with the early Miocene accreted Finisterre Arc (Hill and Raza, 1999; Jaques, 1976; Figures 1, 11). The Finisterre Arc was formed by subduction of the Solomon Sea to the north (Hill and Hall, 2003; van Ufford and Cloos, 2005). The early Miocene high K₂O Finisterre Arc magmas have possible correlatives with middle-to-late Miocene volcanic rocks in eastern Papua New Guinea. The Miocene magmas have negative HFSE anomalies (Figure 12) and these are interpreted to result from HFSE compatible minerals (primarily rutile) in the source regions of subduction zones (Green et al., 1989; Grove et al., 2012; Ryerson and Watson, 1987). In eastern Papua New Guinea, negative

HFSE anomalies associated with Miocene volcanism is evidence in support of the interpretation that the magmas were formed in a subduction zone.

Geochemical and $^{40}\text{Ar}/^{39}\text{Ar}$ data indicate that igneous rocks, ranging in composition from high-K basalt to high-K dacite, were erupted/intruded in the middle to late Miocene on the Papuan Peninsula and throughout the region that was to become the Woodlark Rift (e.g., Woodlark Island, Panapompom Island, the Louisiade Archipelago; Figure 11). $^{40}\text{Ar}/^{39}\text{Ar}$ age spectra from Panapompom Island, the Louisiade Archipelago, and Woodlark Island (Figure 13) in the Woodlark Rift System have loss profiles with lower intercept ages that correspond to the timing of seafloor spreading in the Woodlark Basin (Taylor et al., 1995). The loss profiles likely indicate that some of Miocene magmas in eastern Papua New Guinea were reheated by initiation and westward propagation of Woodlark Basin seafloor spreading, resulting in partial $^{40}\text{Ar}^*$ loss.

Previous workers associated these melts with a brief period of southward subduction beneath the entire length of Papua New Guinea (Cloos, 2005; Page, 1976; Smith, 1982; Weiland, 1999). While a period (11 – 17 Ma) of southward subduction beneath Papua is likely, it is noted that these magmas were produced synchronously with the collision of the Adelbert-Finisterre Arc in central Papua New Guinea (Hill and Raza, 1999). Thus it is possible that some of the Miocene magmas, especially in the Papuan Highlands south of the accreted terranes, may represent melting of continental crust due to collisional processes (Johnson et al., 1978), analogous to late stage magmatism associated with Himalayan orogenesis in Tibet (Chung et al., 2005; Miller et al., 1999).

4.1 Pliocene – Active Volcanism: Lusancay Is., Egum Atoll, Amphlett Is., Nuamata Is., Normanby Is., D’Entrecasteaux Is.

Evidence for Pliocene volcanism in the Woodlark Rift occurs along the Woodlark Rise on Egum Atoll, Amphlett Island Group, and Lusancay Islands (Figures 1, 2) where erosional remnants of larger volcanic complexes are preserved as volcanic necks (Smith, 1981).

Historically active volcanism in the Woodlark Rift occurs along strike of the Woodlark spreading center at Mt. Lamington, Mt. Victory, Mt. Waiwa, Dei Dei geothermal field, SE Goodenough Island, and Dобу Island (Johnson et al., 1978) (Figure 1). The morphology of the volcanic centers changes from large stratocones in the west (i.e. Mt. Lamington), to smaller rhyolitic cinder cones and basalt flows in the east (i.e. Dобу Island).

The greater degree of erosion of volcanic landforms distal to the axis of seafloor spreading suggests volcanism is older on the conjugate margins of the Woodlark Basin. For example, volcanism is older to the north (along the Woodlark Rise) and south (on Normanby and Misima Islands) of Fergusson and Dобу Islands where young and active volcanic landforms are preserved (Smith, 1982).

Papuan Peninsula

Andesite sample 08P010 from the northern coast of the Papuan Peninsula and is located in a geothermal area close to Mt. Waiwa (Figure 1). These andesites have an inferred Miocene age (Davies, 1971) and are comprised of clinopyroxene + biotite + hornblende + plagioclase ± orthopyroxene ± olivine. A $^{40}\text{Ar}/^{39}\text{Ar}$ plateau age of 1.84 ± 0.10 Ma was obtained on biotite analyzed from this sample (Figure 15A). In the Managalase volcanic field, <5 Ma volcanic units have been identified, temporally linking the large stratocones in the western Papuan Peninsula with the young volcanic rocks of the Woodlark Rift System (Ruxton, 1999; Figure 1). These $^{40}\text{Ar}/^{39}\text{Ar}$ results for 08P010 biotite spatially and temporally link young/active volcanism in the Woodlark Basin with active volcanism on the northern coast of the Papuan Peninsula.

Egum Atoll

Egum Atoll, a small ($<1 \text{ km}^2$) deeply eroded volcanic neck, is part of a much larger submarine plateau (~ 30 km in diameter) that comprises the flanks of a volcanic edifice active at ~3 Ma (Smith, 1982) (Figures 1, 2). Phenocrysts in Egum andesite are diopside, augite, plagioclase, and minor olivine in an altered groundmass of Fe-oxide and chlorite (Figure 17F). Clinopyroxene crystals have the 56 – 124 ° cleavage and habit of amphibole suggesting clinopyroxene is pseudomorphic after amphibole. Olivines are small, zoned, and have reaction rims of Fe-oxides.

The geochemistry of volcanic rocks at Egum Atoll indicate they are aluminous, high-K, basaltic andesite to andesite (Figure 16) with LILE enrichment, HREE depletion and negative Nb and Ta anomalies (Figure 17). $^{40}\text{Ar}/^{39}\text{Ar}$ total fusion analysis of clinopyroxene from Egum Atoll yielded an age of $2.79 \pm 0.08 \text{ Ma}$ (Table 2, Appendix 2.1).

One interpretation of pseudomorphic pyroxene in the Lusancay Island volcanics is that amphiboles were crystallized from an arc magma at a time when subduction was active (i.e. Maramuni Arc) in the mid-Miocene (Smith, 1982). At a later time, anhydrous magmas, associated with extension, recrystallized the amphiboles as clinopyroxene (Haschke and Ben-Avraham, 2005). The reaction rim and zoning in olivines suggests that they are possibly xenocrysts derived from the upper plate, which is comprised primarily of the PUB ophiolite (Davies and Ives, 1965).

Xenoliths in Egum Atoll andesite include metapelites (Figures 17I, 17K), felsic gneisses, granite, eclogite, and dunite/pyroxenite (Figure 17J). Gneissic and granitic xenoliths have several potential sources including equivalents of gneisses and granites from Goodenough and Fergusson Islands that host (U)HP eclogites or late Miocene granitic rocks on Woodlark Island

and Misima Island (Adshead and Appleby, 1996; Ashley and Flood, 1981). Ultramafic xenoliths and pyroxenes in altered garnet pyroxenite xenoliths are Ca-rich and are comprised of Mg-rich olivine and diopside, and are potentially correlated with the upper plate of the D'Entrecasteaux Islands core complexes. The ages of xenoliths on Egum Atoll are not known, but they have mineralogic and petrographic similarities to the rocks in the (U)HP terrane and the PUB in the D'Entrecasteaux Islands. The presence of gneissic and granite xenoliths suggests that the lower plate in the D'Entrecasteaux Islands extends to the north under the Woodlark Rise, where the xenoliths have been entrained in magmas associated with rifting.

Lusancay Island Volcanism

The Lusancay Islands are a set of 4 small ($<0.5 \text{ km}^2$) islands (Kawa, Sim Sim, Wagalasu, and Nauria) to the west of the Trobriand Islands (Figures 1, 2). The Lusancay Islands are comprised of deeply eroded, joined, volcanic necks with crosscutting basalt containing abundant xenoliths.

These volcanic rocks overlie a thick sequence of Miocene-Pliocene limestone that comprise most of the Woodlark Rise (Silver et al., 1991). The Lusancay Island volcanic rocks are fine grained with visible phenocrysts of plagioclase, clinopyroxene, biotite, and hornblende. The volcanic necks have abundant xenoliths of eclogite, amphibolite, metasediment, dunite, and gneiss. The xenoliths may be directly sampling the basement rocks (i.e. upper and lower plate equivalents of the D'Entrecasteaux Islands) to the Trobriand Islands. The dacitic suite in the Lusancay islands are typically medium to dark grey but are sometimes red (Wagalasu Island). In thin section, the samples are fine grained with sparse phenocrysts of zoned, pale green clinopyroxene with yellow-brown rims (Figure 17G). The groundmass is made up of plagioclase microlites, with rare epidote, minor biotite with altered rims of hematite and chlorite, and very

rare xenocrystic quartz. The quartz in the groundmass is usually rimmed by oxides but some quartz grains also occur as inclusions in clinopyroxene.

The chemical composition of Lusancay Island volcanic rocks is broadly dacitic with high concentrations of Al and extremely high K (5.4 – 8.0 wt.% (Figure 16). These rocks have extremely high concentrations of LILE and LREE and HFSE and HREE depletion (Figure 18). The trace and REE geochemistry of these rocks show that they are comparable to adakites found in the Aleutian Arc (Kay, 1978). The Lusancay islands have been previously dated at 1.0 – 2.3 Ma via K-Ar whole rock methods (Smith, 1981) (Table 2). $^{40}\text{Ar}/^{39}\text{Ar}$ total fusion of clinopyroxene from the Lusancay Islands yielded an age of 2.92 ± 0.21 Ma (Table 2, Appendix 2.1).

The Lusancay Islands occur south of the Trobriand Trough, a topographic depression to the north of the Woodlark Rise (Figure 1). As previously discussed, the origin of the Woodlark Rise volcanism is controversial, it has been interpreted to represent: (1) a passive margin that was active only in the middle Miocene (Silver et al., 1991), (2) partial melt of Solomon Sea lithosphere formed due to southward subduction at the Trobriand Trough (Martinez et al., 2001), (3) partial melt of an old, previously subducted slab that has been reheated due to westward propagation of upwelling asthenosphere in Woodlark Basin (Haschke and Ben-Avraham, 2005; Johnson et al., 1978; Smith et al., 1979). The chemical signature of adakites is usually attributed to melting of a subducted slab (Castillo, 2006; Smith et al., 1979). However, these magmas were erupted well after Woodlark Basin sea floor spreading began (Taylor et al., 1995) and subduction associated with the Maramuni Arc had ceased (Page, 1976; Smith and Clarke, 1991; Weiland, 1999) so the tectonic significance of the geochemical signature [of subduction] preserved in these rocks is somewhat puzzling. It is probable that Lusancay Island magmas were derived

from melting of a piece of broken eclogitic slab in the mantle from an extinct subduction zone, driven by the westward propagation of the Woodlark Basin sea floor spreading rift tip (Johnson et al., 1978; Smith et al., 1979). This scenario can best account for the composition (adakites) and timing of volcanism (after eastern Papua is undergoing extension in the Woodlark Rift System).

Amphlett Islands

The Amphlett Islands are a group of volcanic islands north of Fergusson Island and south of the Trobriand Trough (Figures 1, 2). They are eroded volcanic islands consisting of massive pyroclastic deposits, several smaller volcanic necks, and lava domes that have been intruded by basaltic dikes. The deeply eroded islands are arranged in an ellipse and may represent the remnant flanks of a large volcano (Smith, 1976b). The lava domes contain xenoliths of gneiss (Figure 17L), granite, and gabbro entrained in a matrix of clinopyroxene + biotite + hornblende + plagioclase \pm orthopyroxene \pm olivine (Figure 17D, Figure 17E).

The Amphlett Island group volcanics are aluminous, high-K, basaltic andesite to andesite (Figure 16) with LILE enrichment, HREE depletion and negative-Nb and negative-Ta anomalies (Figure 19). The trace and REE concentrations of basalt, andesite, and dacite in the Amphlett Island group do not vary substantially with SiO₂ and thus are likely indicative of the source region and not solely the result of crystal fractionation.

⁴⁰Ar/³⁹Ar inverse isochron ages obtained for sanidine and basalt on Apuo Island in the center of the Amphlett Island chain are 3.17 \pm 0.29 Ma (Figure 20C) and 1.92 \pm 0.53 Ma (Figure 20D), respectively. On Yamea Island, at the southern end of the Amphlett island group, a ⁴⁰Ar/³⁹Ar plateau age of 2.59 \pm 0.76 Ma was obtained from (sample PNG10-050a) amphibole (Figure 20A). Yamea Island basalt yielded an ⁴⁰Ar/³⁹Ar inverse isochron age of 2.58 \pm 0.49 Ma.

(Figure 20B). Trapped $^{40}\text{Ar}/^{36}\text{Ar}$ ratios range from 279 to 296 in all Amphlett Island samples; these are all within uncertainty of the atmospheric composition (Figures 20B, 20C, 20D, 20E)).

Nuamata and Normanby Island

Nuamata Island, located north of Goodenough Island, is comprised of welded ash and ignimbrite (Figures 1, 2). Normanby Island is comprised of an active metamorphic core complex that is in fault contact with the upper plate rocks associated with the PUB which are in turn overlain by Pliocene volcanics (Figure 1, 2). Normanby and Nuamata Island volcanic rocks have similar mineral abundances, trace element chemistry, and ages. Nuamata and Normanby Island are comprised of plagioclase + olivine + Fe/Ti oxides \pm orthopyroxene \pm clinopyroxene \pm hornblende \pm biotite (Figure 17C). Olivine and orthopyroxene crystals are rare and may have been incorporated into these magmas as xenocrysts from the upper plate.

Xenoliths in volcanics on Nuamata Island are comprised of metasediments, felsic gneisses, granodiorite, basalt, dunite, and pyroxenite. Gneissic and granitic xenoliths have several potential sources including equivalents of gneisses and granites from the lower plate of Goodenough Island (Monteleone, 2007). $^{40}\text{Ar}/^{39}\text{Ar}$ age spectra from K-feldspar from an amphibolite xenolith (PNG06-043b, Figure 21C) on Nuamata Island has an age gradient interpreted to be a loss profile with a minimum metamorphic age (~9 Ma). This age is within uncertainty of U/Pb zircon and Lu/Hf garnet ages from the metamorphic core complexes on Goodenough Island (Baldwin et al., 2008; Zirakparvar et al., 2011).

The whole rock geochemical composition of Normanby and Nuamata Islands show that the rocks are broadly high-K basaltic andesite to high-K andesite (Figure 16). The trace and REE geochemistry show that these volcanics have LILE enrichment, HREE depletion and negative-Nb and negative-Ta anomalies (Figure 22). There is a noticeable range in REE concentrations in

these sample and they may have undergone extensive magmatic differentiation or were they were derived from slightly different initial compositions.

$^{40}\text{Ar}/^{39}\text{Ar}$ plateau ages were obtained on K-feldspar and amphibole from andesites (PNG06-043a) on Nuamata Island (2.37 ± 0.21 Ma amphibole and 2.19 ± 0.08 Ma K-feldspar; Figure 21C). Trapped $^{40}\text{Ar}/^{36}\text{Ar}$ ratios from Nuamata Island volcanics are slightly higher than atmospheric values, ranging from 339 ± 30 and 300 ± 3 (Figures 21D, 21F). Similar ages were obtained for andesites on Normanby Island (1.7 – 2.6 Ma) (Monteleone, 2007; Table 2). Subaerial volcanism on central Nuamata Island occurs on the northern flank of Goodenough Island upper plate. The $^{40}\text{Ar}/^{39}\text{Ar}$ plateau age obtained on sample PNG10-058 amphibole (2.37 Ma) may be interpreted as a minimum age for initial time when metamorphic core complexes were at the surface because the subaerial ash flow requires that the area around Goodenough Island to be a topographic high, above sea level at that time.

The age and composition of volcanism on Nuamata and Normanby Islands occur to the north and south of active volcanism and metamorphic core complexes on Goodenough and Fergusson Islands (Hill and Baldwin, 1993; Monteleone, 2007). Nuamata and Normanby Island volcanics may have erupted close to the location where metamorphic core complexes currently exist (on Goodenough and Fergusson Islands), and rifted to the north (Nuamata Island) and to the south (Normanby Island) as the lithosphere is extended ahead of the propagating seafloor spreading rift tip.

Goodenough Island

The Moresby Strait, between Goodenough and Fergusson Islands, has four areas where basaltic magmatism erupted to the surface (Figures 1, 2). The largest flow occurs on Wagifa Island, less than 0.5 km southeast of Goodenough Island (Figure 2). Wagifa Island represents a

now dormant, eroded volcanic edifice. North of Wagifa Island, fresh lava flows of vesicular olivine-basalt occur on Goodenough Island and appear to have erupted through vents along transfer faults between the shear zone and sedimentary cover rocks.

Petrography and electron microprobe chemical analyses of PNG10-064B show that Goodenough Island basalts are comprised of plagioclase + olivine + Fe/Ti oxides \pm orthopyroxene \pm clinopyroxene \pm hornblende \pm biotite \pm xenocrystic garnet (Figure 17B, Figure 17H)).

The mafic-intermediate rocks on Goodenough Island and Wagifa Island are high-K, high-Al, calc-alkaline basalt to basaltic andesites (Figure 16). These mafic rocks represent a bimodal rock suite in the D'Entrecasteaux Islands that erupted to the west of active sea-floor spreading center rift tip. N-MORB normalized multi-element patterns of these lavas have incompatible trace and LREE enrichment with respect to heavy rare earth elements and have negative Ta-Nb and mostly positive Sr anomalies (Figure 23).

$^{40}\text{Ar}/^{39}\text{Ar}$ analyses were performed on mineral separates of hornblende, biotite, and K-feldspar from basaltic andesite samples, PNG08-004a (Wagifa Island) (Figures 21A, 21B) and PNG03-117 (Goodenough Island) (Figures 7A, 8A). PNG08-004a biotite yielded a plateau age of 0.409 ± 0.021 Ma (Figure 21A) and this age is interpreted as the timing of cooling through biotite closure temperature, following eruption. The age spectra from PNG03-117 feldspar yielded an age gradient interpreted to represent an argon loss profile. In this sample, the feldspars have likely been incorporated into the magma from the mafic upper plate and have been partially reset. In this case, the maximum eruption age is indicated by the youngest $^{40}\text{Ar}/^{39}\text{Ar}$ steps (1.5 Ma.) and the minimum age of crystallization is indicated by the oldest step (29 Ma; Figure 7A).

Sanaroa, Fergusson, and Dobu Islands

Silicic volcanism occurs on Fergusson, Dobu, and Sanaroa Islands in the Dawson Strait area between Fergusson and Normanby Islands (Figures 1, 2). There are three vents in the Dawson Strait area: Mount Lamonai, Mount Oiau, and Dobu Island (Smith et al., 1977). Outcrops are comprised of pyroclastics, ash fall tuffs, pumice, and flow-banded rhyolite (Smith et al., 1977). Sanaroa Island does not have any volcanic vents that are active, but some units on Sanaroa Island are correlated to volcanic units on Dobu Island (Smith et al., 1977). Igneous rocks in the Dawson Strait area consist of sanidine/anorthoclase + Fe/Ti oxides (illmenite/magnetite) ± olivine ± quartz/nepheline, ± clinopyroxene (Figure 17A). This mineral assemblage is consistent with other silicic volcanic rocks from rift environments (i.e. East African Rift) (Smith, 1976b).

Dawson Strait volcanics are highly fractionated high-K rhyolite and dacite (Hegner and Smith, 1992; Smith et al., 1977; Stoltz et al., 1992) (Figure 16). The felsic volcanic rocks from Dawson Strait are strongly enriched in incompatible trace and rare earth elements with negative Ba, Sr, Eu, and Ti anomalies (Figure 25).

$^{40}\text{Ar}/^{39}\text{Ar}$ ages on sanidines from rhyolites in the Dawson Strait area were obtained from Dobu Island (PNG03-075a, 0.031 ± 0.004 Ma; Figure 24A), SW Fergusson Island (PNG10-067a, 0.81 ± 0.06 Ma; Figure 24E), and Sanaroa Island (PNG08-058a, 1.13 ± 0.03 Ma; Figure 24C). All Dawson Strait samples have $^{36}\text{Ar}/^{40}\text{Ar}$ inverse isochron intercepts within error of atmosphere (Figures 24B, 24D, 24F). These samples are from the bimodal basalt – rhyolite volcanic rock suite in the D'Entrecasteaux Islands, and occur just west the westward propagating seafloor spreading rift tip. Whole rock Hf isotopic data indicate that the felsic volcanic rocks

were derived from juvenile mantle, interpreted to represent the onset on sea floor spreading in the D'Entrecasteaux Islands (Zirakparvar, 2012).

Summary

Geochemical data from the D'Entrecasteaux Islands indicate a bimodal distribution of felsic and mafic volcanic rocks (Figure 16). The D'Entrecasteaux Islands volcanic rocks are similar to bimodal suites that occur in the East African Rift (Gibson, 2009) and the Rio Grande Rift (McMillan et al., 2000). When comparing the bimodal D'Entrecasteaux Islands suite to these other two rifts, the trace element concentrations are similar, suggesting that volcanism in the D'Entrecasteaux Islands occurred by similar tectonic processes; decompression melting in an area of extending continental crust.

Recent tectonic models suggest volcanism in the Woodlark Rift results from active subduction at the Trobriand Trough with exhumation of (U)HP rocks in the back arc (Martinez et al., 2001; Martinez and Taylor, 2002). However, there is also evidence that contradicts that interpretation: i) major, minor, and trace element geochemical signatures of D'Entrecasteaux Islands lavas are similar to lavas in other continental rifts such as the East African Rift and the Rio Grande Rift (Smith, 1976b), ii) there is a lack of hydrous phenocrysts (hornblende, biotite) that are in equilibrium with the magma in which they are entrained, suggesting that they were formed from anhydrous environment, iii) seismic studies have failed to show a well defined increase in P-wave velocities associated with a subducted slab [under the Papuan Peninsula] (Abers et al., 2002; Ferris et al., 2006; Silver et al., 1991), and iv) the lack ^{10}Be enrichment in young lavas suggesting that these magmas have little or no recent pelagic sediment component in their melt source (Gill et al., 1993).

Nb and Ta (HFSE elements) are compatible elements in the minerals (primarily rutile) in the source regions of subduction zones (Green et al., 1989; Grove et al., 2012; Ryerson and Watson, 1987). It is possible that negative HFSE anomalies could have been inherited from a time of previous subduction, because these young volcanic are erupting within a rift. To test this hypothesis, the ratio Nb*/Nb was used as a proxy for the subduction modified component in the volcanic rock and calculated as follows. Nb* is the concentration of niobium, determined from the log-linear extrapolation of N-MORB normalized La and Ce concentrations. This value is the concentration of Nb if there was not a negative anomaly present. Nb is the NMORB normalized concentration of Nb measured in the sample. Using the same method, Ta*/Ta is calculated. The magnitude of Nb*/Nb and Ta*/Ta is used to estimate the subduction component inherited from the source region for Woodlark Rift System magmas. Plots of Nb*/Nb and Ta*/Ta vs. age show that the intensity of the geochemical signature associated with subduction is decreases from the Miocene to the present (Figures 26, 27).

These trends are consistent with Miocene subduction beneath eastern Papua New Guinea that imposed negative Nb and Ta anomalies on the overlying mantle wedge. Relict Nb and Ta anomalies are still present in the Pliocene but decrease with time as magma was produced increasingly from upwelling E-MORB-like mantle associated with the Woodlark Basin (Chadwick et al., 2009). Processes that may affect the relict geochemical signature in the mantle beneath the Woodlark Rift System are diffusion, convection, and mixing.

5.1 Conclusions

The evolution of volcanism in eastern Papua New Guinea starts in the late Cretaceous/Paleocene when arc continent collision and PUB ophiolite obduction occurred. The

Shadowa Complex has been determined to be Paleocene in age and contains Late Cretaceous microfossils (Rogerson and Hilyard, 1989; Smith, 1976b). The Shadowa Complex could represent a slice of Coral Sea lithosphere obducted onto the Papuan Margin during the Eocene/Miocene, or it might represent an unrecognized section of the PUB.

In the Oligocene, volcanism is dominated by MORB compositions that make up large portions of the upper plate in eastern Papua New Guinea. The upper plate in the Woodlark Rift System has three potential associations: 1) Cretaceous oceanic lithosphere associated with the Pacific Plate or 2) Oligocene lithosphere associated with the Solomon Sea or 3) early Eocene Coral Sea lithosphere. $^{40}\text{Ar}/^{39}\text{Ar}$ results from Goodenough Island basalt, pillow lava from Woodlark Island, and Panapompom Island basalt provide evidence suggesting part the upper plate in the Woodlark Rift is at least Oligocene in age (i.e. 29-32 Ma; Figures 7A, 7B, 7C). The Oligocene basalt may be a minor section of Solomon Sea basalt and gabbro that overthrusts older Mesozoic oceanic lithosphere (PUB) identified on the Papuan Peninsula (Davies, 1971) and Moresby Seamount (Monteleone et al., 2001).

In the Miocene, magmas were erupted in a E-W trending belt throughout eastern Papua New Guinea (i.e. Maramuni Arc; Figure 9), and these are most likely related to a south dipping subduction zone (Cloos, 2005; Page, 1976; Smith, 1982; Weiland, 1999). The whole rock trace element compositions of Maramuni Arc rocks have LILE enrichment and HFSE depletion, which are also indicators of subduction during this time (Figure 12). It is also noted that the rocks are alkaline (Jakeš and Smith, 1970) and were erupted during the time of Finisterre Arc collision in central Papua New Guinea (Hill and Raza, 1999), so collisional processes might be the cause of some of the Miocene volcanism.

After 8 Ma, volcanism and is scarce until ~3 Ma. During this time, the Woodlark Basin formed (Taylor et al., 1995) and metamorphic core complexes were exhumed to the surface (Baldwin et al., 1993) and extensional basins formed via microplate rotation (Wallace et al., 2004). Pliocene magmatism in the Woodlark Rift initially has geochemical characteristics of subduction zone volcanism (i.e. negative Nb and Ta anomalies). It is likely that the ‘arc-like’ geochemical signatures were inherited from a relict subduction modified mantle wedge. Decompression melting during rifting is mostly responsible for active volcanism in the Woodlark Rift System. This hypothesis is supported when the intensity of HFSE anomalies are traced over time (Figure 26, 27).

Figures

Figure 1. Geologic and tectonic map of southeastern Papua with geologic units highlighted (after Baldwin et al., 2008). The sea floor spreading anomalies of Taylor et al. (1995) are indicated in the Woodlark Basin. AUS = Australia, LA = Louisiade Archipelago, RI = Rossel Island, MI = Misima Island, PI = Panapompom Island, PP = Papuan Peninsula, DI = D'Entrecasteaux Islands, G = Goodenough Island, F = Fergusson Island, N = Normanby Island, MVF = Managalase Volcanic Field, WI = Woodlark Island, TI = Trobriand Islands, LI = Lusancay Islands, F-AA = Finisterre-Adelbert Arc, SBP = South Bismarck Plate, WLK = Woodlark Plate.

Figure 2. Map showing sample localities for igneous rocks used in this study. Red stars denote sample locations. D.S. = Dawson Strait, M.S. = Morsby Strait.

Figure 3. Oceanic lithosphere in eastern Papua New Guinea with ages indicated. Samples locations for obducted oceanic lithosphere are indicated by star symbols. The blue star indicates the sample location of the Paleocene Dabi Volcanics. Red Stars indicate the sample locations altered basalts from the upper plate. PUB. = Papuan Ultramafic Belt, SS = Solomon Sea, SG = Shadowa Gabbro, KV = Kutu Volcanics, LA = Louisiade Archipelago, MI = Misima Island, PI = Panapompom Island, WI = Woodlark Island.

Figure 4. Photomicrographs of rocks for upper plate rocks of the Woodlark Rift System. A) altered gabbro sample PMG03-188 from Panapompom Island. Mineral assemblage is orthopyroxene + olivine + plagioclase + Fe-oxides ± epidote ± chlorite. Image is in crossed polarized light. B) pillow basalt sample PNG10-017 from Woodlark Island. Mineral assemblage is orthopyroxene + clinopyroxene + plagioclase +Fe-oxides ± serpentine ± chlorite. Image is in cross polarized light. C) basalt sample PNG03-117 from Goodenough Island. Phenocrysts are

olivine + clinopyroxene + plagioclase +Fe-oxide. Image is in plane polarized light. D) serpentinite sample PNG03-058 from Normanby Island. Mineral assemblage is serpentine + chlorite+ calcite + plagioclase +Fe-oxides. Image is in plane polarized light. E) gabbro sample 08P-002 from the Papuan Peninsula. Mineral assemblage is clinopyroxene + orthopyroxene + plagioclase +Fe-oxides ± chlorite. F) basalt sample 08P-024 from the Cape Vogel basin. Phenocrysts are clinoenstatite + plagioclase + clinopyroxene + olivine +Fe-oxide ± chlorite. Image is in crossed polarized light.

Figure 5. K₂O vs. SiO₂ classification plots for samples from the upper plate in the Woodlark Rift System (after Ewart, 1982).

Figure 6. N-MORB normalized multi-element diagram from the upper plate in the Woodlark Rift System. Elements are listed with the most incompatible elements on the left and the least incompatible on the right. N-MORB normalization values are from McDonough and Sun (1995).

Figure 7. ⁴⁰Ar/³⁹Ar age spectra for feldspar and whole rock samples from the upper plate in the Woodlark Rift System..

Figure 8. Inverse isochron plots for feldspar and whole rock samples from the upper plate in the Woodlark Rift System..

Figure 9. Map of eastern Papua New Guinea with Miocene volcanic rocks (in red) and Miocene plutonic rocks (in yellow) highlighted. Published geochronologic ages are color coded according to reference.

Figure 10. Photomicrographs of Miocene igneous rocks from the Woodlark Rift. A) altered andesite sample 08P006 from the Papuan Peninsula. Phenocrysts are amphibole + quartz + K-feldspar +Fe-oxides. Image is in plane polarized light. B) diorite sill sample PNG09-005a from

the Louisiade Archipelago. Mineral assemblage is amphibole + quartz + K-feldspar +Fe-oxides. Image is in cross polarized light. C) dacite sample PNG10-005b from Woodlark Island. Phenocrysts are amphibole + quartz + K-feldspar +Fe-oxides. Image is in plane polarized light. D) granite sample PNG10-014b from Woodlark Island. Mineral assemblage is amphibole + biotite+ quartz + plagioclase +K-feldspar +Fe-oxides. Image is in cross polarized light. E) diorite sample PNG03-199 from Panapompom Island. Mineral assemblage is amphibole + biotite+ quartz + plagioclase +Fe-oxides.

Figure 11. K_2O vs. SiO_2 classification plots for Miocene igneous rocks in the Woodlark Rift System (after Ewart, 1982). Compositions range from basalt to dacite, but all samples at all locations contain a calc-alkaline to alkaline component.

Figure 12. N-MORB normalized multi-element diagram for Miocene igneous rocks from the Woodlark Rift System. The patterns show LILE enrichment and depletion in HFSE. Elements are listed with the most incompatible elements on the left and the least incompatible on the right. N-MORB normalization values are from McDonough and Sun (1995).

Figure 13. $^{40}Ar/^{39}Ar$ composite age spectra for whole rock and amphibole samples from Miocene igneous rocks in the Woodlark Rift System. 08P006 amphibole yielded a plateau age that comprises 99.2 % of the ^{39}Ar released and an age of 17.03 ± 0.94 Ma. PNG10-005b amphibole yielded a plateau age that comprises 84.5 % of the ^{39}Ar released and an age of 13.42 ± 1.01 Ma. PNG10-014a amphibole yielded a plateau age that comprises 95.8 % of the ^{39}Ar released and an age of 12.42 ± 0.37 Ma. PNG09-005 amphibole yielded a plateau age that comprises 79.2% of the ^{39}Ar released and an age of 11.84 ± 0.16 Ma. Sample PNG03-199 (whole rock) yielded a plateau age that comprises 81.6% of the ^{39}Ar released and an age of 8.07 ± 0.32 Ma.

Figure 14. Inverse isochron plots for whole rock and amphibole samples from Miocene igneous rocks. A) The inverse isochron for 08P006 amphibole yields an age of 16.5 ± 1.5 Ma. (MSWD = 7.5), regressed through all data points. $^{40}\text{Ar}/^{36}\text{Ar}$ intercept is 316 ± 15 , slightly higher than atmospheric values. B) The inverse isochron for PNG09-005 amphibole yields an age of 11.48 ± 0.33 Ma. (MSWD = 2.1), regressed through 7 of 9 data points. $^{40}\text{Ar}/^{36}\text{Ar}$ intercept is 301.9 ± 8.0 , concordant with atmospheric values. C) The inverse isochron for PNG03-199 whole rock yields an age of 8.4 ± 1.4 Ma. (MSWD = 28), regressed through 8 of 9 data points. $^{40}\text{Ar}/^{36}\text{Ar}$ intercept is 285 ± 20 , concordant with atmospheric values. D) The inverse isochron for PNG10-014b amphibole yields an age of 12.6 ± 0.97 Ma. (MSWD = 7.6), regressed through all data points. $^{40}\text{Ar}/^{36}\text{Ar}$ intercept is 271 ± 16 , slightly lower than atmospheric values. The inverse isochron for PNG10-005b amphibole yields an age of 12.9 ± 1.4 Ma. (MSWD = 0.55), regressed through 8 of 11 data points. $^{40}\text{Ar}/^{36}\text{Ar}$ intercept is 301.8 ± 9.5 , concordant with atmospheric values.

Figure 15. A) $^{40}\text{Ar}/^{39}\text{Ar}$ age spectra and inverse isochron plots for biotite from sample 08P010 from the northern coast of the Papuan Peninsula. 08P010 biotite yielded a plateau that comprises 99.98% of the ^{39}Ar released and yields an age of 1.84 ± 0.10 Ma. B) 08P010 biotite inverse isochron yields an age of 1.76 ± 0.27 Ma. (MSWD = 4.5), regressed through all points. $^{40}\text{Ar}/^{36}\text{Ar}$ intercept is 297.6 ± 7.7 , concordant with the atmospheric values.

Figure 16. K_2O vs. SiO_2 classification plots for young lavas in the Woodlark Rift (after Ewart, 1982). Samples range in composition from basalt to rhyolite but all sample locations contain a high-K, calc alkaline component. The Lusancay Island samples are dacitic with extremely high K_2O concentrations (5.4 – 8.0 wt. %).

Figure 17. Photomicrographs of samples from the Woodlark Rift. A) high-K rhyolite sample PNG03-075a from Dobu Island. Phenocrysts are sanidine + quartz + Fe-oxides + fayalite. Image

is in plane polarized light. B) basaltic andesite sample PNG08-004a from Wagifa Island.

Phenocrysts are amphibole + biotite + plagioclase + Fe-oxide (after amphibole and biotite).

Image is in plane polarized light. C) andesite sample PNG06-043a from Nuamata Island.

Phenocrysts are amphibole + clinopyroxene + plagioclase + Fe-oxide (after amphibole). Image is in plane polarized light. D) basalt sample PNG08-042 from Yamea Island (Amphlett Island group).

Phenocrysts are olivine + plagioclase + amphibole + biotite + Fe-oxide (after amphibole and biotite). Image is in plane polarized light. E) dacite sample PNG10-046a from Apuo Island.

Phenocrysts are K-feldspar + quartz + amphibole + Fe-oxide. Image is in plane polarized light.

F) andesite sample PNG10-042f from Egum Atoll. Phenocrysts are clinopyroxene + quartz + plagioclase + Fe-oxide (after amphibole). Image is in plane polarized light. G) dacite sample

PNG10-054a from Simsims Island (Lusancay Island group). Phenocrysts are clinopyroxene + quartz + biotite + Fe-oxide. Image is in plane polarized light. H) vesicular basalt sample

PNG10-064b from Goodenough Island. Phenocrysts are clinopyroxene + orthopyroxene + olivine + plagioclase + plagioclase. Image is in plane polarized light. I) xenolith sample PNG10-

043k from Egum Atoll. The assemblage contains diopsid + sanidine + aerinite. Image is in plane polarized light. J) xenolith sample PNG10-043l from Egum Atoll. The assemblage

contains enstatite + diopsid + Fe-oxide. Image is in plane polarized light. K) xenolith sample

PNG10-044d from Egum Atoll. The assemblage contains anorthite + diopsid + garnet + Fe-oxide. Image is in plane polarized light. L) gneiss xenolith sample PNG10-047b from Amphlett

Island group. The assemblage contains quartz + K-feldspar + biotite + amphibole Image is in plane polarized light.

Figure 18. N-MORB normalized multi-element diagram from samples from the Lusancay Island group. The patterns show LILE enrichment and depletion in HREE and HFSE. Elements are

listed with the most incompatible elements on the left and the least incompatible on the right. N-MORB normalization values are from McDonough and Sun (1995).

Figure 19. N-MORB normalized multi-element diagram from samples from the Amphlett Island group. The patterns show LILE enrichment and depletion in HREE and HFSE. Elements are listed with the most incompatible elements on the left and the least incompatible on the right. N-MORB normalization values are from McDonough and Sun (1995).

Figure 20. A) $^{40}\text{Ar}/^{39}\text{Ar}$ composite age spectra and inverse isochron plots for whole rock basalt, sanidine, and amphibole from samples from the Amphlett Island group. B) The inverse isochron for PNG08-042 basalt yields an age of 2.58 ± 0.45 Ma. (MSWD = 34), regressed through 7 of 8 data points. $^{40}\text{Ar}/^{36}\text{Ar}$ intercept is 292 ± 42 , concordant with the atmospheric values. C) The inverse isochron for PNG10-046a sanidine yields an age of 3.17 ± 0.29 Ma. (MSWD = 26), regressed through all data points. $^{40}\text{Ar}/^{36}\text{Ar}$ intercept is 296.1 ± 7.2 , concordant with the atmospheric values. D) The inverse isochron for PNG10-046b basalt yields an age of 1.92 ± 0.53 Ma. (MSWD = 72), regressed through all data points. $^{40}\text{Ar}/^{36}\text{Ar}$ intercept is 279 ± 50 , concordant with the atmospheric values. PNG10-050a amphibole yielded a plateau age that comprises 90.2 % of the ^{39}Ar released and an age of 2.37 ± 0.21 Ma. E) The inverse isochron for PNG10-050a amphibole yields an age of 2.59 ± 0.76 Ma. (MSWD = 6.1), regressed through 7 of 11 data points. $^{40}\text{Ar}/^{36}\text{Ar}$ intercept is 295.6 ± 21 , concordant with the atmospheric values.

Figure 21. $^{40}\text{Ar}/^{39}\text{Ar}$ age spectra and inverse isochron plots for K-feldspar, basalt, biotite, and amphibole from samples from the Goodenough and Nuamata Islands. A) PNG08-004a biotite age spectrum yielded a plateau age that comprises 78.5 % of the ^{39}Ar released and an age of 0.409 ± 0.021 Ma. B) The inverse isochron for PNG08-004a biotite yields an age of $0.364 \pm$

0.050 Ma. (MSWD = 1.4), regressed through 11 of 12 data points. $^{40}\text{Ar}/^{36}\text{Ar}$ intercept is 298.3 ± 4.9 , concordant with the atmospheric values. C) PNG06-043a K-feldspar age spectrum yielded a plateau age that comprises 62.3 % of the ^{39}Ar released and an age of 2.19 ± 0.08 Ma. D) The inverse isochron for PNG06-043a K-feldspar yielded an age of 1.6 ± 0.29 Ma. (MSWD = 9), regressed through 7 of 10 data points. $^{40}\text{Ar}/^{36}\text{Ar}$ intercept is 339 ± 30 , suggesting that this sample has a non-atmospheric trapped $^{40}\text{Ar}/^{36}\text{Ar}$ component. E) The inverse isochron for PNG06-046b K-feldspar yields an age of 2.00 ± 0.21 Ma. (MSWD = 11.1), regressed through all data points. $^{40}\text{Ar}/^{36}\text{Ar}$ intercept is 297.17 ± 17 , concordant with the atmospheric values. C) PNG10-058a amphibole age spectrum yielded a plateau age that comprises 84.5 % of the ^{39}Ar released and an age of 2.37 ± 0.21 Ma. F) The inverse isochron for PNG10-058a amphibole yields an age of 2.18 ± 0.23 Ma. (MSWD = 0.79), regressed through all data points. $^{40}\text{Ar}/^{36}\text{Ar}$ intercept is 300.1 ± 3.1 , concordant with the atmospheric values.

Figure 22. N-MORB normalized multi-element diagram from samples from the Normanby and Nuamata Islands. The patterns show LILE enrichment and depletion in HREE and HFSE except for PNG03-058a. PNG03-058a is characterized by slight LILE and LREE enrichment with HREE and HSFE similar to N-MORB. These concentrations are consistent with altered sea floor basalt and this sample is considered part of the PUB upper plate on Normanby Island. Elements are listed with the most incompatible elements on the left and the least incompatible on the right. N-MORB normalization values are from McDonough and Sun (1995).

Figure 23. N-MORB normalized multi-element diagram from samples from the Goodenough Island. The patterns show LILE enrichment and depletion HFSE with HREE concentrations similar to N-MORB. Elements are listed with the most incompatible elements on the left and the

least incompatible on the right. N-MORB normalization values are from McDonough and Sun (1995).

Figure 24. $^{40}\text{Ar}/^{39}\text{Ar}$ age spectra and inverse isochron plots for sanidine from samples from the Dawson Strait area. A) PNG03-075a age spectrum yielded a plateau age that comprises 50.5 % of the ^{39}Ar released and an age of 0.031 ± 0.004 Ma. B) The inverse isochron for PNG03-075a yields an age of 0.019 ± 0.011 Ma. (MSWD = 0.48), regressed through 6 of 11 data points. $^{40}\text{Ar}/^{36}\text{Ar}$ intercept is 303 ± 4 , concordant with the atmospheric values. C) PNG08-058a age spectrum yielded an integrated age of 1.13 ± 0.03 Ma. D) The inverse isochron for PNG08-058a yields an age of 1.17 ± 0.21 Ma. (MSWD = 9.8), regressed through 8 of 9 data points. $^{40}\text{Ar}/^{36}\text{Ar}$ intercept is 286 ± 15 , concordant with the atmospheric values. E) PNG10-067a age spectrum yielded a plateau age that comprises 73.2 % of the ^{39}Ar released and an age of 0.81 ± 0.06 Ma. F) The inverse isochron for PNG08-058a yields an age of 0.82 ± 0.12 Ma. (MSWD = 32), regressed through 8 of 9 data points. $^{40}\text{Ar}/^{36}\text{Ar}$ intercept is 281 ± 10 , concordant with the atmospheric values.

Figure 25. N-MORB normalized multi-element diagram from samples from the Dawson Strait volcanics. The patterns show LILE enrichment and depletion HFSE with HREE concentrations at or below N-MORB values. Elements are listed with the most incompatible elements on the left and the least incompatible on the right. N-MORB normalization values are from McDonough and Sun (1995).

Figure 26. Plot of Nb^*/Nb vs. $^{40}\text{Ar}/^{39}\text{Ar}$ age for samples analyzed in this study. The best fit lines used a logarithmic equation and suggest that the Nb^*/Nb ratio decreases significantly for samples <4 Ma. N-MORB normalization values are from McDonough and Sun (1995).

Figure 27. Plot of Ta*/Ta vs. $^{40}\text{Ar}/^{39}\text{Ar}$ age for samples analyzed in this study. The best fit lines used a logarithmic equation and suggest that the Ta*/Ta ratio decreases significantly for samples <4 Ma. N-MORB normalization values are from McDonough and Sun (1995).

Figure 1

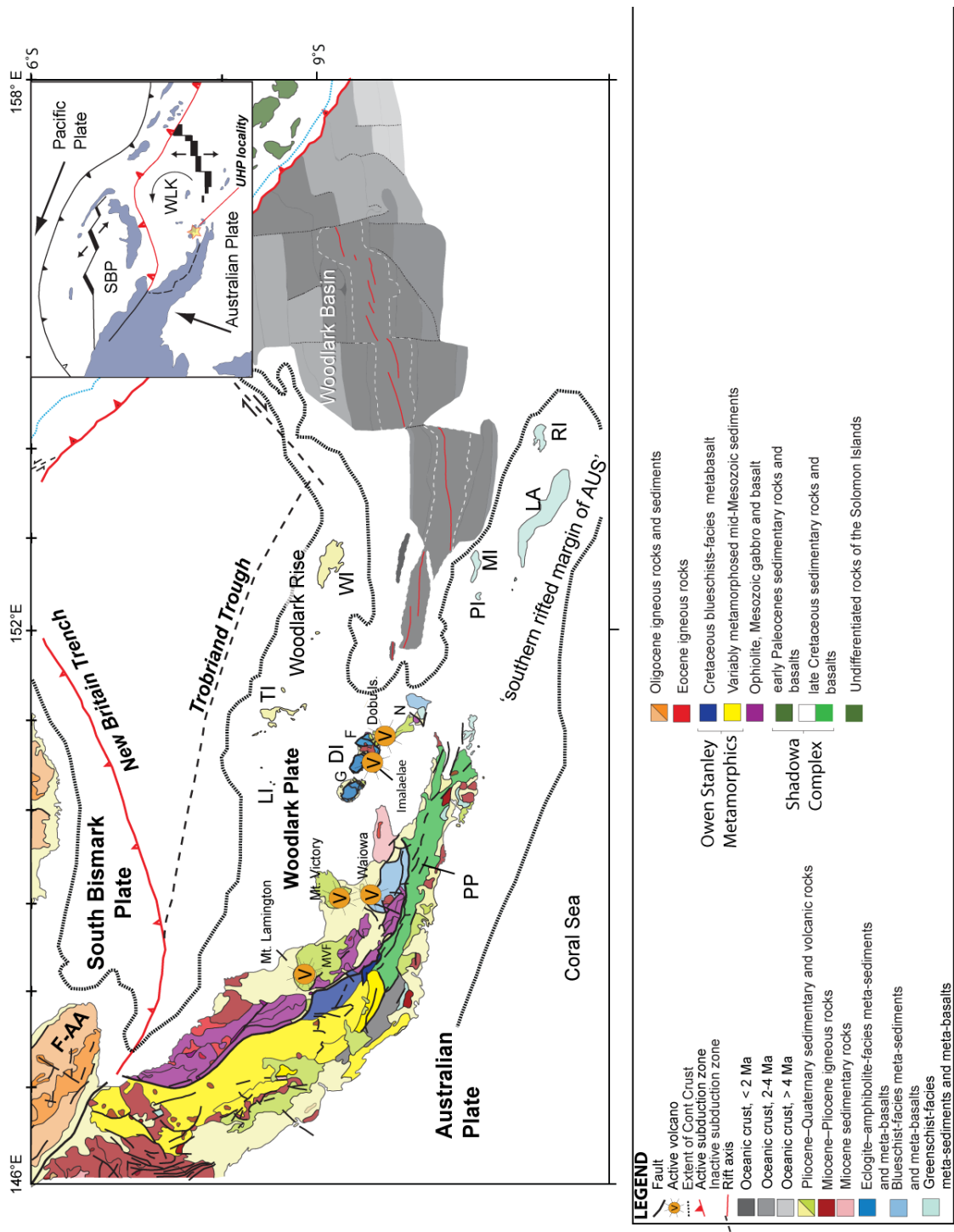


Figure 2

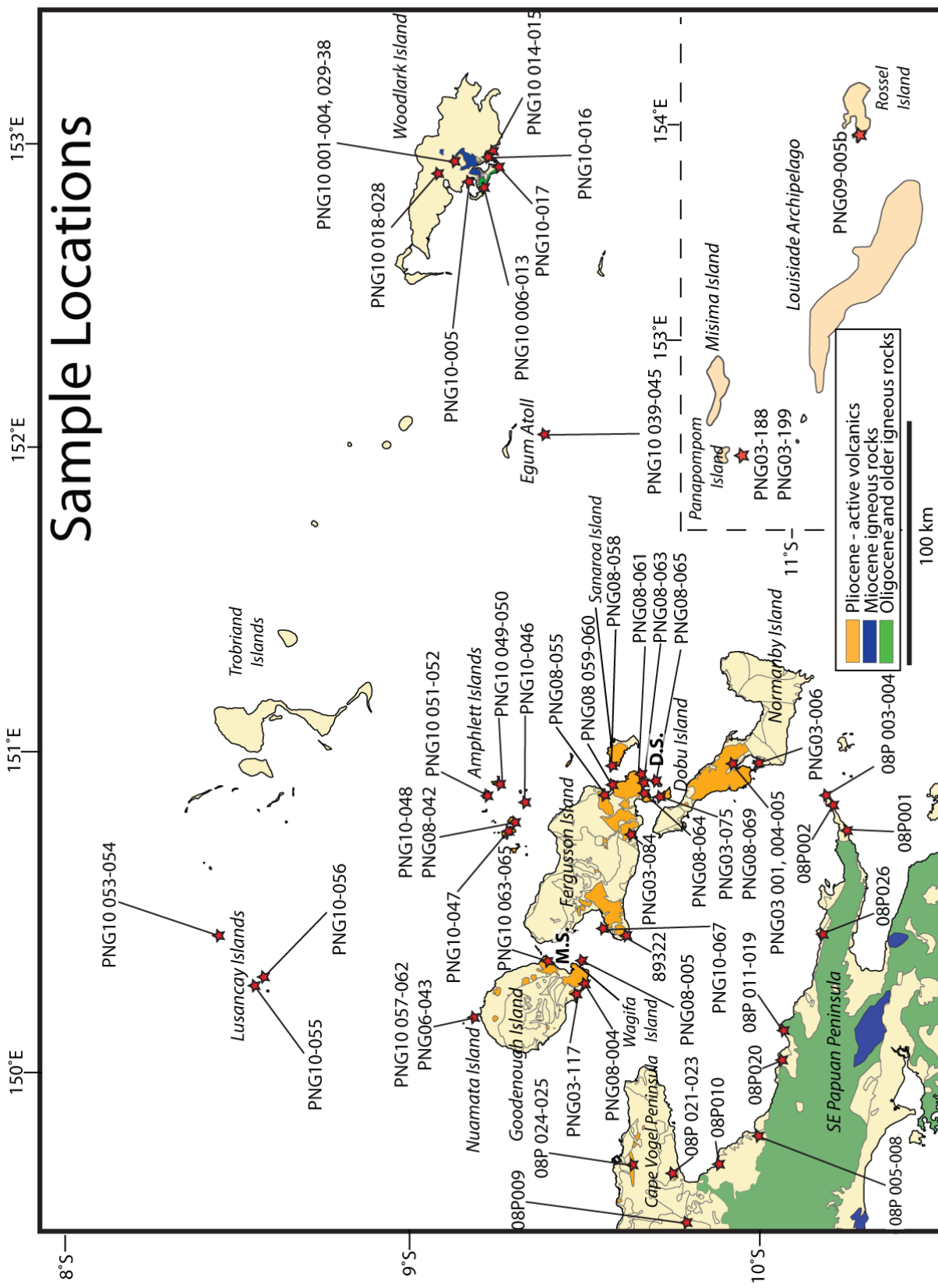


Figure 3.

Oceanic Lithosphere in Eastern Papua

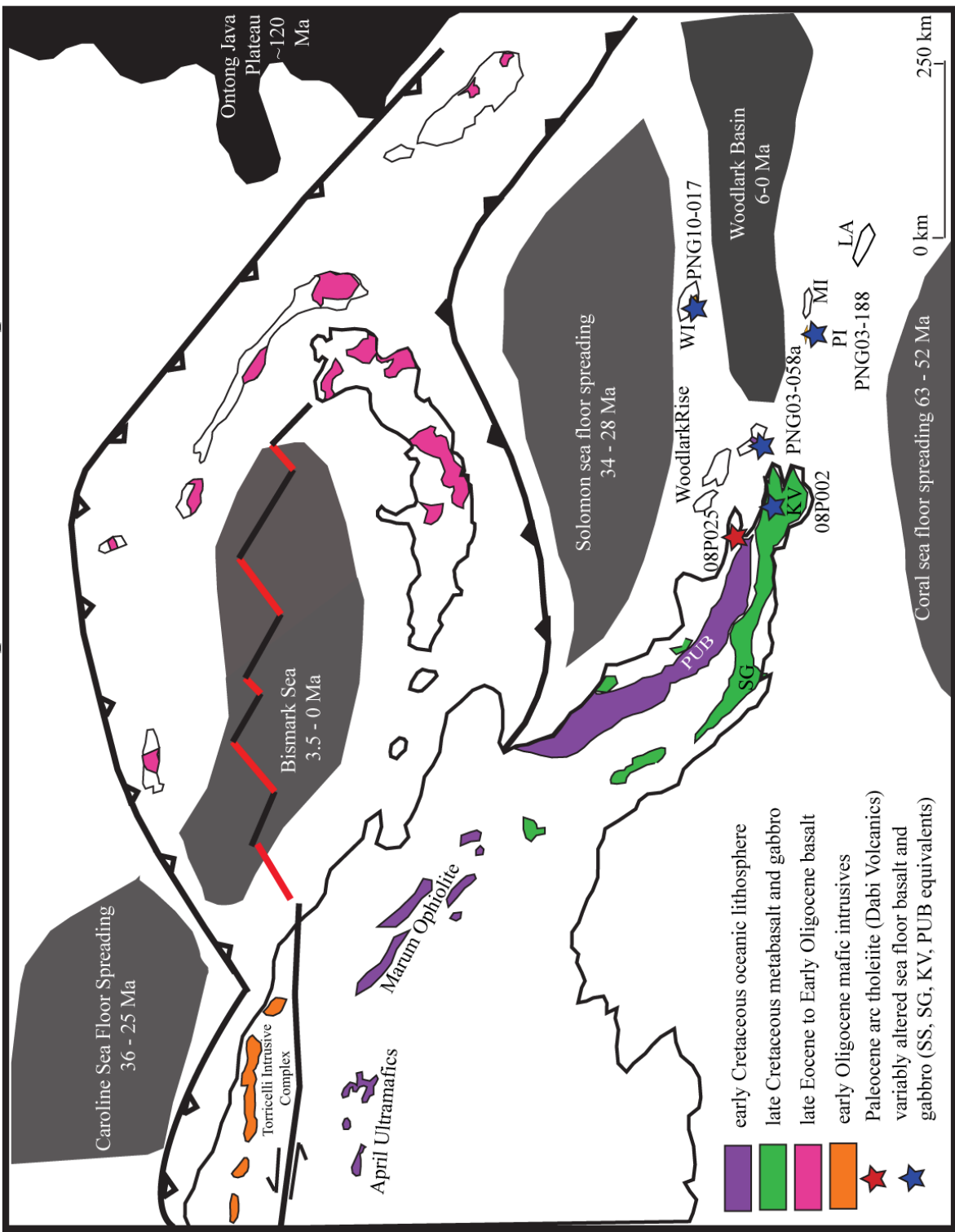
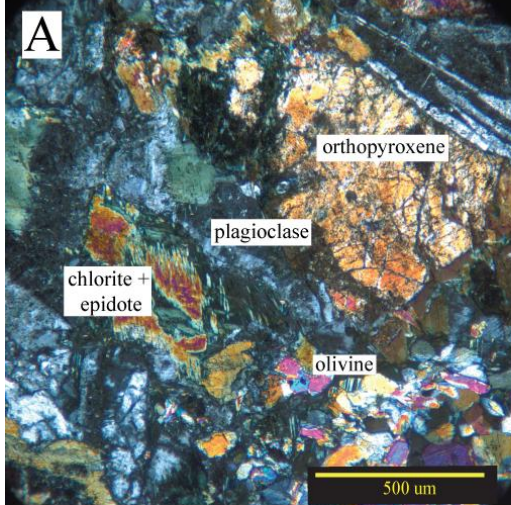
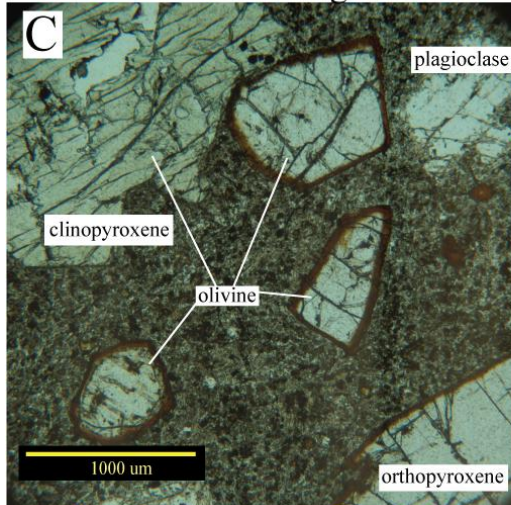


Figure 4

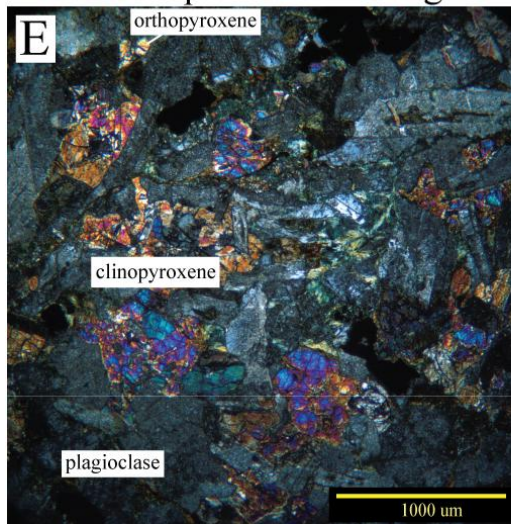
PNG03-188 Panapompom Is. gabbro



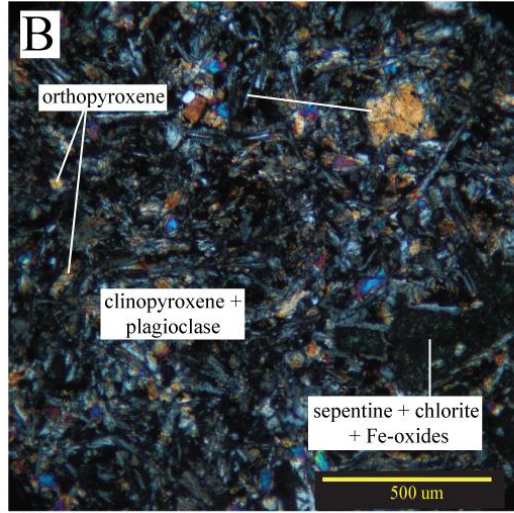
PNG03-117 Goodenough Is. Basalt



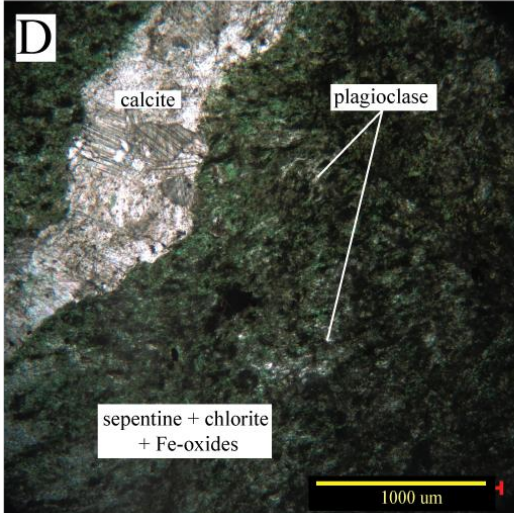
08P-002 Papuan Peninsula gabbro



PNG10-017 Woodlark Is. basalt



PNG03-058a Normanby Is. serp. ultramafics



08P-024 Dabi Volcanics

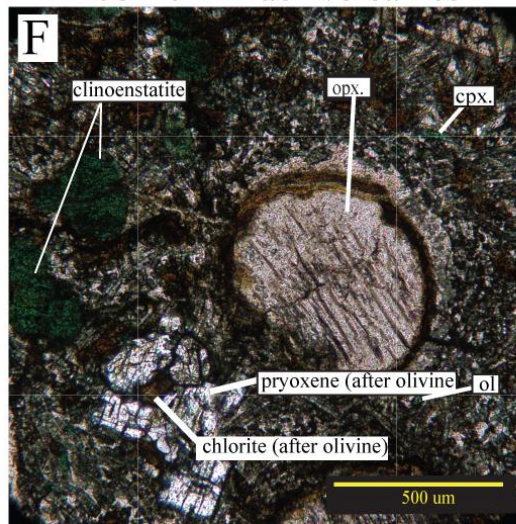


Figure 5.

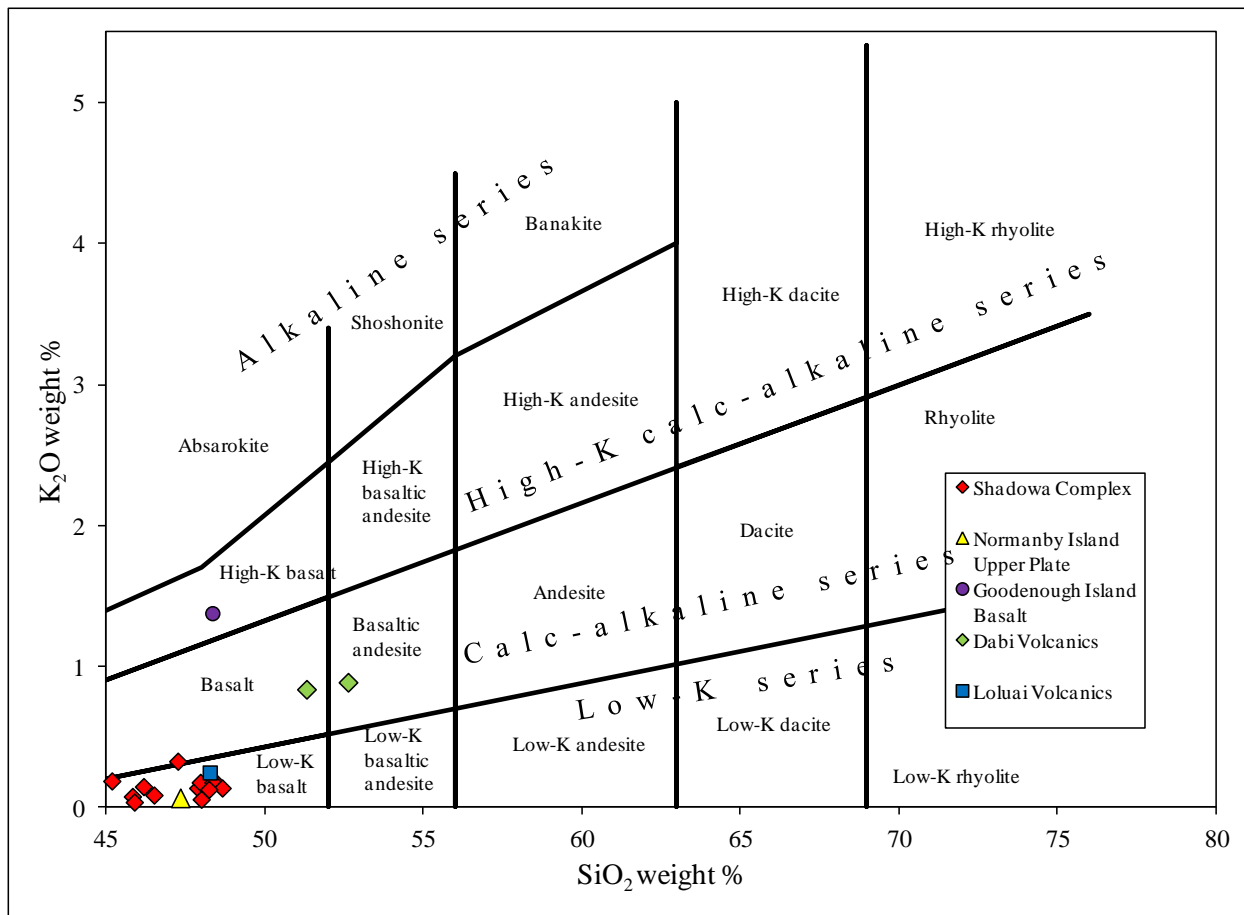


Figure 6.

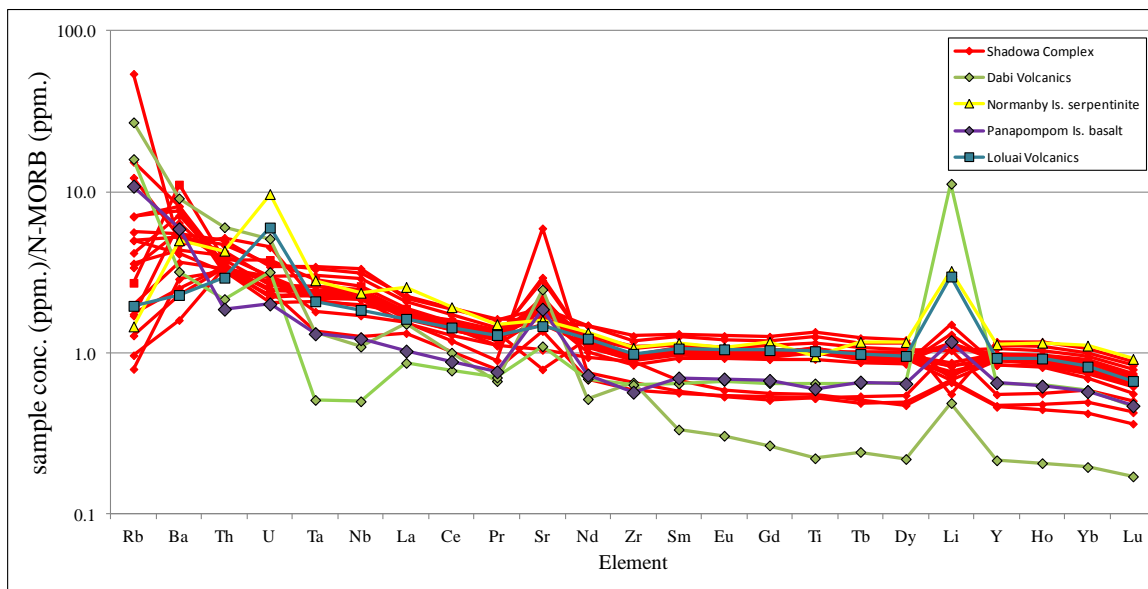


Figure 7.

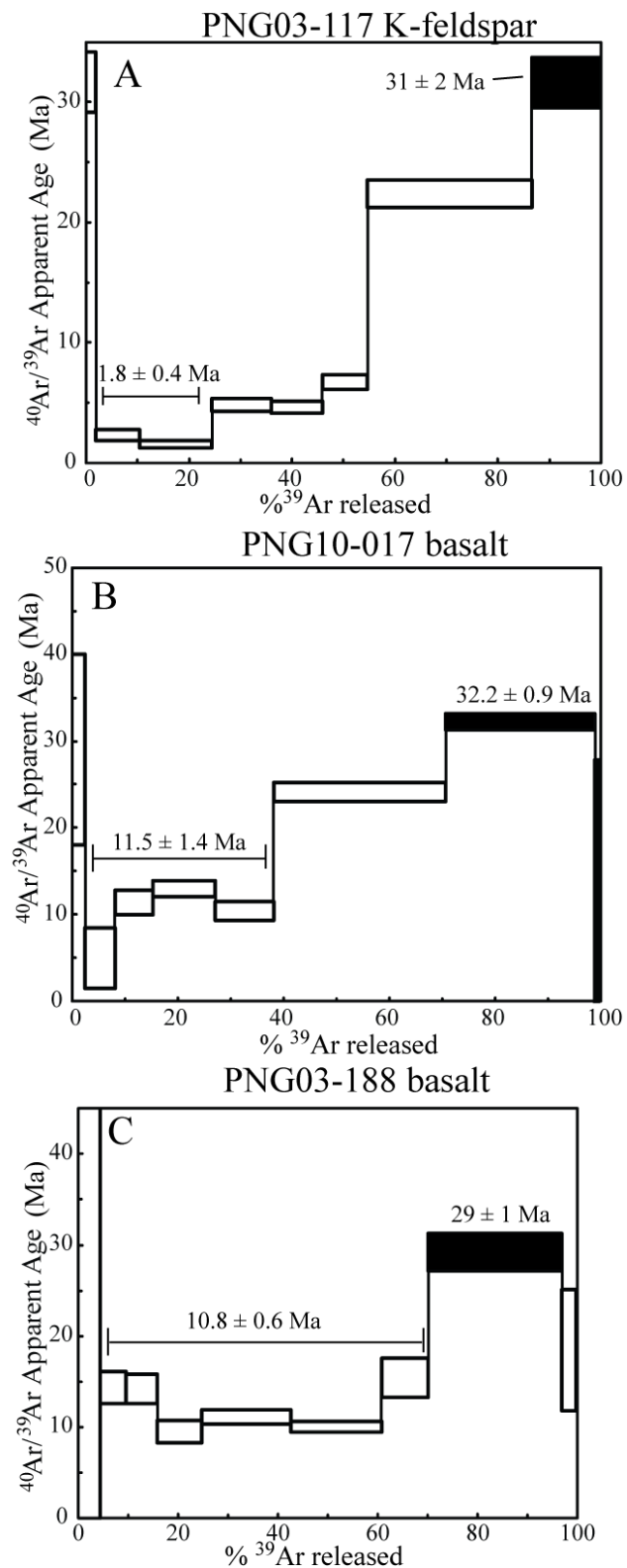


Figure 8.

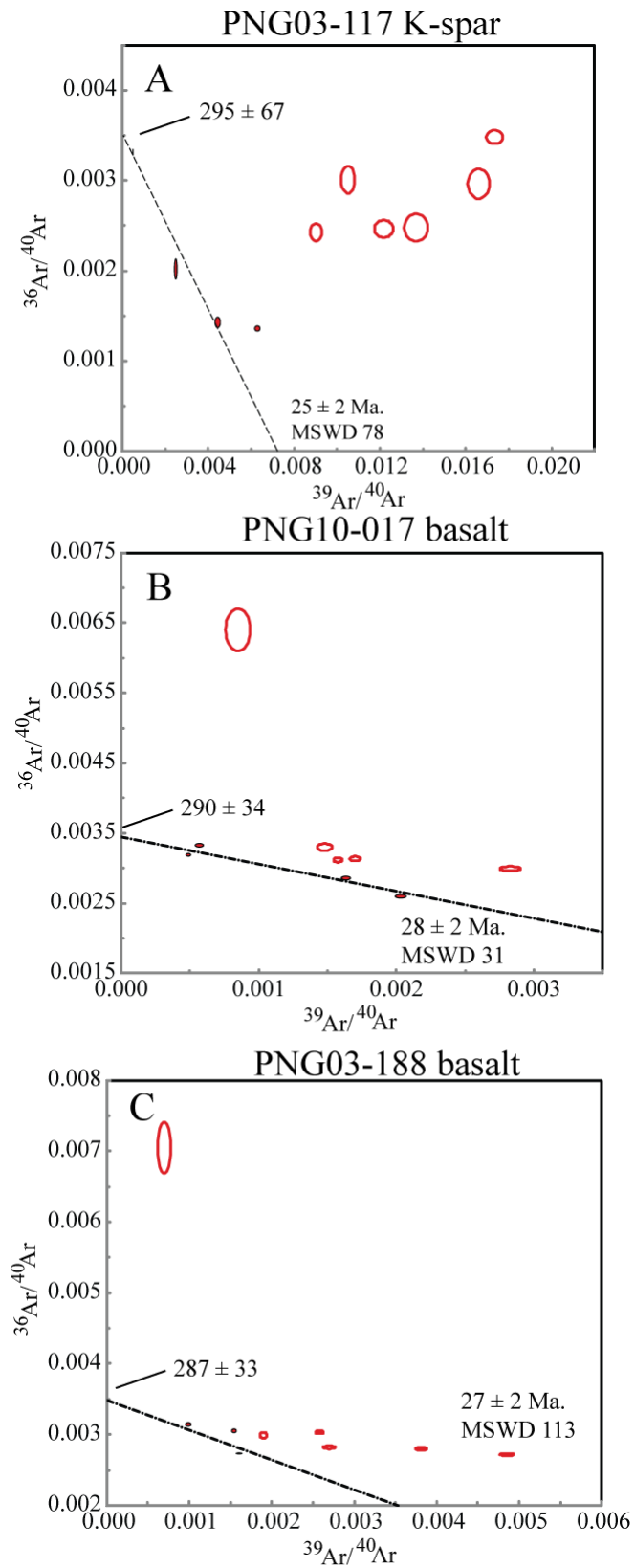


Figure 9.

Miocene Igneous Rocks in Eastern Papua New Guinea

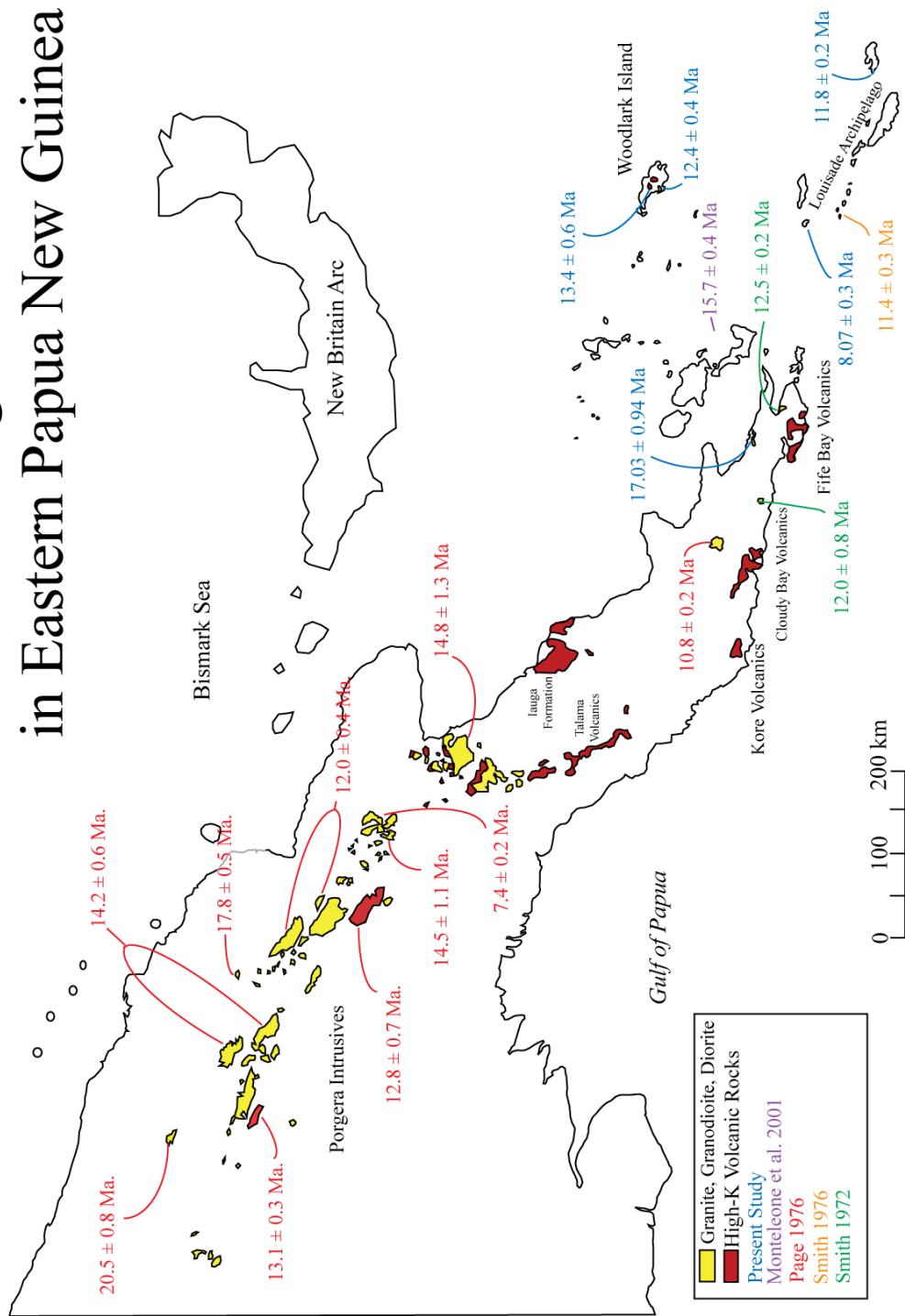


Figure 10.

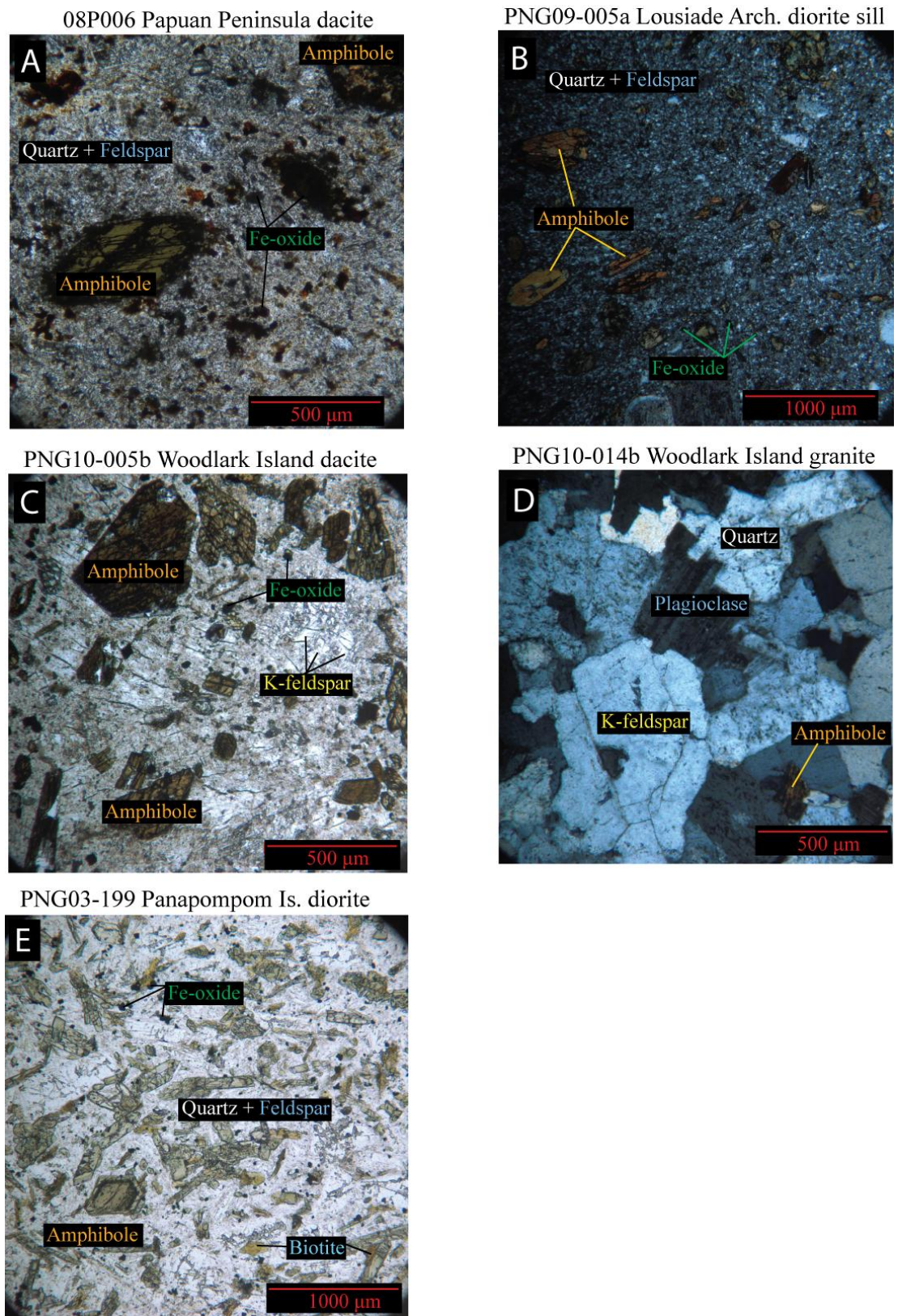


Figure 11.

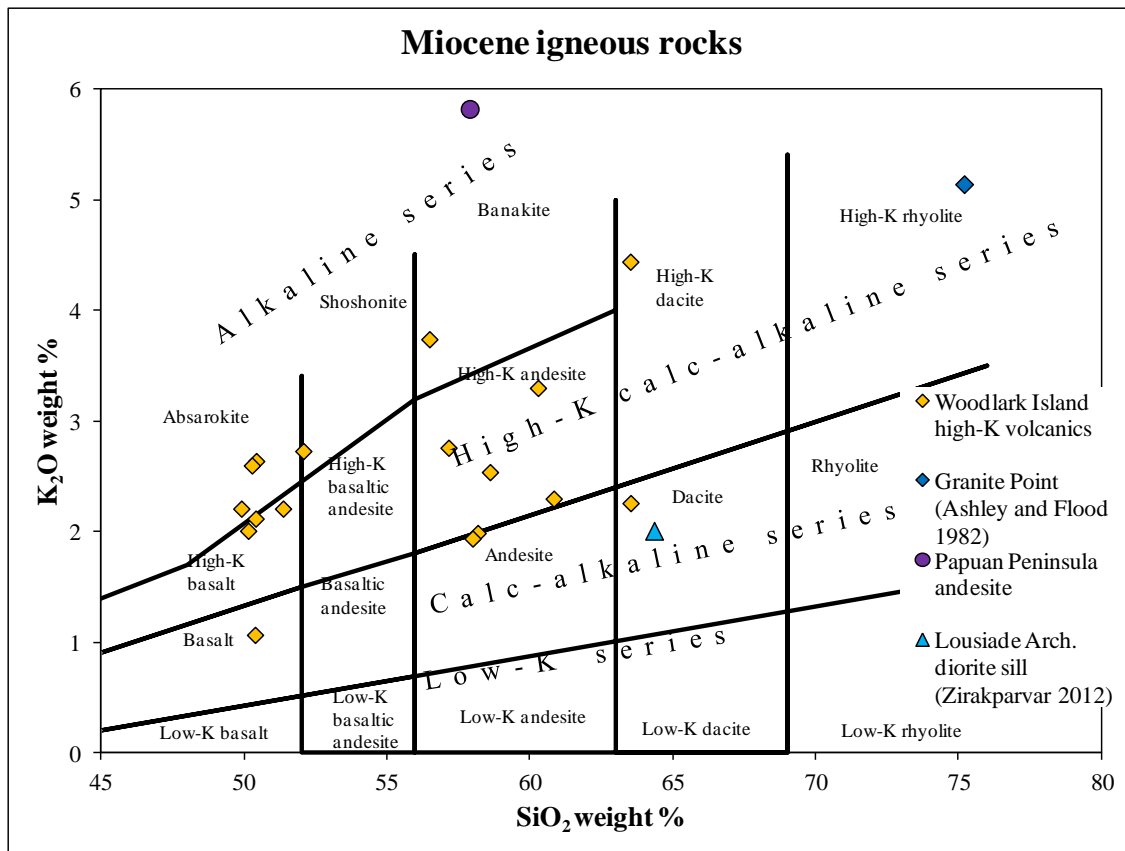


Figure 12.

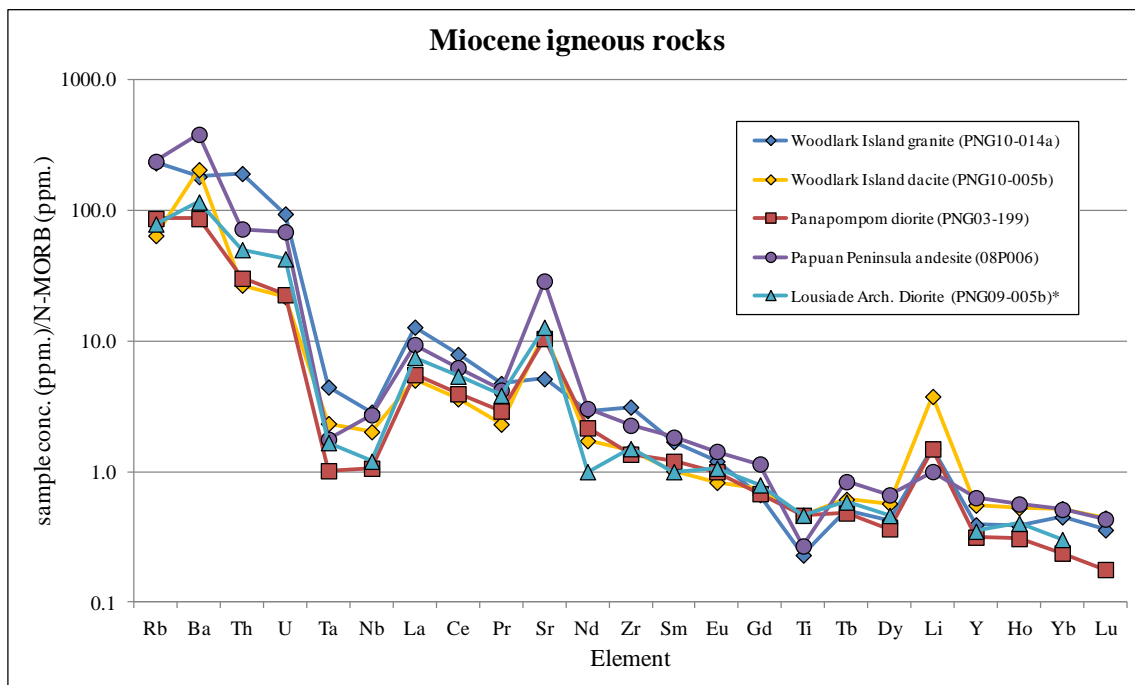


Figure 13.

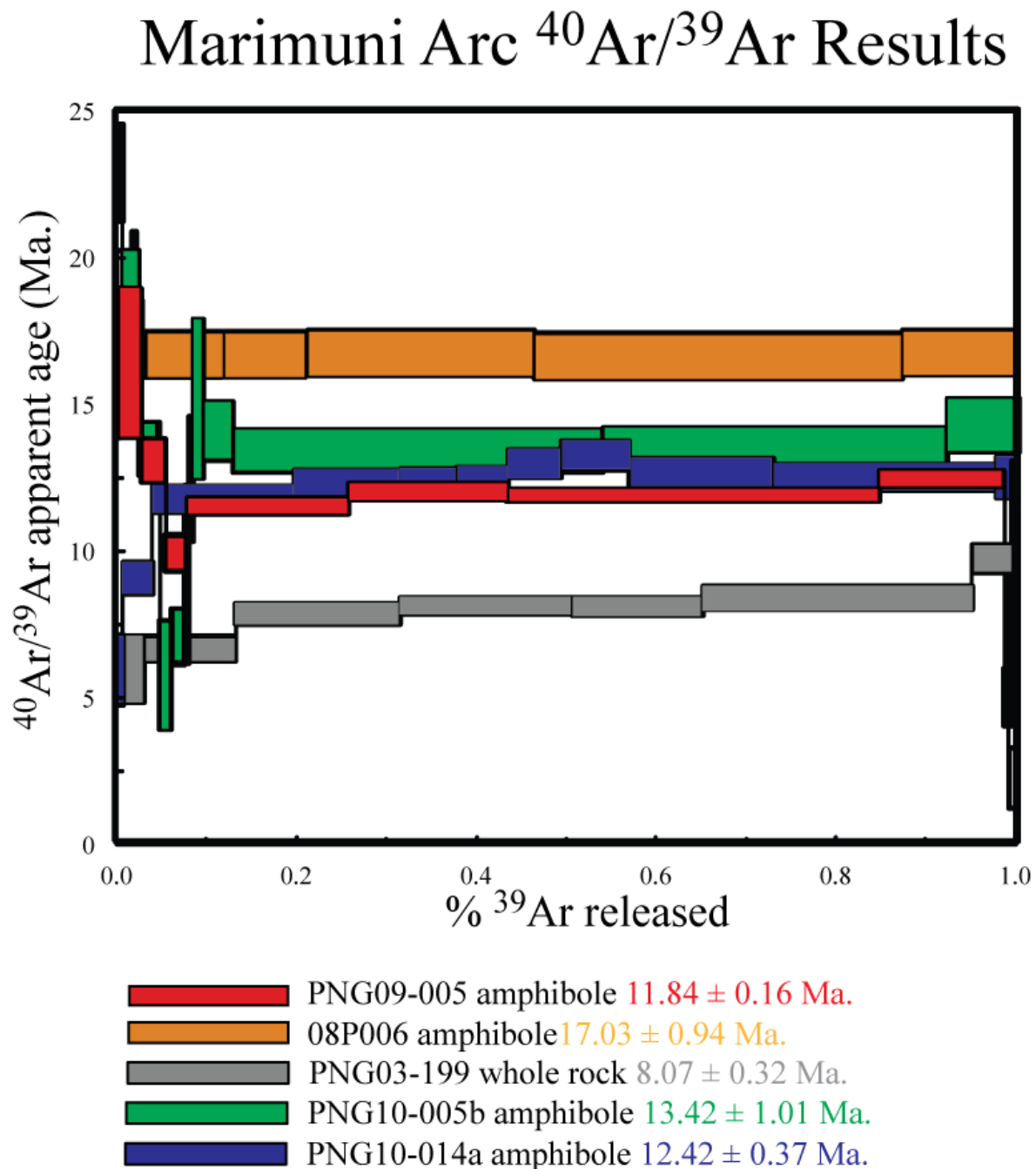


Figure 14.

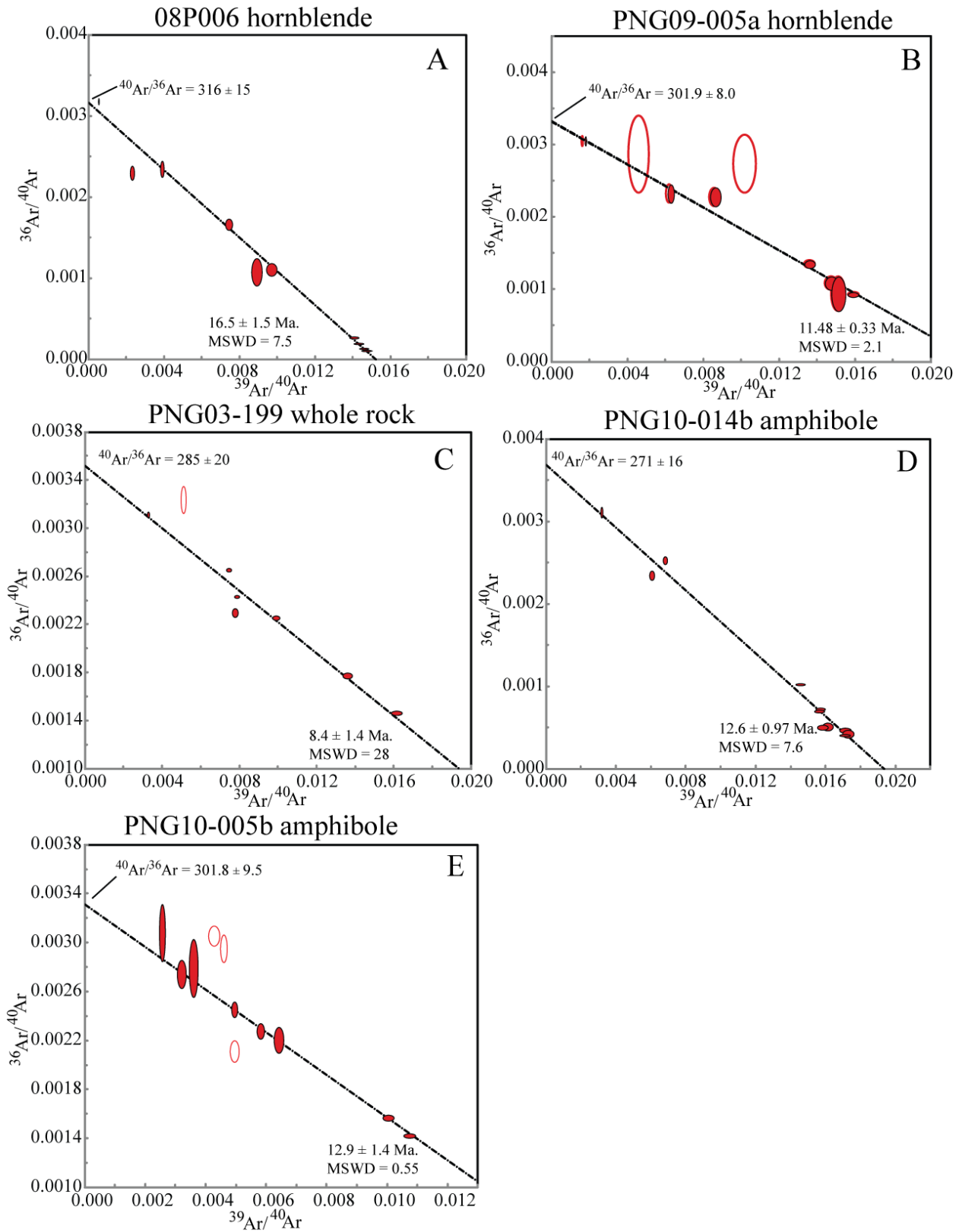


Figure 15.

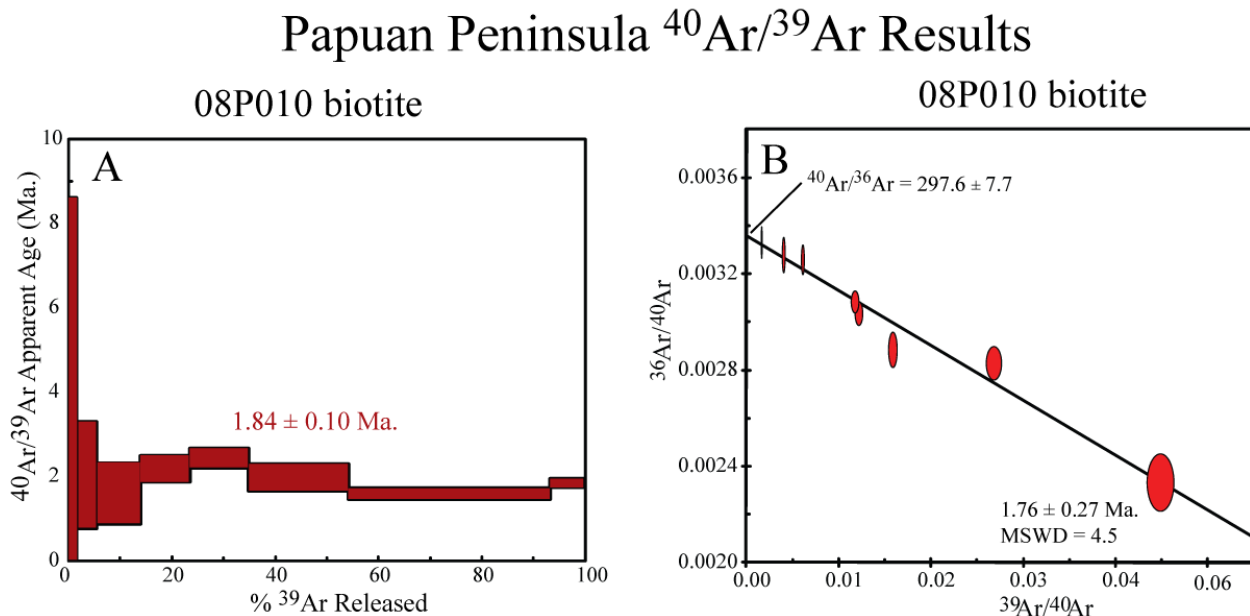


Figure 16.

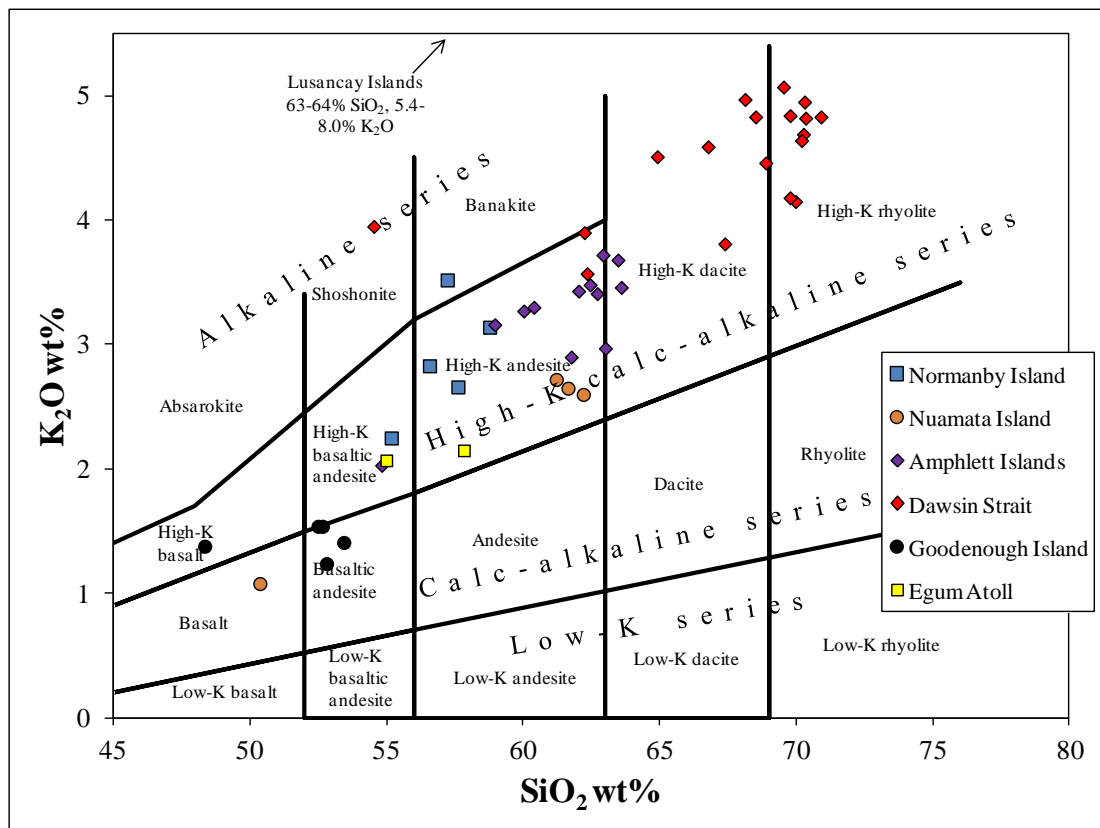


Figure 17.

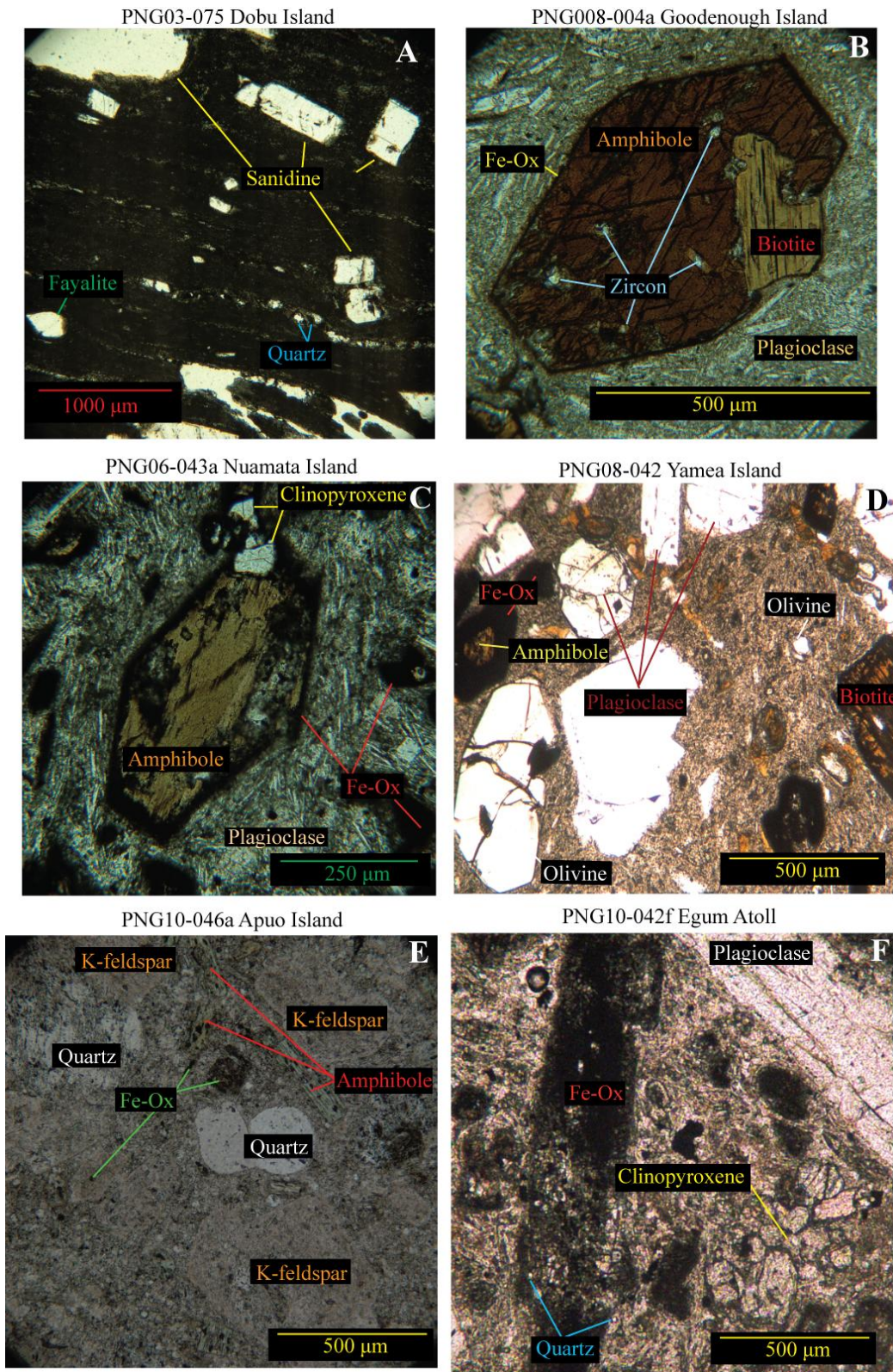


Figure 17 continued.

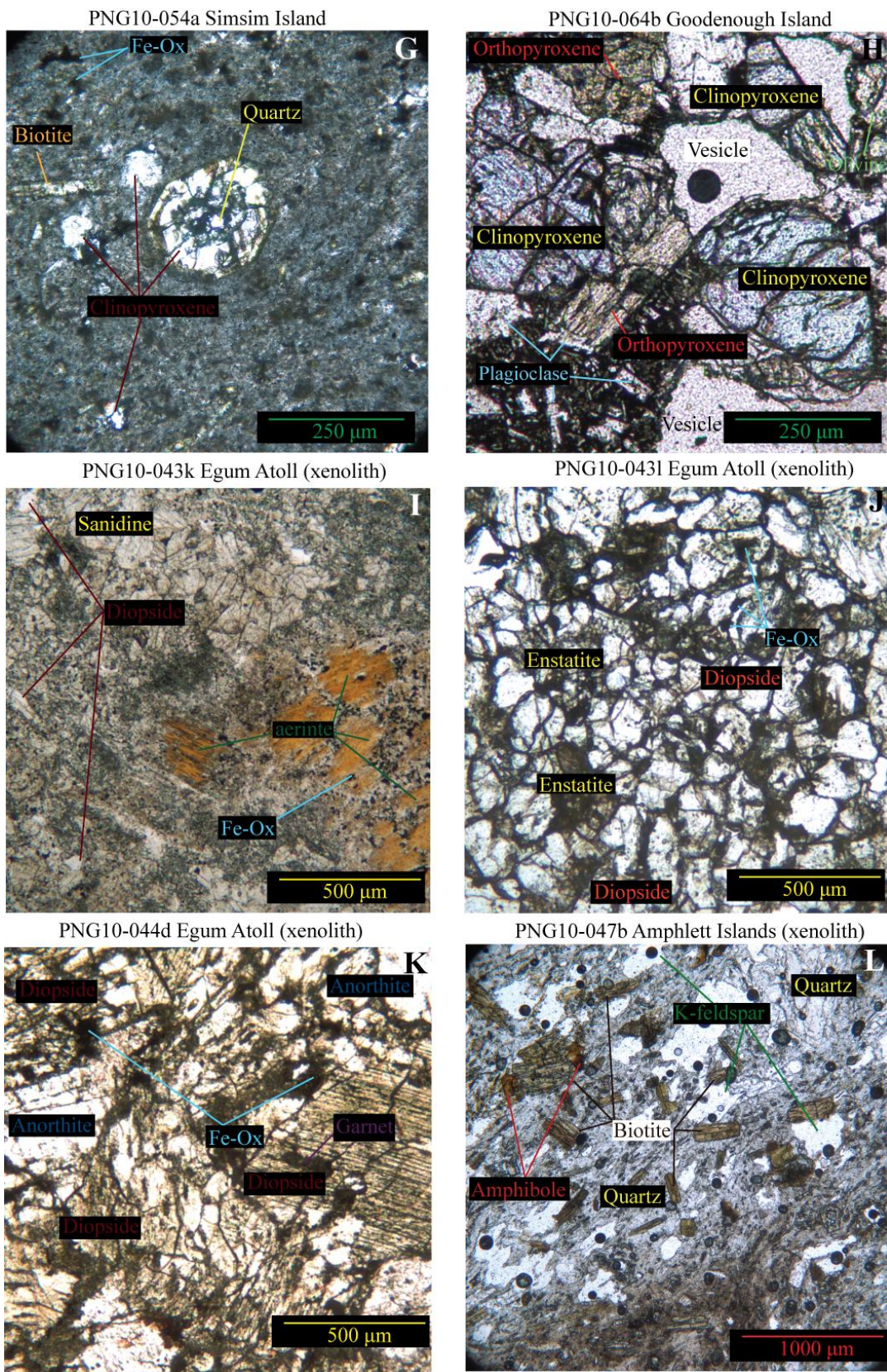


Figure 18.

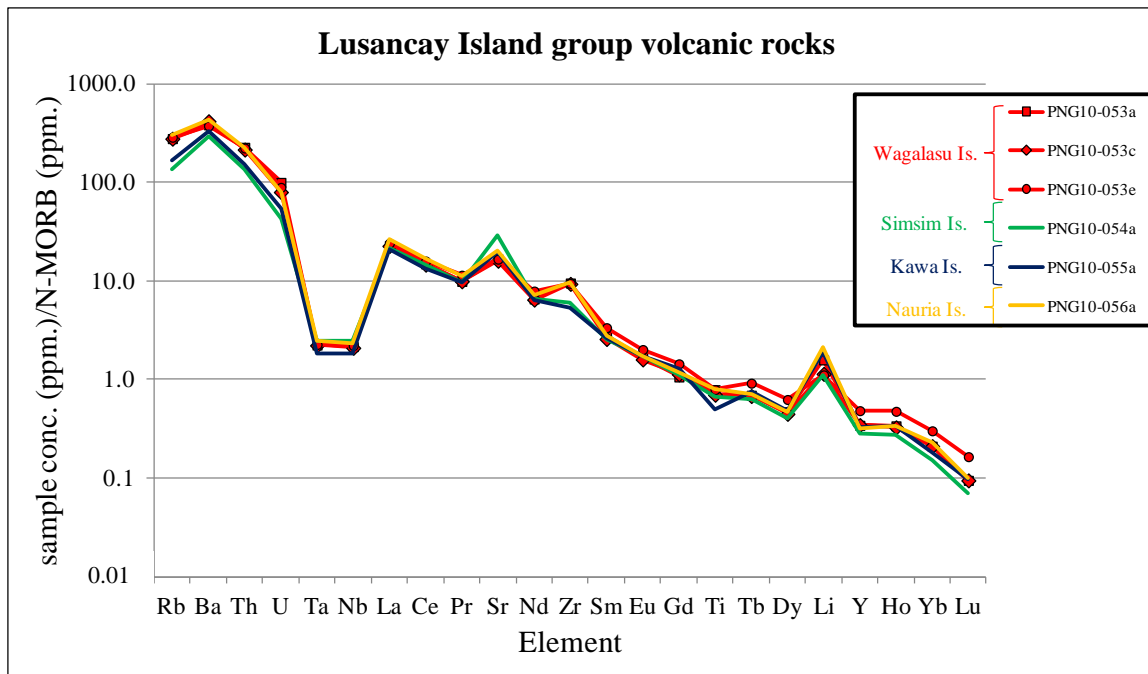


Figure 19.

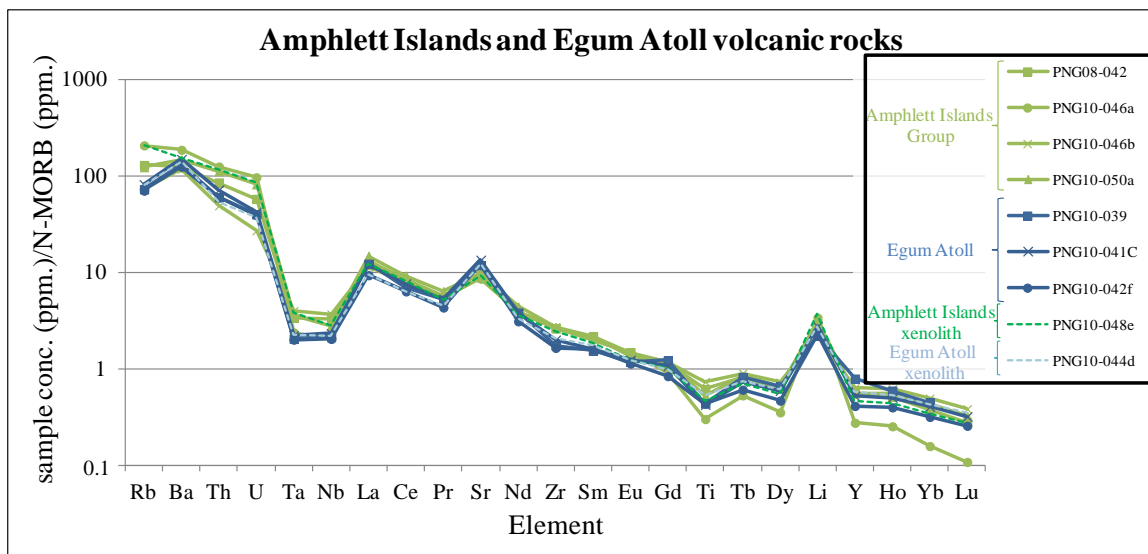


Figure 20.

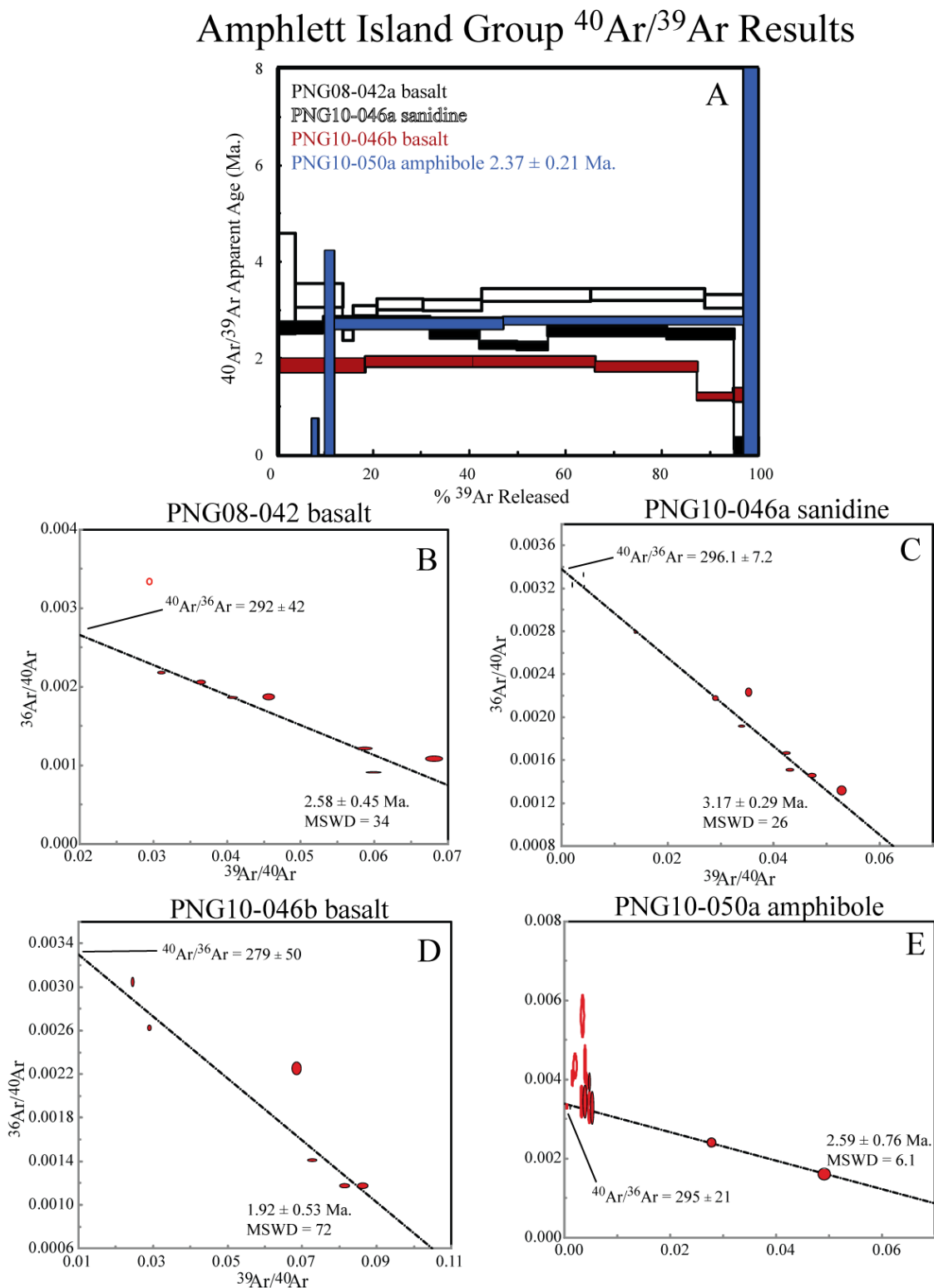


Figure 21.

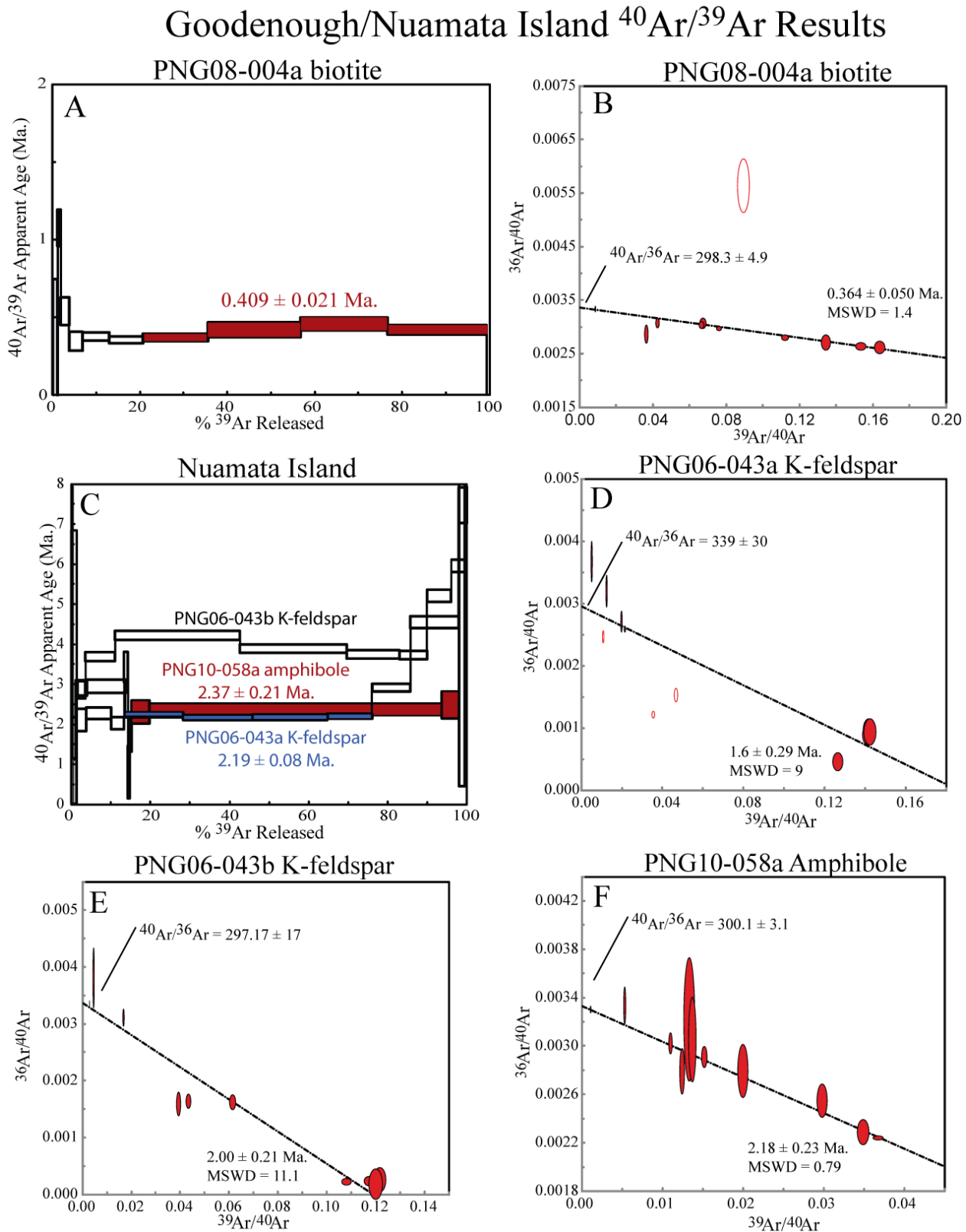


Figure 22.

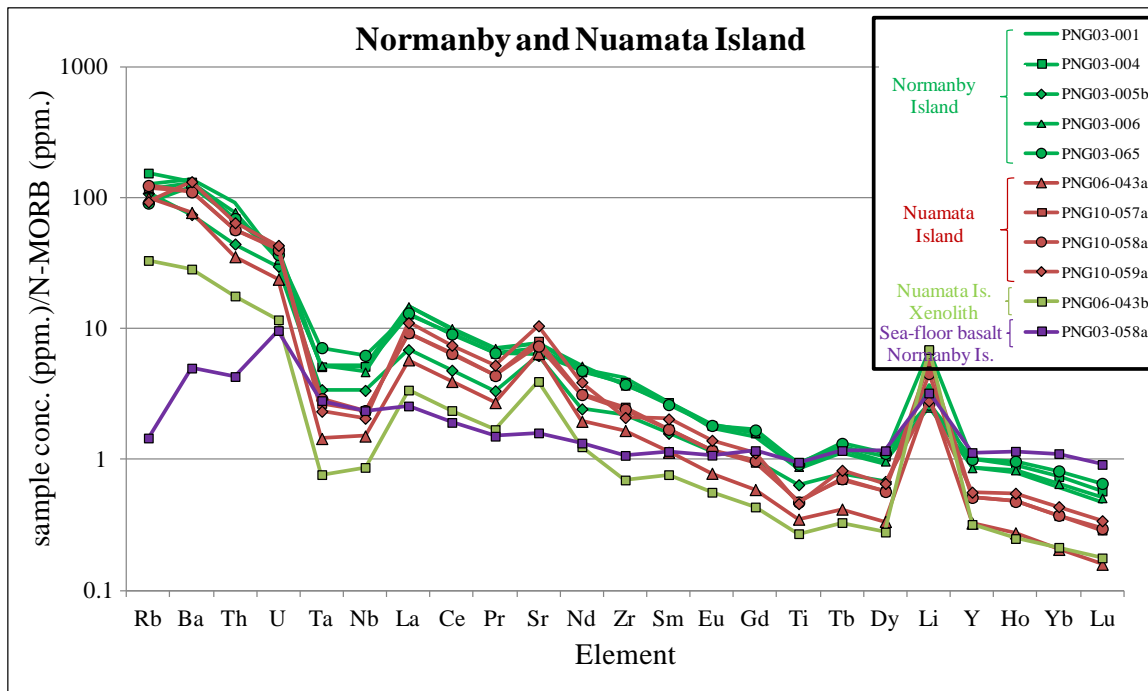


Figure 23.

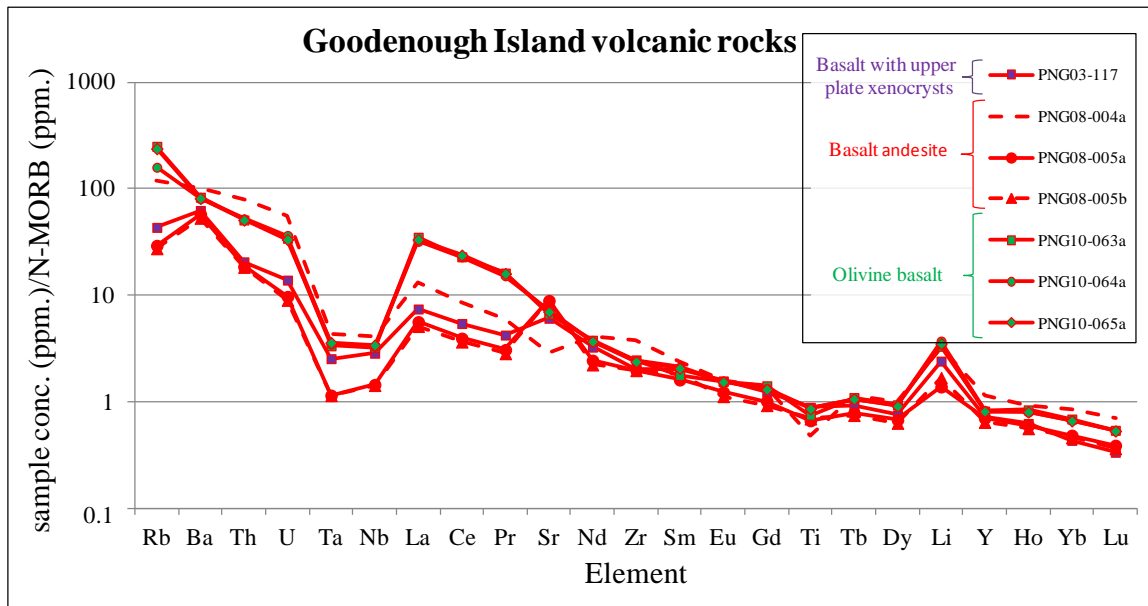


Figure 24.

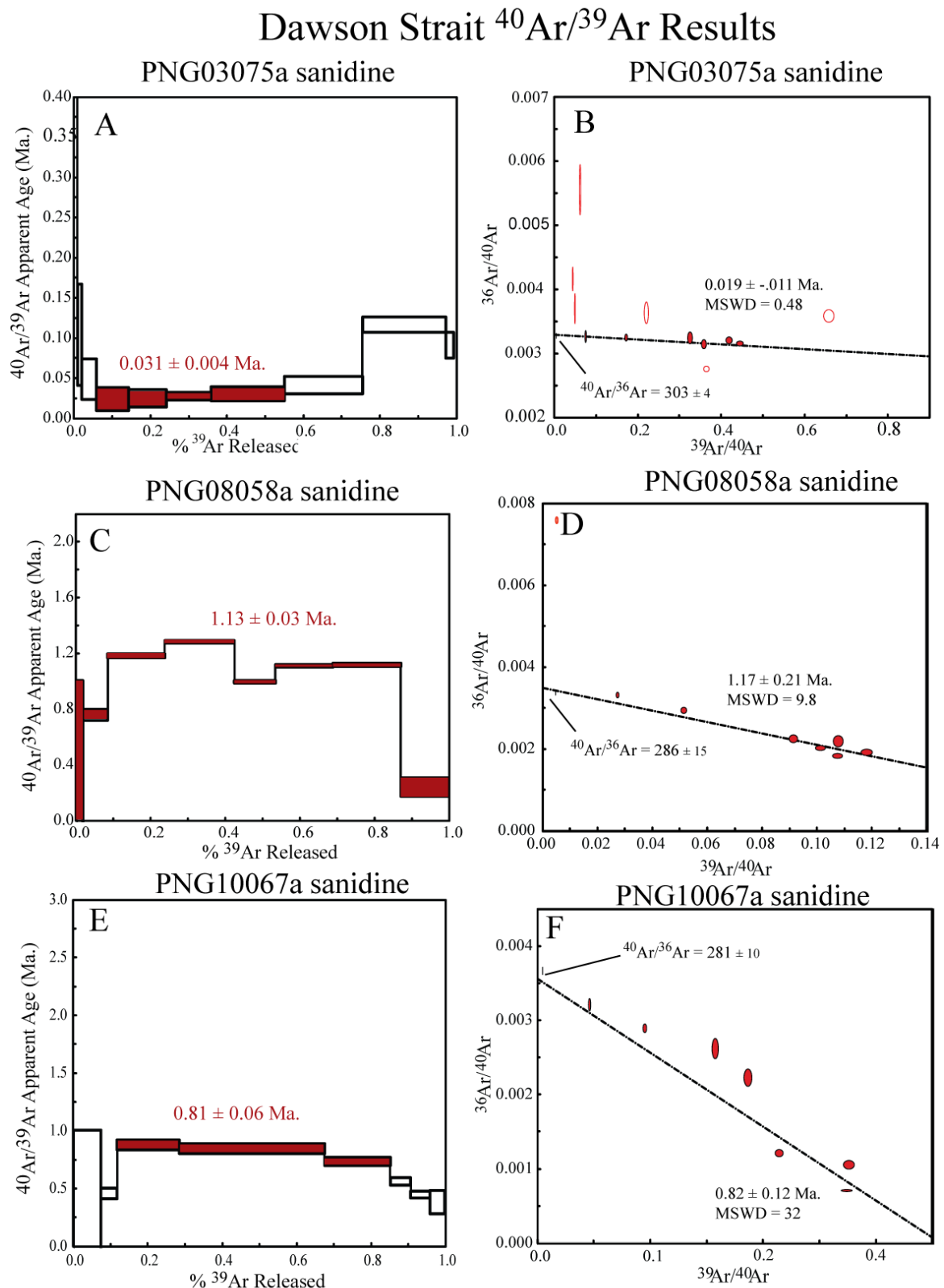


Figure 25.

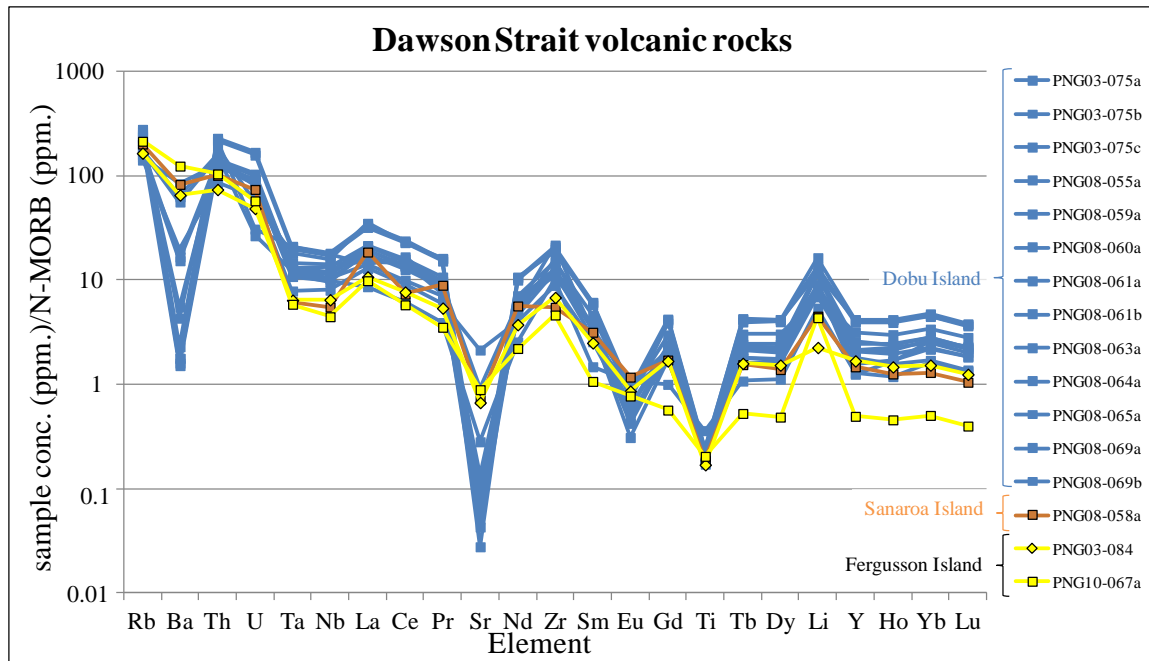


Figure 26.

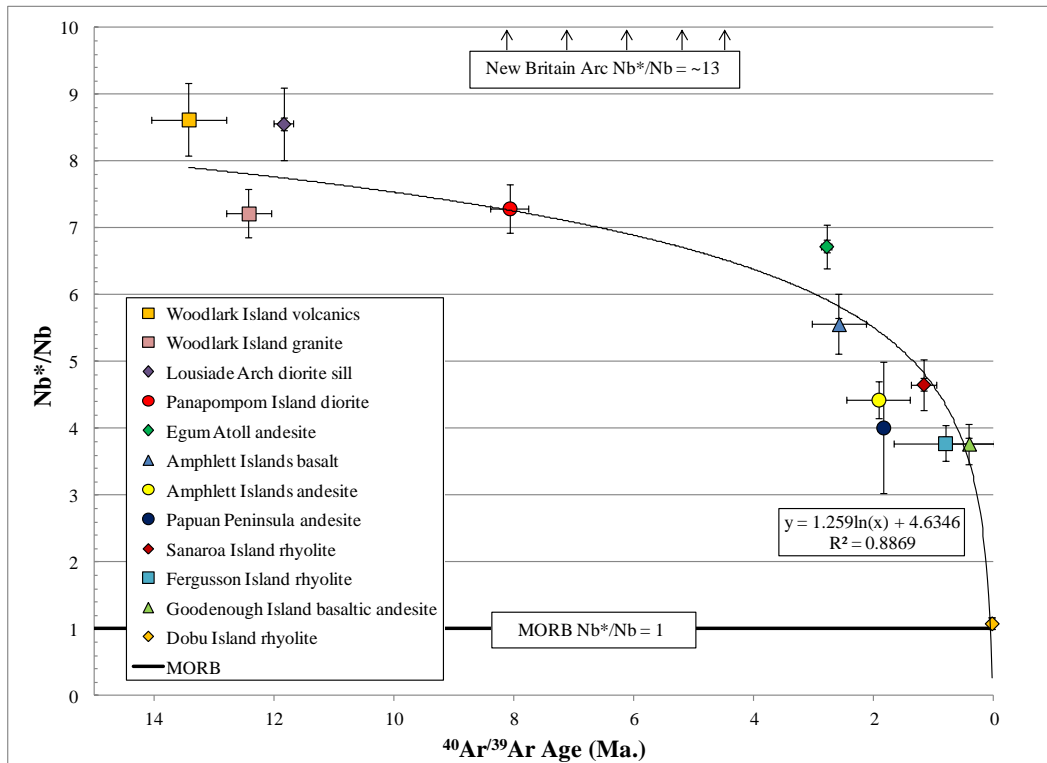


Figure 27.

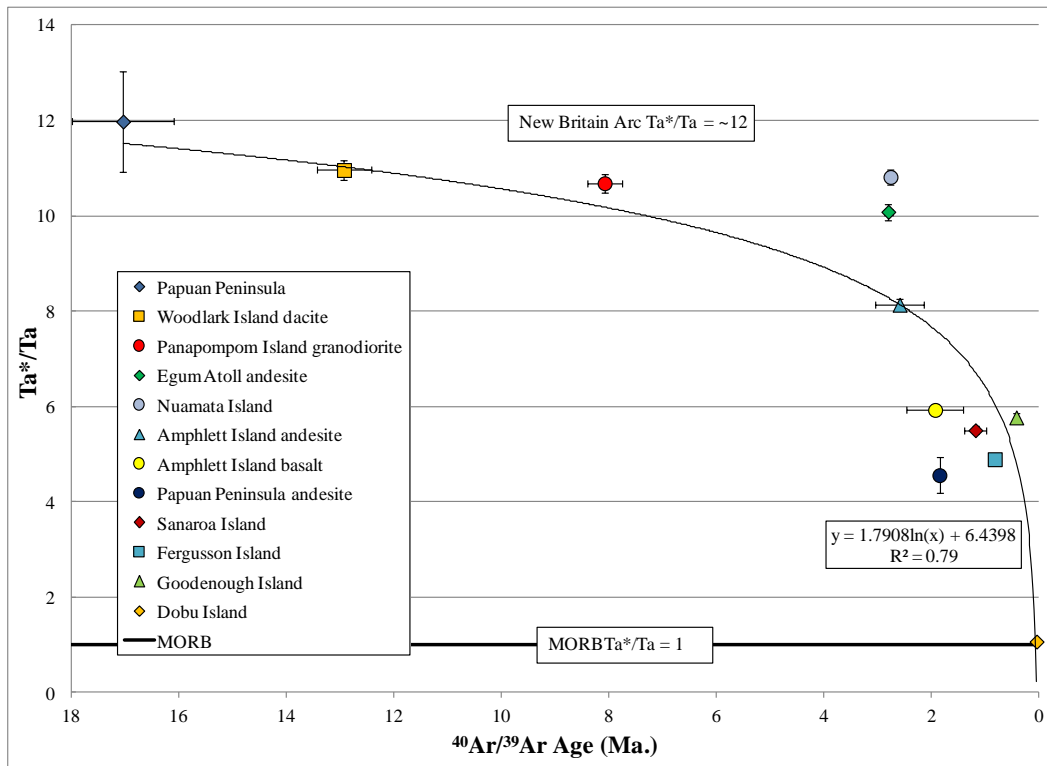


Table 1. Whole rock geochemical standard concentrations. (major element in wt%, trace elements in ppm)

	BIR-1	NIST-688	BCR-2	NIST-278	BHVO-2	Detection	Analytical
	Basalt	Basalt	Basalt	Rhyolite	Basalt	Limits	Precision
SiO ₂	47.84	48.79	54.09	72.61	49.93	0.01	0.006
TiO ₂	0.96	1.17	2.24	0.25	2.71	0.01	0.007
Al ₂ O ₃	15.4	17.38	13.57	14.26	13.82	0.01	0.02
FeO	10.2	9.28	12.1	1.84	11.11	0.04	0.01
MnO	0.17	0.16	0.19	0.05	0.17	0.01	
MgO	9.6	8.53	3.5	0.24	7.31	0.01	0.009
CaO	12.58	12.1	6.96	0.98	11.44	0.01	0.008
Na ₂ O	1.69	2.13	3.27	4.8	2.28	0.01	0.005
K ₂ O	0.03	0.19	1.72	4.15	0.53	0.01	0.01
P ₂ O ₅	0.04	0.14	0.35	0.03	0.27	0.01	0.02
Trace Element Concentrations (ppm.)							
Li	3.4	7	12	47	4.6	0.03	2.4
Be	0.58	0.7	1.6	1.9	1.1	0.001	1.6
Sc	43.8	37.3	32.8	4.96	31.5	0.1	6.4
V	317	242	415	9	320	0.02	9.5
Cr	382	331	14.2	5.9	293	0.003	4.1
Co	52	48.7	37	1.5	45.3	0.005	4.1
Ni	169	152	12.1	3.6	123	0.1	5.2
Cu	125	96	18	5.3	137	0.03	3.1
Zn	71	72	129.5	53	1.06	0.5	5.3
Ga	16	17	22	16.8	21.4	0.02	1.3
As	0.45	2.4	0.64	4.7	0.45	0.4	3.4
Rb	0.23	1.91	47.9	127.5	10.2	0.005	3
Sr	109	169	346	64	400	0.03	3.1
Y	16.2	18.4	37.7	39	27.2	0.002	3.4
Zr	15.5	58	188	288	176	0.01	2.6
Nb	0.55	5.5	14	18	18.8	0.007	3.8
Mo	0.054	0.41	1.7	3.2	3	0.006	3.1
Sn	0.65	1.66	2.7	4.16	2.05	0.003	3.5
Sb	0.54	0.29	0.61	1.7	0.16	0.0009	1.2
Cs	0.005	0.23	0.96	5.2	0.1	0.0003	2.7
Ba	7	181	675	918	135	0.02	3.9
La	0.61	5.21	24.9	31.4	15.6	0.0004	2.5
Ce	1.99	12.2	53.7	62	38.6	0.002	3.2
Pr	0.39	1.89	6.8	7.06	5.5	0.0002	2.1
Nd	2.5	8.8	28.4	27.6	25.1	0.001	2.4
Sm	1.11	2.6	6.63	5.72	6.27	0.0003	4.1
Eu	0.53	0.99	1.95	0.78	2.07	0.0002	3.9
Gd	1.9	2.96	6.68	5.3	6.4	0.0004	1.7
Tb	0.37	0.49	1.06	1.02	0.954	0.0001	2.2
Dy	2.48	3.3	6.34	6.29	5.36	0.0005	3.6
Ho	0.57	0.74	1.28	1.31	1.03	0.0001	3.1
Er	1.7	2.07	3.63	3.97	2.5	0.0002	2.2
Tm	0.26	0.3	0.557	0.64	0.335	0.0001	2.7
Yb	1.66	2.06	3.39	4.46	2.02	0.0004	1.4
Lu	0.259	0.325	0.509	0.71	0.29	0.0001	2.4
Hf	0.59	1.56	4.88	8.1	4.4	0.002	1.6
Ta	0.039	0.3	0.79	1.26	1.22	0.003	1
Pb	3	3.26	11	16.4	2.5	0.001	1.8
Th	0.03	0.32	5.99	12.4	1.1	0.0006	0.9
U	0.01	0.32	1.73	4.58	0.426	0.0002	0.7

Table 2. Summary of geochronologic ages for Pliocene to active volcanic rocks in Eastern Papua New Guinea.

Pliocene - active volcanism in Eastern Papua				
Location	Age	Rock Type	Reference	Comments
Mt. Lamington	historically active volcano	basalt - andesite	Johnson et al. 1978	last known eruption 1951
Waiowa	historically active volcano	basalt - andesite	Johnson et al. 1978	last known eruption 1943-44
Mt. Victory	historically active volcano	basalt - andesite	Johnson et al. 1978	last known eruption 1890s
Fergusson Island	1.01 -0.4 Ma.	rhyolite	Smtih and Compston 1982, Baldwin et al. 1993	K-Ar, $^{40}\text{Ar}/^{39}\text{Ar}$ - whole rock
Normanby Island	1.7 - 2.6 Ma.	andesite/ granodiorite	Monteleone 2007	$^{40}\text{Ar}/^{39}\text{Ar}$ - K-feldspar, biotite, hornblende
Liusancay Islands	2.79 , 2.3 - 1.02 Ma.	dacite	Present study , Smith 1976	$^{40}\text{Ar}/^{39}\text{Ar}$ - clinopyroxene, K-Ar - whole rock
Amphlett Islands	3.8 Ma.	andesite	Smith 1976	K-Ar - whole rock
Egum Atoll	2.92 , 2.9 Ma.	andesite	Present study , Smith 1976	$^{40}\text{Ar}/^{39}\text{Ar}$ - clinopyroxene, K-Ar - whole rock
Managalase Plateau	5.5 - 0.08 Ma.	high K basalt - dacite	Ruxton 1999	$^{40}\text{Ar}/^{39}\text{Ar}$ - whole rock

Appendix 1. Sample locations and descriptions.

<u>Sample:</u>	<u>Location:</u>	<u>Rock Type:</u>		
PNG03075C	Dobu Island (Z 56 - 8922462N, 265417E)	High-K Rhyolite		
<u>Hand Sample Description:</u>				
Flow banded rhyolite with small (< 1 mm) phenocrysts of feldspar				
<u>Mineralogy:</u>	<u>Properties:</u>			
Plagioclase	90° Cleavages. 1 st order birefringence. Albite twinning			
Sanidine/Anorthoclase	90° Cleavages. 1 st order birefringence Grid twinning (albite and pericline) characteristic of anorthoclase. Carlsbad twinning is more characteristic of sanidines.			
Olivine	Deep green pleochroism –Fayolitic?, No cleavages, high 2 nd order pink/yellow interferences.			
Oxides	Opaque isotropic minerals			
Apatite	High relief mineral with 1 st order interference colors. Inclusions in feldspars.			
<u>Structural and Textural Observations:</u>				
-Groundmass is comprised of feldspars, but they are not microlites like in the mafic rocks.				
-oxides comprise a higher amount of this sample and it appears to be slightly altered.				

<u>Sample:</u> PNG03117	<u>Location:</u> SE Goodenough Island (Z 56 - 8950195N, 200566E)	<u>Rock Type:</u> Basaltic Andesite
<u>Hand Sample Description:</u> Mafic rock with ~20% crystals, there are visible phenocrysts of feldspar and black augite.		
<u>Mineralogy:</u>	<u>Properties:</u>	
Olivine	Colorless to pale green pleochroism, No cleavages, high 2 nd order pink/yellow interferences.	
Clinopyroxene	Non-pleochroic. High 1 st to low 2 nd order interference colors.	
Plagioclase	90° cleavages, low 1 st order interference colors, colorless in plain light, albite twinning	
Oxides	Isotropic minerals in groundmass	
<u>Structural and Textural Observations:</u> -Feldspar microlites seem to flow around olivine/pyroxene phenocrysts. -Pyroxene phenocrysts seem to have no reaction rim. -Olivines are zoned with more Mg rich cores and altered rims. -There appear to be two generations of feldspar		

<u>Sample:</u> PNG03-188	<u>Location:</u> Panapompom Island (10°46'28"S, 152°22'44"E)	<u>Rock Type:</u> Altered Basalt
<u>Hand Sample Description:</u> Phenocrysts of plagioclase (~0.5 mm) and clinopyroxene (~1 mm) in a dark grey groundmass.		
<u>Mineralogy:</u>	<u>Properties:</u>	
Clinopyroxene	Non-pleochroic. High 1 st to low 2 nd order interference colors.	
Orthopyroxene	1 st order yellow, euhedral grains, octahedral crystals, parallel extinction	
Chlorite	Colorless-pale green pleochroism. Anomalously low interference colors.	
Plagioclase	90° cleavages, low 1 st order interference colors, colorless in plain light, albite twinning	
Fe-Oxides	Isotropic	
Apatite	High relief mineral with 1 st order interference colors.	
<u>Structural and Textural Observations:</u> -clinopyroxene and orthopyroxene are being replaced by chlorite -mineralogy and composition is similar to basalts on the Papuan Peninsula and Woodlark Island		

<u>Sample:</u> PNG03-199	<u>Location:</u> Panapompom Island (10°46'28"S, 152°22'44"E)	<u>Rock Type:</u> Diorite
<u>Hand Sample Description:</u> Phenocrysts of amphibole (~1 mm) and plagioclase (~0.5 mm) in dark grey matrix.		
<u>Mineralogy:</u>	<u>Properties:</u>	
Amphibole	56-120 cleavage, pale green brown pleochroism, low 2 nd order birefringence	
Plagioclase	90° cleavages, low 1 st order interference colors, colorless in plain light, albite twinning	
Quartz	No cleavages and undulatory extinction.	
Biotite	Brown pleochroism, one perfect cleavage. Extinction parallel to cleavage	
Fe-oxides	Isotropic minerals	
Apatite	Small, high relief mineral in the groundmass	
<u>Structural and Textural Observations:</u> -Minerals are euhedral with grain boundaries that do not appear to be reacted with the magma.		

<u>Sample:</u> PNG06043A	<u>Location:</u> Nuamata Island (Z 56 - 8984744N, 192257E)	<u>Rock Type:</u> Andesite
<u>Hand Sample Description:</u> Andesite with fine grained, grey groundmass and phenocrysts of amphibole (~1 mm).		
<u>Mineralogy:</u>	<u>Properties:</u>	
Hornblende	56-120 cleavage, pale green brown pleochroism, low 2 nd order birefringence	
Plagioclase/Sanidine	Low birefringent microlites in the groundmass. albite twinning.	
Biotite	Brown pleochroism, one perfect cleavage. Extinction parallel to cleavage	
Quartz	No cleavages and undulatory extinction.	
Apatite	Fine grained high relief mineral in the groundmass	
Oxides	Isotropic	
Pyroxene	Pale green pleochroism. High 1 st to low 2 nd order interference colors.	
<u>Structural and Textural Observations:</u> - Biotite and hornblende have a thick cloudy oxide rim and sometimes completely replaced, it is likely that they were in disequilibrium with the magma at the time of eruption -Feldspar microlites in the groundmass are flowing around larger hornblende phenocrysts.		

<u>Sample:</u> PNG06043B	<u>Location:</u> Nuamata Island (Z 56 - 8984744N, 192257E)	<u>Rock Type:</u> Amphibolite Xenolith
<u>Hand Sample Description:</u> Coarse grained with crystals of amphibole, biotite, quartz, and feldspar		
<u>Mineralogy:</u>	<u>Properties:</u>	
Biotite	Brown pleochroism, one perfect cleavage. Extinction parallel to cleavage	
Hornblende	56-120 cleavage, pale green brown pleochroism, low 2 nd order birefringence	
Mica	Non-pleochroic mineral in between biotite and hornblende grains with high birefringence.	
Plagioclase	90° cleavages, low 1 st order interference colors, colorless in plain light, albite twinning	
Quartz	No cleavages and undulatory extinction. Only sample where quartz is not interstitial.	
Oxides	Isotropic	
Zircon	Highly birefringent inclusions in biotite with radiation halos	
<u>Structural and Textural Observations:</u> -100% crystallinity - this xenolith is a plutonic igneous rock. -Hornblende, biotite, and mica grains are all intergrown and appear to be altered. -large quartz grains		

<u>Sample:</u> PNG08004A	<u>Location:</u> Wagifa Island (Z 56 – 8939288N, 212420E)	<u>Rock Type:</u> Andesite
<u>Hand Sample Description:</u> Visible phenocrysts of biotite (~0.25 mm), amphibole (~0.5 mm), and feldspar (~0.1 mm) in a fine grained groundmass.		
<u>Mineralogy:</u>	<u>Properties:</u>	
Biotite	Brown pleochroism, one perfect cleavage. Extinction parallel to cleavage	
Hornblende	56-120 cleavage, pale green brown pleochroism, low 2 nd order birefringence	
Sanidine/Plagioclase	Low birefringent microlites in the groundmass. albite twinning.	
Zircon	Highly birefringent inclusions in amphibole.	
Oxides	Isotropic	
<u>Structural and Textural Observations:</u> - Amphibole and Biotite have an isotropic rim of oxide - Feldspar microlites are flowing around the hornblende phenocrysts - Zircon occurs as inclusions in the amphibole.		

<u>Sample:</u> PNG09-005A	<u>Location:</u> Louisiade Archipelago (152°35'63"S, 11°7'33"E)	<u>Rock Type:</u> Diorite
<u>Hand Sample Description:</u> Phenocrysts of amphibole (~1 mm) and plagioclase (~0.5 mm) in light grey matrix.		
<u>Mineralogy:</u>	<u>Properties:</u>	
Hornblende	56-120 cleavage, pale green brown pleochroism, low 2 nd order birefringence	
K-Feldspar	90° Cleavages. 1 st order birefringence. Grid twinning.	
Oxide	Isotropic	
Apatite	Small, high relief mineral in the groundmass	
Zircon	High birefringent, high relief, occurs as inclusions	
<u>Structural and Textural Observations:</u> -Zircon occurs as inclusions in larger amphibole phenocrysts -Phenocrysts are euhedral		

<u>Sample:</u> PNG08042A	<u>Location:</u> Yabwaia Island (Z 56, 257987E, 8971252N)	<u>Rock Type:</u> Basalt
<u>Hand Sample Description:</u> Visible phenocrysts of plagioclase and small olivine (<0.5 mm) in a glassy, black groundmass.		
<u>Mineralogy:</u>	<u>Properties:</u>	
Plagioclase	90° cleavages, low 1 st order interference colors, colorless in plain light, albite twinning	
Orthopyroxene	1 st order yellow, euhedral grains, octahedral crystals, parallel extinction	
Olivine	Pale green pleochroism, No cleavages, high 2 nd order pink/yellow interferences.	
Zircon	Highly birefringent inclusions in orthopyroxene.	
Apatite	High relief mineral with 1 st order interference colors. Inclusions in olivine and orthopyroxene.	
Oxides	Isotropic	
<u>Structural and Textural Observations:</u> -Feldspars have oscillatory zoning -Microlites in the groundmass are aligned with flow -Fine grained oxide rim around olivine		

<u>Sample:</u> PNG08-058A	<u>Location:</u> Sanaroa Island (9°37'48"S, 150°59'25"E)	<u>Rock Type:</u> Rhyolite
<u>Hand Sample Description:</u> Flow-banded rhyolite with vesicles (~2-3 mm) and visible crystals of sanidine		
<u>Mineralogy:</u>	<u>Properties:</u>	
Sanidine/Anorthoclase	90° Cleavages. 1 st order birefringence. Grid twinning (albite and pericline) characteristic of anorthoclase. Carlsbad twinning is more characteristic of sanidines.	
Plagioclase	90° Cleavages. 1 st order birefringence. Albite twinning	
Olivine	Deep green pleochroism –Fayolitic?, No cleavages, high 2 nd order pink/yellow interferences.	
Quartz	Fine grained intestinal material in bands with undulatory extinction.	
Oxides	Isotropic.	
Hornblende	56-120 cleavage, pale green brown pleochroism, low 2 nd order birefringence	
<u>Structural and Textural Observations:</u> -Plagioclase and Sanidine and variably altered -Hornblendes and olivines are rare and resorbed in groundmass -Oxide minerals are rare		

<u>Sample:</u> 08P001	<u>Location:</u> Papuan Peninsula (10.30.,35S, 150.76.050E)	<u>Rock Type:</u> Altered Basalt
--------------------------	---	-------------------------------------

Hand Sample Description:

-green-black groundmass with small irregular crystals of plagioclase

<u>Mineralogy:</u>	<u>Properties:</u>
Olivine	No pleochroism, No cleavages, high relief, high 2 nd order pink/yellow interferences.
Clinopyroxene	Non-pleochroic. High 1 st to low 2 nd order interference colors.
Orthopyroxene	Non-pleochroic. 2 nd order interference colors. 90 degree cleavage angle
Biotite	Brown pleochroism, one perfect cleavage. Extinction parallel to cleavage
Chlorite	Colorless-pale green pleochroism. Anomalously low interference colors.
Calcite	Non-pleochroic with 75° cleavage with extremely high birefringence.
Fe-Oxides	Small, irregular, and isotropic

Structural and Textural Observations:

- Rock is highly altered by hydrothermal processes.

<u>Sample:</u> 08P006	<u>Location:</u> Papuan Peninsula (10°03'31"S, 149°85'67"E)	<u>Rock Type:</u> Diorite
<u>Hand Sample Description:</u> Fairly Coarse grained with phenocrysts of amphibole (~2.5 mm), feldspar (~1 mm), and quartz (~1 mm) in a finer grain groundmass of feldspar/quartz.		
<u>Mineralogy:</u>	<u>Properties:</u>	
K-Feldspar	90° Cleavages. 1 st order birefringence. Non-pleochroic.	
Quartz	1 st order birefringence with undulatory extinction.	
Amphibole	56-120 cleavage, pale green brown pleochroism, low 2 nd order birefringence	
Biotite	Brown pleochroism, one perfect cleavage. Extinction parallel to cleavage	
Oxides	Isotropic	
Plagioclase	90° Cleavages. 1 st order birefringence. Albite twinning	
<u>Structural and Textural Observations:</u> -Groundmass us comprised of amphibole, Fe-oxides, and feldspar -Amphibole shows signs of alteration and does not appear to be in equilibrium with the magma -Some biotite is comely replaced by oxide minerals -Sample looks altered and in disequilibrium in thin section.		

<u>Sample:</u> 08P010	<u>Location:</u> Papuan Peninsula (10°03'31"S, 149°85'67"E)	<u>Rock Type:</u> Andesite
<u>Hand Sample Description:</u> Andesite with light grey groundmass with phenocrysts of amphibole and biotite		
<u>Mineralogy:</u>	<u>Properties:</u>	
Plagioclase	90° Cleavages. 1 st order birefringence. Albite twinning	
Analcite/Nephline	Low birefringence, low relief, small inclusions of muscovite?	
Hornblende	56-120 cleavage, pale green brown pleochroism, low 2 nd order birefringence	
Biotite	Brown pleochroism, one perfect cleavage. Extinction parallel to cleavage	
Chlorite	Colorless-pale green pleochroism. Anomalously low interference colors.	
Serpentine	Colorless-pale green pleochroism. Low interference colors. Higher relief than the chlorite grains.	
Fe-Oxides	Isoropic minerals in groundmass	
Zircon	Inclusions in Analcite/Nephline	
Apatite	Inclusions in Analcite/Nephline	
<u>Structural and Textural Observations:</u> -Chlorite/Serpentine/Fe-oxides mineralization is replacing groundmass minerals, amphibole, and biotite		

<u>Sample:</u> 08P025	<u>Location:</u> Cape Vogel Peninsula (9.66.758S, 149.82757E)	<u>Rock Type:</u> Basaltic Andesite		
<u>Hand Sample Description:</u> Fine-grained, green-grey groundmass with small visible crystals of pyroxene/amphibole and feldspar				
<u>Mineralogy:</u>	<u>Properties:</u>			
Plagioclase	90° Cleavages. 1 st order birefringence.			
Fe Oxides	Isotropic			
Serpentine	Colorless-pale green pleochroism. Anomalously low interference colors.			
Chlorite	Colorless-pale green pleochroism. Anomalously low interference colors.			
Amphibole	56-120 cleavage, pale green brown pleochroism, low 2 nd order birefringence			
pyroxene	Colorless - pale green pleochroism. High 1 st to low 2 nd order interference colors.			
<u>Structural and Textural Observations:</u>				
<ul style="list-style-type: none"> - Plagioclase occurs as microlites in the groundmass - Fe-Ox, serpentine, and chlorite are fine grained alteration products in the groundmass and pseudomorphic replacements for pyroxene and amphibole phenocrysts. - Amphibole and clinopyroxene are fine grained in groundmass, larger xts seem to be altered and replaced. - Some crystals of clinopyroxene are clinoenstatite 				

<u>Sample:</u> PNG10-005b	<u>Location:</u> Woodlark Island (Z56 - 466328E, 8986740N)	<u>Rock Type:</u> Dacite
<u>Hand Sample Description:</u> Phenocrysts of amphibole (~1 mm) and plagioclase (~1.5 mm) in a grey crystal rich groundmass		
<u>Mineralogy:</u>	<u>Properties:</u>	
Quartz	Fine grained intestinal material in bands with undulatory extinction.	
Plagioclase	90° Cleavages. 1 st order birefringence. Albite twinning	
Hornblende	56-120 cleavage, pale green brown pleochroism, low 2 nd order birefringence	
Apatite	High relief, low birefringence inclusions in feldspars.	
Zircon	Trace grains of high relief and high birefringence.	
<u>Structural and Textural Observations:</u> -Quartz and plagioclase make up about 85% of phenocrysts -Hornblende makes up about 10% of phenocrysts -Oxides rim the hornblendes. -Sericitic alteration in groundmass -Rare resorbed biotite grains		

<u>Sample:</u> PNG10-014a	<u>Location:</u> Woodlark Island (9°14'15"S, 152°46'98"E)	<u>Rock Type:</u> Granite
<u>Hand Sample Description:</u> I-type granite with crystals of amphibole, biotite, quartz, plagioclase, and K-feldspar		
<u>Mineralogy:</u>	<u>Properties:</u>	
Amphibole	56-120 cleavage, pale green brown pleochroism, low 2 nd order birefringence	
Biotite	Brown pleochroism, one perfect cleavage. Extinction parallel to cleavage	
Quartz	No cleavages and undulatory extinction.	
Plagioclase	90° cleavages, low 1 st order interference colors, colorless in plain light, albite twinning	
K-feldspar	90° Cleavages. 1 st order yellow birefringence	
Fe-Oxides	Isopropic	
Apatite	High relief mineral with 1 st order interference colors. Inclusions in feldspars	
Zircon	Highly birefringent inclusions in feldspar and in biotite with radiation halos	
<u>Structural and Textural Observations:</u> -crystals to be in equilibrium and do not appear to be altered like younger samples.		

<u>Sample:</u> PNG10-017	<u>Location:</u> Woodlark Island (9°15'37"S, 152°44'71"E)	<u>Rock Type:</u> Pillow Basalt		
<u>Hand Sample Description:</u> Pillow lava that lacks any visible phenocrysts.				
<u>Mineralogy:</u>	<u>Properties:</u>			
Plagioclase	90° Cleavages. 1 st order birefringence. Albite twinning			
Olivine	Colorless, No cleavages, high 2 nd order pink/yellow interferences.			
Clinopyroxene	Pale green pleochroism. High 1 st to low 2 nd order interference colors.			
Orthopyroxene	Non-pleochroic. High 1 st to low 2 nd order interference colors.			
Serpentine	Colorless-pale green pleochroism. Curved fractures. Anomalously low interference colors.			
<u>Structural and Textural Observations:</u>				
<ul style="list-style-type: none"> -Plagioclase xtals occur mainly as microlites making up the groundmass -Olivines are rare with altered rims of serpentine -Pyroxenes are the main phenocrysts -some sericitic alteration of plagioclase 				

<u>Sample:</u> PNG10-042f	<u>Location:</u> Egum Atoll (E151 56.766, S9 22.929)	<u>Rock Type:</u> Dacite
<u>Hand Sample Description:</u> 1-2 mm phenocrysts of pyroxene with finer crystals of plagioclase in the groundmass		
<u>Mineralogy:</u>	<u>Properties:</u>	
Clinopyroxene	Colorless - pale green pleochroism. High 1 st to low 2 nd order interference colors.	
Plagioclase	90° Cleavages. 1 st order birefringence.	
Oxide	Isotropic minerals	
Hornblende	56-120 cleavage, pale green brown pleochroism, low 2 nd order birefringence	
Anorthoclase	90° Cleavages. 1 st order birefringence. Grid twinning (albite and pericline) characteristic of anorthoclase.	
<u>Structural and Textural Observations:</u> <ul style="list-style-type: none"> -All hornblende is relict in groundmass -Clinopyroxene psedomorphic after amphibole -Fe-Oxides also replace amphibole -anorthoclase crystals are rare 		

<u>Sample:</u> PNG10-046a	<u>Location:</u> Apuo Island (Amphlett Is) (E150 51.265, S9 19.077)	<u>Rock Type:</u> Rhyolite
<u>Hand Sample Description:</u> Light tan groundmass with small (<1 mm) crystals of feldspar.		
<u>Mineralogy:</u>	<u>Properties:</u>	
Sanidine	90° Cleavages. 1 st order birefringence. Carlsbad twinning is more characteristic of sanidines.	
Quartz	Fine grained intestinal with undulatory extinction in groundmass.	
Zircon	high relief and high birefringence inclusions in sanidine	
Apatite	High relief, low birefringence inclusions in sanidine.	
Clinopyroxene	Rare (<1% of phenocrysts). Non-pleochroic, but has a higher relief and birefringence (low 2 nd order) than the feldspars.	
Oxides	Isotropic crystals	
<u>Structural and Textural Observations:</u> -Holocrystalline rock with fine grained groundmass of quartz and clinopyroxene -clinopyroxene crystals might be xenocrysts from nearby basalt flow		

<u>Sample:</u> PNG10-046b	<u>Location:</u> Apuo Island (Amphlett Is) (E150 51.265, S9 19.077)	<u>Rock Type:</u> Basalt
<u>Hand Sample Description:</u> Glassy black groundmass with visible crystals of olivine (2-3 mm) and finer plagioclase		
<u>Mineralogy:</u>	<u>Properties:</u>	
Olivine	Colorless to pale green pleochroism, No cleavages, high 2 nd order pink/yellow interferences.	
Plagioclase	90° Cleavages. 1 st order birefringence.	
Fe Oxide	Isotropic mineral in groundmass	
Orthopreoxene	Non-pleochroic. High 1 st to low 2 nd order interference colors. Mineral becomes extinct along 90° cleavages.	
<u>Structural and Textural Observations:</u> -plagioclase forms microlites that display a preferred orientations that is likely aligned with flow direction after eruption		

<u>Sample:</u> PNG10-050A	<u>Location:</u> Yamea Island (Amphletts) (E150 53.716, S9 15.669)	<u>Rock Type:</u> Basaltic Andesite
<u>Hand Sample Description:</u> -vesicular andesite with grey-red groundmass and visible phenocrysts of amphibole (~3 mm), pyroxene (~2 mm), and fine feldspar.		
<u>Mineralogy:</u>	<u>Properties:</u>	
Plagioclase	90° Cleavages. 1 st order birefringence. Albite twinning	
Hornblende	56-120 cleavage, pale green brown pleochroism, low 2 nd order birefringence	
Oxides	Isotropic	
Augite	Pale green pleochroism. High 1 st to low 2 nd order interference colors. Inclined extinction.	
<u>Structural and Textural Observations:</u> -Plagioclase is resorbed with numerous inclusions -augite seems to be altered and out of equilibrium -flow aligned microlites in the groundmass		

<u>Sample:</u> PNG10-058a	<u>Location:</u> Nuamata Island (E150 11.835, S9 10.510)	<u>Rock Type:</u> Dacite		
<u>Hand Sample Description:</u> - medium grey crystal rich groundmass with visible crystals of amphibole (~1 mm) and feldspar				
<u>Mineralogy:</u>	<u>Properties:</u>			
Sanidine/Anorthoclase	90° Cleavages. 1 st order birefringence. Grid twinning (albite and pericline) characteristic of anorthoclase. Carlsbad twinning is more characteristic of sanidines.			
Amphibole	56-120 cleavage, pale green brown pleochroism, low 2 nd order birefringence			
Oxides	Isotropic. Crystal form (hexagonal) suggest hematite – illmenite.			
Zircon	Trace grains of high relief and high birefringence.			
Apatite	High relief, low birefringence inclusions in feldspars.			
<u>Structural and Textural Observations:</u> -apatite and zircon occur as inclusions in amphibole and feldspar -amphiboles have a reaction rim of Fe-oxides				

<u>Sample:</u> PNG10-064b	<u>Location:</u> Goodenough Island (9 24.868S, 150 22.053E)	<u>Rock Type:</u> Vesicular Basalt
<u>Hand Sample Description:</u> Black, vesicular, glassy grounds visible phenocrysts of plagioclase (1-2 mm) and olivine (~3 mm) with xenocrysts of garnet.		
<u>Mineralogy:</u>	<u>Properties:</u>	
Olivine	Colorless, No cleavages, high 2 nd - 3 rd order pink/yellow interferences.	
Clinopyroxene	Pale green pleochroism. High 1 st to low 2 nd order interference colors.	
Orthopyroxene	Non-pleochroic. High 1 st to low 2 nd order interference colors. Mineral becomes extinct along 90° cleavages.	
Plagioclase	90° Cleavages. 1 st order birefringence. Albite twinning	
<u>Structural and Textural Observations:</u> -vesicular basalt with zoned olivines -some olivines/pyroxenes occur as aggregates		

<u>Sample:</u> PNG10-067a	<u>Location:</u> Fergusson Island (E150 27.921, S9 33.884)	<u>Rock Type:</u> Rhyolite
<u>Hand Sample Description:</u> -white-pink, fine-grained groundmass with visible crystals of feldspar		
<u>Mineralogy:</u>	<u>Properties:</u>	
Sanidine/Anorthoclase	90° Cleavages. 1 st order birefringence. Grid twinning (albite and pericline) characteristic of anorthoclase. Carlsbad twinning is more characteristic of sanidines.	
Quartz	Fine grained intestinal material in bands with undulatory extinction.	
Oxides	Isotropic. Crystal form (hexagonal) suggest hematite – illmenite.	
Apatite	High relief, low birefringence inclusions in feldspars.	
Serpentine	Colorless-pale green pleochroism. Curved fractures. Anomalously low interference colors.	
<u>Structural and Textural Observations:</u> -rock has flow banding with light layers of quartz and feldspar and tan layers of fine grained matrix that has minor serpentinization in small areas.		

Appendix 2.1 $^{40}\text{Ar}/^{39}\text{Ar}$ Data Tables - < 3.5 Ma. igneous rocks

PNG03-075 Dobu Island rhyolite			sanidine			60.10 mg (250 μm - 50 μm fraction)			J= 1.35126E-03 \pm 3.00%								
step	T (C)	t (min.)	^{36}Ar	%err	^{37}Ar	%err	^{38}Ar	%err	^{39}Ar	%err	^{40}Ar	%err	$\Sigma^{39}\text{Ar}$	% $^{40}\text{Ar}^*$	$^{40}\text{Ar}/^{39}\text{ArK}$	Age (Ma)	1s.d.
1	400	12	2.06E-06	\pm 2.93	2.19E-06	\pm 37.05	5.44E-07	\pm 4.02	2.12E-05	\pm 1.25	4.93E-04	\pm 0.28	0.004	2.83	7.125	1.736	0.7725
2	500	12	2.05E-06	\pm 1.78	1.21E-06	\pm 50.34	9.75E-07	\pm 5.47	4.65E-05	\pm 1.29	6.27E-04	\pm 0.09	0.020	3.18	0.289	0.070	0.0220
3	600	12	3.19E-06	\pm 1.10	2.02E-07	\pm 378.35	2.48E-06	\pm 2.20	1.67E-04	\pm 1.21	9.78E-04	\pm 0.14	0.059	3.66	0.143	0.034	0.0078
4	700	12	3.57E-06	\pm 1.91	5.51E-07	\pm 107.21	4.96E-06	\pm 2.12	3.54E-06	\pm 1.22	1.10E-03	\pm 0.12	0.142	3.77	0.068	0.016	0.0050
5	775	12	3.19E-06	\pm 1.17	2.14E-06	\pm 37.53	5.43E-06	\pm 1.51	4.13E-04	\pm 1.25	9.92E-04	\pm 0.17	0.242	5.01	0.078	0.019	0.0047
6	850	12	2.71E-06	\pm 1.76	1.70E-06	\pm 50.78	6.36E-06	\pm 0.79	4.95E-04	\pm 1.22	7.56E-04	\pm 0.26	0.358	6.11	0.130	0.032	0.0039
7	950	12	5.94E-06	\pm 0.85	3.54E-06	\pm 27.12	1.07E-05	\pm 1.17	8.29E-04	\pm 1.20	1.87E-03	\pm 0.08	0.550	6.39	0.104	0.025	0.0041
8	1025	12	7.79E-06	\pm 1.42	9.55E-07	\pm 102.34	1.24E-05	\pm 0.63	8.80E-04	\pm 1.20	2.47E-03	\pm 0.06	0.754	6.73	0.143	0.035	0.0046
9	1100	12	7.13E-06	\pm 1.09	1.44E-06	\pm 70.15	1.27E-05	\pm 1.13	9.34E-04	\pm 1.21	2.57E-03	\pm 0.09	0.972	18.04	0.456	0.111	0.0056
10	1175	12	1.12E-06	\pm 3.03	2.18E-06	\pm 52.01	1.12E-06	\pm 3.15	6.75E-05	\pm 1.54	3.07E-04	\pm 0.41	0.992	7.78	0.424	0.103	0.0134
11	1350	12	2.06E-06	\pm 2.93	2.19E-06	\pm 37.05	5.44E-07	\pm 4.02	2.12E-05	\pm 1.25	4.93E-04	\pm 0.28	0.997	2.33	5.71	13.9	0.0550
12	1500	12	1.15E-06	\pm 4.61	2.23E-06	\pm 44.52	2.56E-07	\pm 8.64	1.25E-05	\pm 1.35	2.07E-04	\pm 0.58	1.000	6.42	1.09	2.67	0.0891
													Total Gas Age =			0.077	0.002
													Plateau Age (based on steps 5 - 9) =			0.031	0.004
													Isochron Age =			0.019	0.011

PNG03-117 Goodenough Island basaltic andesite			K-feldspar	31.20 mg (250 μm - 50 μm fraction)			J= 1.30219E-04 \pm 4.67%										
step	T (C)	t (min.)	^{36}Ar	%err	^{37}Ar	%err	^{38}Ar	%err	^{39}Ar	%err	^{40}Ar	%err	$\Sigma^{39}\text{Ar}$	% $^{40}\text{Ar}^*$	$^{40}\text{Ar}/^{39}\text{ArK}$	Age (Ma)	1s.d.
1	400	12	2.49E-04	\pm 0.54	1.76E-03	\pm 79.28	4.80E-05	\pm 1.46	2.19E-05	\pm 2.74	7.52E-02	\pm 0.18	0.223	1.95	65.656	15.36	18.874
2	500	12	1.02E-06	\pm 3.35	2.32E-04	\pm 30.12	1.95E-07	\pm 11.40	1.16E-06	\pm 1.80	5.01E-04	\pm 1.41	0.235	40.08	135.98	31.67	2.283
3	600	12	1.42E-06	\pm 3.02	4.79E-05	\pm 235.04	3.88E-07	\pm 7.17	4.95E-06	\pm 1.26	4.71E-04	\pm 1.49	0.285	11.02	9.8753	2.318	0.376
4	700	12	1.50E-06	\pm 3.41	9.17E-05	\pm 120.68	3.78E-07	\pm 7.30	8.39E-06	\pm 1.44	5.06E-04	\pm 1.39	0.370	12.34	6.6486	1.561	0.245
5	800	12	1.24E-06	\pm 3.65	6.01E-05	\pm 160.22	3.77E-07	\pm 9.74	6.84E-06	\pm 2.11	5.00E-04	\pm 1.65	0.440	26.78	20.617	4.837	0.479
6	900	12	1.18E-06	\pm 2.09	1.72E-04	\pm 42.24	2.81E-07	\pm 13.54	5.84E-06	\pm 1.87	4.80E-04	\pm 1.49	0.499	27.16	19.663	4.614	0.454
7	1000	12	1.39E-06	\pm 2.35	1.43E-04	\pm 83.06	3.54E-07	\pm 5.28	5.16E-06	\pm 1.45	5.72E-04	\pm 1.23	0.551	28.24	28.716	6.733	0.505
8	1150	12	4.21E-06	\pm 1.42	9.71E-05	\pm 77.56	1.14E-06	\pm 2.98	1.89E-05	\pm 1.25	3.06E-03	\pm 0.24	0.743	59.30	95.748	22.35	1.063
9	1300	12	2.68E-06	\pm 2.67	2.95E-05	\pm 480.96	5.21E-07	\pm 10.11	7.96E-06	\pm 1.98	1.86E-03	\pm 0.38	0.824	57.50	135.78	31.62	2.021
10	1500	12	3.48E-06	\pm 1.23	2.90E-04	\pm 26.74	8.79E-07	\pm 3.64	1.73E-05	\pm 1.26	1.00E-03	\pm 0.72	1.000	2.95	0.2231	0.052	0.129
													Total Gas Age =			0.629	0.09
													Plateau Age (based on steps 5 - 10) =			1.32	0.43
													Isochron Age =			0.366	0.49

PNG08-004a Goodenough Island basaltic andesite			Biotite	34.80 mg (250 μm - 50 μm fraction)			J= 1.44350E-04 \pm 3.21%										
step	T (C)	t (min.)	^{36}Ar	%err	^{37}Ar	%err	^{38}Ar	%err	^{39}Ar	%err	^{40}Ar	%err	$\Sigma^{39}\text{Ar}$	% $^{40}\text{Ar}^*$	$^{40}\text{Ar}/^{39}\text{ArK}$	Age (Ma)	1s.d.
1	550	12	4.33E-06	\pm 1.00	2.29E-06	\pm 22.76	8.84E-07	\pm 3.97	1.12E-05	\pm 1.28	1.29E-03	\pm 0.12	0.011	1.07	1.3672	0.3560	0.194
2	650	12	5.97E-07	\pm 3.87	9.73E-08	\pm 408.94	2.12E-07	\pm 11.89	7.55E-06	\pm 1.50	2.08E-04	\pm 0.44	0.019	14.99	4.1317	1.0756	0.086
3	725	12	1.33E-06	\pm 1.99	1.63E-06	\pm 28.50	4.64E-07	\pm 3.64	1.83E-05	\pm 1.40	4.29E-04	\pm 0.15	0.038	8.76	20.691	0.5388	0.055
4	800	12	1.39E-06	\pm 2.00	3.03E-06	\pm 8.12	6.59E-07	\pm 2.51	3.03E-05	\pm 1.54	4.52E-04	\pm 0.22	0.069	8.87	1.3251	0.3450	0.044
5	850	12	1.21E-06	\pm 3.40	3.62E-06	\pm 8.33	9.50E-07	\pm 3.76	5.93E-05	\pm 1.17	4.42E-04	\pm 0.18	0.130	19.39	1.4363	0.3740	0.015
6	900	12	1.23E-06	\pm 2.83	1.08E-06	\pm 1.80	1.20E-06	\pm 1.16	7.62E-05	\pm 1.16	4.66E-04	\pm 0.14	0.208	22.24	1.3566	0.3532	0.013
7	950	12	2.50E-06	\pm 1.83	2.65E-05	\pm 2.25	2.21E-06	\pm 1.65	1.45E-04	\pm 1.22	9.44E-04	\pm 0.15	0.356	21.62	1.41275	0.3679	0.015
8	1000	12	9.46E-06	\pm 1.38	3.63E-04	\pm 0.82	4.25E-06	\pm 1.69	2.06E-04	\pm 1.15	3.10E-03	\pm 0.08	0.567	9.77	1.60973	0.4192	0.018
9	1050	12	7.64E-06	\pm 0.84	5.17E-04	\pm 0.52	3.93E-06	\pm 1.13	1.95E-04	\pm 1.14	2.56E-03	\pm 0.09	0.766	11.69	1.74761	0.4551	0.018
10	1100	12	5.58E-06	\pm 1.15	3.18E-04	\pm 0.74	3.83E-06	\pm 0.99	2.22E-04	\pm 1.14	1.98E-03	\pm 0.11	0.993	16.83	1.61094	0.4195	0.015

PNG06-043a Nuamata Island andesite				K-feldspar	26.00 mg (250µm - 50µm fraction)				J=	1.31954E-04 ± 2.58%							
step	T (C)	t (min.)	^{36}Ar	%err	^{37}Ar	%err	^{38}Ar	%err	^{39}Ar	%err	^{40}Ar	%err	$\Sigma^{39}\text{Ar}$	% $^{39}\text{Ar}^*$	$^{40}\text{Ar} + ^{39}\text{ArK}$	Age (Ma)	1s.d.
1	400	12	1.35E-06	± 5.87	7.71E-05	± 88.62	3.29E-07	± 7.79	1.26E-06	± 3.97	3.68E-04	± 0.37	0.003	8.74	20.8908	4.98	2.83
2	500	12	7.49E-07	± 5.15	5.52E-05	± 115.16	1.87E-07	± 17.04	2.56E-06	± 2.25	2.34E-04	± 0.55	0.010	5.34	6.9710	1.66	0.45
3	600	12	1.55E-06	± 4.17	1.53E-04	± 45.19	4.98E-07	± 4.54	1.04E-05	± 1.37	5.69E-04	± 0.28	0.039	19.69	12.2161	2.91	0.13
4	700	12	4.61E-06	± 1.18	2.67E-04	± 28.70	1.35E-06	± 3.12	3.55E-05	± 1.24	1.77E-03	± 0.12	0.137	23.16	12.3741	2.94	0.10
5	775	12	3.62E-07	± 12.67	1.94E-04	± 25.67	5.96E-07	± 6.01	5.28E-05	± 1.27	3.73E-04	± 0.50	0.282	128.72	9.4097	2.24	0.06
6	850	12	4.06E-07	± 11.24	9.76E-05	± 93.36	7.66E-07	± 7.09	6.41E-05	± 1.20	4.54E-04	± 0.26	0.458	126.40	9.0907	2.16	0.06
7	950	12	2.53E-07	± 21.00	9.35E-05	± 71.91	8.20E-07	± 4.88	6.84E-05	± 1.28	5.42E-04	± 0.28	0.646	113.78	9.1406	2.17	0.06
8	1050	12	2.76E-07	± 15.07	1.31E-04	± 77.52	5.33E-07	± 10.51	4.14E-05	± 1.28	2.91E-04	± 0.51	0.760	127.96	9.2707	2.21	0.06
9	1150	12	1.19E-06	± 4.81	7.94E-05	± 80.62	6.66E-07	± 5.68	3.52E-05	± 1.20	7.74E-04	± 0.19	0.857	54.54	12.2357	2.91	0.08
10	1300	12	1.58E-06	± 3.11	1.94E-04	± 35.35	8.44E-07	± 5.53	4.42E-05	± 1.28	1.29E-03	± 0.20	0.979	63.88	19.1014	4.54	0.13
11	1500	12	2.11E-06	± 2.56	1.20E-04	± 53.76	5.28E-07	± 9.82	7.81E-06	± 1.46	8.53E-04	± 0.29	1.000	27.04	31.4464	7.47	0.32
														Total Gas Age =	2.76	0.07	
														Plateau Age (based on steps 5 - 8) =	2.19	0.08	
														Isochron Age =	1.28	0.29	

PNG06-043b Nuamata Island amph. xenolith				K-feldspar	34.82 mg (250µm - 50µm fraction)				J=	1.31954E-04 ± 2.58%							
step	T (C)	t (min.)	^{36}Ar	%err	^{37}Ar	%err	^{38}Ar	%err	^{39}Ar	%err	^{40}Ar	%err	$\Sigma^{39}\text{Ar}$	% $^{39}\text{Ar}^*$	$^{40}\text{Ar} + ^{39}\text{ArK}$	Age (Ma)	1s.d.
1	400	12	1.51E-05	± 0.80	4.18E-05	± 147.35	2.96E-06	± 1.70	6.51E-06	± 1.87	4.50E-03	± 0.07	0.018	0.47	5.6764	1.35	2.50
2	500	12	1.52E-06	± 3.16	1.32E-04	± 54.30	3.45E-07	± 10.81	7.54E-06	± 1.31	4.89E-04	± 0.21	0.038	7.96	6.8299	1.63	0.12
3	600	12	7.54E-07	± 5.43	6.86E-05	± 109.69	4.96E-07	± 8.21	2.80E-05	± 1.27	4.62E-04	± 0.33	0.113	51.71	8.7672	2.09	0.06
4	775	12	2.53E-07	± 16.05	1.56E-04	± 33.47	1.28E-06	± 4.74	1.18E-04	± 1.17	1.09E-03	± 0.20	0.429	106.87	10.0222	2.38	0.06
5	850	12	2.18E-07	± 21.67	1.24E-04	± 49.64	1.20E-06	± 3.98	1.04E-04	± 1.16	8.88E-04	± 0.17	0.700	107.26	9.2549	2.20	0.06
6	950	12	1.14E-07	± 52.91	1.34E-05	± 553.54	4.98E-07	± 6.07	5.19E-05	± 1.29	4.27E-04	± 0.30	0.834	107.88	8.8958	2.12	0.06
7	1050	12	4.25E-08	± 93.97	1.94E-05	± 285.48	3.75E-07	± 10.48	2.67E-05	± 1.37	2.23E-04	± 0.72	0.903	105.64	8.8769	2.11	0.06
8	1150	12	9.10E-07	± 5.01	5.62E-05	± 91.45	5.45E-07	± 9.30	2.34E-05	± 1.29	5.52E-04	± 0.29	0.964	51.33	12.3683	2.94	0.09
9	1300	12	5.50E-07	± 8.60	3.28E-05	± 166.48	2.26E-07	± 15.62	1.32E-05	± 1.50	3.44E-04	± 0.37	0.998	52.76	14.0369	3.34	0.11
10	1500	12	8.46E-07	± 9.10	4.85E-05	± 142.34	1.74E-07	± 17.59	6.67E-07	± 6.26	2.22E-04	± 0.84	1.000	12.78	38.0274	9.08	5.32
														Total Gas Age =	2.34	0.06	
														Plateau Age (based on steps 6 - 10) =	2.37	0.21	
														Isochron Age =	2.00	0.21	

PNG10-058a Nuamata Island andesite				hornblende	56.83 mg (250µm - 50µm fraction)				J=	1.36390E-04 ± 4.92%							
step	T (C)	t (min.)	^{36}Ar	%err	^{37}Ar	%err	^{38}Ar	%err	^{39}Ar	%err	^{40}Ar	%err	$\Sigma^{39}\text{Ar}$	% $^{39}\text{Ar}^*$	$^{40}\text{Ar} + ^{39}\text{ArK}$	Age (Ma)	1s.d.
1	500	12	1.95E-06	± 2.99	1.61E-05	± 3.27	4.49E-07	± 5.11	2.89E-06	± 1.73	5.85E-04	± 0.18	0.010	1.27	0.8815	0.22	0.67
2	600	12	1.04E-06	± 5.22	1.93E-05	± 3.84	2.58E-07	± 7.97	7.34E-06	± 2.08	3.71E-04	± 0.47	0.035	17.28	8.4421	2.08	0.25
3	700	12	1.24E-06	± 2.95	2.61E-05	± 2.41	5.34E-07	± 4.39	1.88E-05	± 1.36	5.39E-04	± 0.16	0.098	32.22	9.1141	2.24	0.12
4	800	12	8.46E-07	± 3.51	2.06E-05	± 3.16	2.68E-07	± 8.64	9.83E-06	± 1.42	3.31E-04	± 0.27	0.131	24.55	8.1030	1.99	0.12
5	850	12	6.19E-07	± 4.43	8.87E-06	± 2.92	1.50E-07	± 13.98	2.68E-06	± 1.64	2.21E-04	± 0.39	0.141	17.41	13.8400	3.40	0.31
6	890	12	2.94E-07	± 10.38	7.79E-06	± 3.15	2.08E-08	± 88.74	1.19E-06	± 3.37	9.13E-05	± 0.86	0.145	4.71	3.1451	0.77	0.62
7	930	12	3.70E-07	± 7.48	1.36E-05	± 4.06	1.27E-07	± 16.11	1.63E-06	± 1.94	1.21E-04	± 1.02	0.150	9.68	6.8707	1.69	0.36
8	1000	12	2.65E-06	± 2.01	1.97E-04	± 1.13	6.99E-07	± 2.90	1.36E-05	± 1.57	9.10E-04	± 0.21	0.196	13.87	9.2577	2.28	0.22
9	1100	12	1.35E-05	± 0.49	3.38E-03	± 0.48	5.44E-06	± 1.08	2.20E-04	± 1.17	6.00E-03	± 0.05	0.942	33.71	9.5360	2.34	0.12
10	1200	12	3.63E-06	± 1.86	3.34E-04	± 0.89	9.05E-07	± 4.08	1.28E-05	± 1.34	1.20E-03	± 0.12	0.986	10.54	9.9783	2.45	0.21
11	1350	12	2.18E-05	± 0.55	2.50E-04	± 1.24	4.20E-06	± 0.98	4.26E-06	± 1.40	6.59E-03	± 0.07	1.000	2.30	23.6623	5.81	3.27
														Total Gas Age =	2.33	0.11	
														Plateau Age (based on steps 6 - 10) =	2.37	0.21	
														Isochron Age =	2.18	0.14	

P08-010 Papuan Peninsula basaltic andesite				biotite	33.1 mg (250µm - 150µm fraction)				J=	1.43950E-04 ± 3.00%							
step	T (C)	t (min.)	^{36}Ar	%err	^{37}Ar	%err	^{38}Ar	%err	^{39}Ar	%err	^{40}Ar	%err	$\Sigma^{39}\text{Ar}$	% $^{39}\text{Ar}^*$	$^{40}\text{Ar} + ^{39}\text{ArK}$	Age (Ma)	1s.d.
1	500	12	1.00E-05	0.79	5.52E-06	51.91	1.90E-06	1.78	5.17E-06	1.43	3.01E-03	0.08	0.015	1.42	3.2868	2.41	1.37
2	600	12	1.23E-05	0.92	6.41E-06	37.69	2.51E-06	1.79	1.51E-05	1.32	3.75E-03	0.06	0.054	2.96	5.2597	2.02	0.45
3	700	1															

PNG08-042a Yamea Island basalt					whole rock					115.1 mg					J= 1.27928E-04 ± 2.63%						
step	T (C)	t (min.)	^{36}Ar	%err	^{37}Ar	%err	^{38}Ar	%err	^{39}Ar	%err	^{40}Ar	%err	$\chi^{20}\text{Ar}$	%err	$\chi^{39}\text{Ar}$	%err*	$^{40}\text{Ar}^{*}/^{39}\text{ArK}$	Age (Ma)	1s.d.		
1	500	12	1.82E-05 ± 0.49		3.42E-04 ± 1.26		5.95E-06 ± 1.05		2.55E-04 ± 1.13		8.31E-03 ± 0.04		0.10	35.26	11.33481	2.664	0.02				
2	600	12	9.15E-06 ± 0.54		4.46E-07 ± 0.90		7.95E-06 ± 1.65		5.94E-04 ± 1.13		9.93E-03 ± 0.04		0.32	72.76	12.07670	2.796	0.01				
3	700	12	5.76E-06 ± 0.82		3.25E-04 ± 1.05		3.70E-06 ± 1.77		2.76E-04 ± 1.15		4.70E-03 ± 0.04		0.42	63.82	10.86564	2.521	0.01				
4	800	12	3.38E-06 ± 2.16		3.59E-04 ± 0.62		2.91E-06 ± 2.40		2.10E-04 ± 1.14		3.08E-03 ± 0.12		0.50	67.64	9.94476	2.305	0.01				
5	900	12	7.22E-06 ± 1.37		3.85E-04 ± 1.11		3.25E-06 ± 1.58		1.74E-04 ± 1.15		3.83E-03 ± 0.11		0.56	44.39	9.73782	2.275	0.02				
6	1100	12	3.06E-05 ± 0.38		1.84E-03 ± 0.66		1.36E-05 ± 0.80		6.64E-04 ± 1.14		1.64E-02 ± 0.06		0.81	44.77	11.02131	2.574	0.01				
7	1300	12	2.15E-05 ± 0.77		1.53E-03 ± 0.61		8.18E-06 ± 1.21		3.77E-04 ± 1.13		1.04E-02 ± 0.06		0.95	38.99	10.77135	2.524	0.01				
8	1500	12	1.51E-05 ± 1.24		5.93E-04 ± 0.81		3.58E-06 ± 1.91		1.37E-04 ± 1.14		4.53E-03 ± 0.12		1.000	0.02	0.3228	0.074	0.021	Total Gas Age =	2.46	0.03	
																		Isochron Age =	2.58	0.45	

PNG10-042f Egum Atoll andesite					clinopyroxene					41.6 mg					J= 1.26590E-04 ± 1.97%						
step	T (C)	t (min.)	^{36}Ar	%err	^{37}Ar	%err	^{38}Ar	%err	^{39}Ar	%err	^{40}Ar	%err	$\chi^{20}\text{Ar}$	%err*	$^{40}\text{Ar}^{*}/^{39}\text{ArK}$	Age (Ma)	1s.d.				
TF	1500	12	3.88E-05 ± 0.53		9.40E-03 ± 0.46		8.95E-06 ± 1.16		1.52E-04 ± 1.14		1.31E-02 ± 0.07		-		12.50	12.2428	2.79	0.08			

PNG10-046a Apou Island dacite					sanidine					78.23 mg (250μm - 50μm fraction)					J= 1.43845E-04 ± 2.91%						
step	T (C)	t (min.)	^{36}Ar	%err	^{37}Ar	%err	^{38}Ar	%err	^{39}Ar	%err	^{40}Ar	%err	$\chi^{20}\text{Ar}$	%err*	$^{40}\text{Ar}^{*}/^{39}\text{ArK}$	Age (Ma)	1s.d.				
1	400	12	2.49E-05 ± 0.48		6.00E-06 ± 14.94		4.76E-06 ± 1.36		1.08E-05 ± 1.22		7.67E-03 ± 0.02		0.003	4.25	24.1235	8.074	0.93				
2	500	12	1.32E-04 ± 0.33		2.89E-04 ± 1.03		2.63E-05 ± 0.72		1.53E-04 ± 1.19		4.12E-02 ± 0.03		0.039	4.92	11.0309	3.549	0.29				
3	600	12	8.65E-05 ± 0.28		4.37E-07 ± 0.92		2.12E-05 ± 0.66		4.14E-04 ± 1.14		3.09E-02 ± 0.03		0.137	17.22	12.0984	3.303	0.05				
4	700	12	5.72E-06 ± 1.15		7.61E-09 ± 9.13		1.88E-06 ± 3.33		8.92E-05 ± 1.17		2.55E-03 ± 0.11		0.158	33.77	9.4146	2.492	0.03				
5	775	12	5.31E-06 ± 2.25		1.86E-08 ± 6.53		3.28E-06 ± 2.04		2.11E-04 ± 1.14		4.01E-03 ± 0.06		0.208	60.86	11.4294	2.984	0.01				
6	850	12	1.26E-05 ± 0.89		2.57E-08 ± 4.60		7.00E-06 ± 1.42		4.05E-04 ± 1.13		8.61E-03 ± 0.06		0.304	56.76	11.9406	3.121	0.01				
7	950	12	2.03E-05 ± 0.48		2.98E-08 ± 3.78		9.89E-06 ± 1.03		5.11E-04 ± 1.13		1.21E-02 ± 0.03		0.425	50.56	11.8276	3.098	0.01				
8	1050	12	5.44E-05 ± 0.31		8.37E-08 ± 2.28		2.15E-05 ± 0.78		9.52E-04 ± 1.13		2.83E-02 ± 0.03		0.651	43.15	12.5866	3.309	0.02				
9	1150	12	3.53E-05 ± 0.50		7.74E-08 ± 1.60		1.83E-05 ± 0.57		9.98E-04 ± 1.13		2.33E-02 ± 0.04		0.888	55.16	12.7140	3.324	0.01				
10	1300	12	3.21E-05 ± 0.67		2.82E-08 ± 2.72		1.09E-05 ± 0.65		4.22E-04 ± 1.14		1.47E-02 ± 0.06		0.988	35.41	12.0549	3.186	0.02				
11	1500	12	4.92E-05 ± 0.40		2.82E-09 ± 22.32		9.65E-06 ± 0.91		5.26E-05 ± 1.18		1.48E-02 ± 0.04		1.000	1.59	1.2217	1.059	0.27	Total Gas Age =	3.22	0.09	
																		Isochron Age =	3.17	0.24	

PNG10-046b Apou Island basalt					whole rock					57.93 mg					J= 1.33741E-04 ± 4.92%						
step	T (C)	t (min.)	^{36}Ar	%err	^{37}Ar	%err	^{38}Ar	%err	^{39}Ar	%err	^{40}Ar	%err	$\chi^{20}\text{Ar}$	%err*	$^{40}\text{Ar}^{*}/^{39}\text{ArK}$	Age (Ma)	1s.d.				
1	500	12	1.57E-05 ± 0.68		2.59E-06 ± 28.60		4.98E-06 ± 0.77		1.72E-04 ± 1.13		5.95E-03 ± 0.07		0.175	22.27	7.45570	1.865	0.02				
2	600	12	4.28E-06 ± 0.65		2.34E-04 ± 1.47		3.55E-06 ± 1.09		2.19E-04 ± 1.14		3.01E-03 ± 0.10		0.398	58.04	7.97920	1.939	0.01				
3	700	12	3.57E-06 ± 1.12		5.31E-04 ± 1.06		3.58E-06 ± 2.32		2.45E-04 ± 1.15		3.01E-03 ± 0.09		0.647	65.01	8.03479	1.948	0.01				
4	800	12	2.82E-06 ± 1.49		6.87E-04 ± 0.89		3.02E-06 ± 1.17		2.05E-04 ± 1.15		2.38E-03 ± 0.08		0.856	64.99	7.62286	1.848	0.01				
5	900	12	2.37E-06 ± 1.71		4.56E-04 ± 1.19		1.06E-06 ± 1.95		7.17E-05 ± 1.18		1.05E-03 ± 0.17		0.929	33.18	4.96821	1.222	0.01				
6	1200	12	6.04E-06 ± 0.92		1.62E-03 ± 0.49		1.74E-06 ± 2.87		4.85E-05 ± 1.15		1.98E-03 ± 0.11		0.978	9.88	4.81386	1.251	0.03				
7	1500	12	4.44E-06 ± 1.24		5.58E-04 ± 1.59		9.73E-07 ± 3.50		2.14E-05 ± 1.18		1.17E-03 ± 0.19		1.000	-	-	-	-	Total Gas Age =	1.75	0.08	
																		Platau Age (based on steps 7 - 10) =	2.75	0.06	
																		Isochron Age =	2.59	0.76	

PNG10-050a Yamea Island andesite					clinopyroxene					78.2 mg					J= 1.27480E-04 ± 1.57%						
step	T (C)	t (min.)	^{36}Ar	%err	^{37}Ar	%err	^{38}Ar	%err	^{39}Ar	%err	^{40}Ar	%err	$\chi^{20}\text{Ar}$	%err*	$^{40}\text{Ar}^{*}/^{39}\text{ArK}$	Age (Ma)	1s.d.				
TF	1500	12	3.37E-05 ± 0.40		2.19E-02 ± 0.43		6.62E-06 ± 1.46		5.20E-05 ± 1.19		9.95E-03 ± 0.04		-	0.14	12.6933	2.92	0.21				

Appendix 2.2 $^{40}\text{Ar}/^{39}\text{Ar}$ Data Tables - Miocene igneous rocks

PNG03-199 diorite				whole rock 48.23 mg				J= 1.27480E-04 ± 2.76%										
step	T (C)	t (min.)		^{36}Ar	%err	^{37}Ar	%err	^{38}Ar	%err	^{39}Ar	%err	^{40}Ar	%err	$\chi^{20}\text{Ar}$	% $^{40}\text{Ar}^*$	$^{40}\text{Ar}/^{39}\text{ArK}$	Age (Ma)	1s.d.
1	500	12	1.90E-05 ± 0.50	9.00E-05 ± 2.50	3.72E-06 ± 1.47	1.92E-05 ± 1.36	6.11E-03 ± 0.06	0.031	7.93	22.815	5.934	0.567						
2	600	12	2.25E-05 ± 0.37	1.50E-07 ± 1.62	4.88E-06 ± 0.93	6.24E-05 ± 1.24	8.45E-03 ± 0.04	0.133	21.47	27.803	6.635	0.167						
3	700	12	2.57E-05 ± 0.53	3.47E-04 ± 0.88	6.11E-06 ± 1.35	1.12E-04 ± 1.18	1.14E-02 ± 0.07	0.316	33.25	33.297	7.802	0.091						
4	800	12	1.06E-05 ± 0.85	2.98E-04 ± 1.33	3.17E-06 ± 1.43	1.17E-04 ± 1.15	7.21E-03 ± 0.03	0.505	56.75	34.955	8.084	0.041						
5	900	12	1.17E-05 ± 0.81	2.43E-04 ± 1.14	3.24E-06 ± 1.19	8.95E-05 ± 1.20	6.57E-03 ± 0.05	0.651	47.50	34.675	8.048	0.074						
6	1100	12	5.73E-05 ± 0.35	9.79E-04 ± 0.63	1.34E-05 ± 0.62	1.38E-04 ± 1.14	2.35E-02 ± 0.04	0.949	28.04	35.489	8.363	0.066						
7	1200	12	7.51E-06 ± 1.02	3.17E-04 ± 1.63	1.80E-06 ± 2.55	2.52E-05 ± 1.24	3.27E-03 ± 0.10	0.990	32.05	41.383	9.701	0.165						
8	1350	12	3.86E-06 ± 2.25	1.23E-04 ± 2.29	6.27E-07 ± 5.28	5.93E-06 ± 1.71	1.19E-03 ± 0.23	0.999	4.32	7.702	2.228	0.612						
9	1500	12	2.07E-06 ± 3.96	2.26E-04 ± 1.91	6.06E-08 ± 59.52	3.43E-07 ± 7.31	3.23E-05 ± 0.08	1.000	-*	-*	-*	-*						
Total Gas Age =																		
Plateau Age (based on steps 3 - 6) =																		
Isochron Age =																		

08P-006 Papuan Peninsula andesite				amphibole 35.37 mg				J= 1.40317E-04 ± 4.41%										
step	T (C)	t (min.)		^{36}Ar	%err	^{37}Ar	%err	^{38}Ar	%err	^{39}Ar	%err	^{40}Ar	%err	$\chi^{20}\text{Ar}$	% $^{40}\text{Ar}^*$	$^{40}\text{Ar}/^{39}\text{ArK}$	Age (Ma)	1s.d.
1	500	12	8.55E-06 ± 0.87	1.10E-04 ± 16.34	1.52E-06 ± 2.80	9.74E-07 ± 4.01	2.69E-03 ± 0.08	0.001	5.99	200.714	50.11	29.35						
2	600	12	1.57E-06 ± 2.44	1.14E-04 ± 36.07	3.07E-07 ± 10.87	1.48E-06 ± 3.51	6.81E-04 ± 0.22	0.003	32.06	165.936	41.52	4.13						
3	700	12	1.95E-06 ± 2.72	1.73E-04 ± 14.55	3.59E-07 ± 8.22	3.12E-06 ± 1.89	8.30E-04 ± 0.16	0.008	30.66	90.816	22.84	1.08						
4	800	12	1.66E-06 ± 2.66	4.38E-05 ± 101.98	4.12E-07 ± 5.66	7.35E-06 ± 1.69	1.00E-03 ± 0.19	0.018	50.83	70.420	17.74	0.45						
5	850	12	3.75E-07 ± 10.29	7.20E-06 ± 606.03	1.67E-07 ± 12.73	3.07E-06 ± 2.14	3.48E-04 ± 0.32	0.022	68.12	77.850	19.60	0.85						
6	890	12	6.09E-07 ± 4.66	1.20E-05 ± 350.36	3.00E-07 ± 9.26	5.28E-06 ± 1.99	5.48E-04 ± 0.19	0.030	67.15	69.658	17.55	0.47						
7	930	12	1.20E-06 ± 3.51	1.82E-04 ± 22.63	1.10E-06 ± 4.27	6.25E-05 ± 1.16	4.45E-03 ± 0.09	0.117	92.07	66.116	16.66	0.06						
8	960	12	9.59E-07 ± 2.93	8.78E-05 ± 55.71	1.15E-06 ± 4.37	6.89E-05 ± 1.19	4.82E-03 ± 0.07	0.214	94.12	66.173	16.67	0.07						
9	1010	12	1.65E-06 ± 3.05	3.32E-04 ± 13.96	2.61E-06 ± 1.39	1.79E-04 ± 1.14	1.23E-02 ± 0.05	0.464	96.03	66.272	16.70	0.04						
10	1100	12	2.20E-06 ± 1.49	6.45E-04 ± 7.11	4.20E-06 ± 1.24	2.93E-04 ± 1.13	1.98E-02 ± 0.03	0.874	96.71	65.898	16.60	0.04						
11	1300	12	6.50E-07 ± 5.65	3.11E-04 ± 21.75	1.24E-06 ± 2.41	9.00E-05 ± 1.14	6.12E-03 ± 0.06	1.000	96.86	66.433	16.74	0.04						
Total Gas Age =																		
Plateau Age (based on steps 4 - 9) =																		
Isochron Age =																		

PNG09-005a Louisiana Archipelago diorite sill				hornblende 10.63 mg				J= 1.42623E-04 ± 0.50%										
step	T (C)	t (min.)		^{36}Ar	%err	^{37}Ar	%err	^{38}Ar	%err	^{39}Ar	%err	^{40}Ar	%err	$\chi^{20}\text{Ar}$	% $^{40}\text{Ar}^*$	$^{40}\text{Ar}/^{39}\text{ArK}$	Age (Ma)	1s.d.
1	600	12	3.81E-06 ± 1.41	3.52E-05 ± 2.08	7.33E-07 ± 4.54	2.03E-06 ± 1.59	1.25E-03 ± 0.14	0.028	9.91	64.003	16.39	1.83						
2	750	12	7.19E-07 ± 3.62	1.69E-06 ± 14.25	1.31E-07 ± 9.09	1.92E-06 ± 1.76	3.10E-04 ± 0.31	0.054	31.41	51.023	13.08	0.58						
3	850	12	4.89E-07 ± 3.76	5.73E-06 ± 4.84	1.07E-07 ± 19.57	1.84E-06 ± 2.02	2.15E-04 ± 0.50	0.079	32.77	38.677	9.92	0.53						
4	925	12	1.29E-06 ± 2.59	7.26E-05 ± 1.50	3.71E-07 ± 3.30	1.30E-05 ± 1.38	9.57E-04 ± 0.15	0.258	60.18	44.938	11.53	0.16						
5	975	12	9.50E-07 ± 5.51	8.09E-05 ± 1.59	3.90E-07 ± 3.84	1.29E-05 ± 1.51	8.72E-04 ± 0.18	0.434	67.82	46.822	12.01	0.18						
6	1025	12	1.77E-06 ± 2.23	1.99E-04 ± 0.87	7.00E-07 ± 3.55	3.03E-05 ± 1.18	1.90E-03 ± 0.17	0.849	72.55	46.408	11.90	0.07						
7	1075	12	6.26E-07 ± 16.71	6.19E-04 ± 1.62	2.37E-07 ± 6.51	1.01E-05 ± 1.65	6.66E-04 ± 0.18	0.987	72.21	48.574	12.46	0.21						
8	1125	12	1.63E-07 ± 9.58	3.02E-06 ± 10.64	2.42E-08 ± 38.23	6.07E-07 ± 3.58	5.97E-05 ± 1.34	0.996	19.26	19.497	5.01	0.93						
9	1200	12	1.92E-07 ± 12.16	6.62E-07 ± 43.21	4.31E-08 ± 29.21	3.07E-07 ± 7.85	6.69E-05 ± 1.22	1.000	15.20	33.514	8.60	4.41						
Total Gas Age =																		
Plateau Age (based on steps 4 - 9) =																		
Isochron Age =																		

PNG10-005b Woodlark Island andesite				hornblende 28.54 mg				J= 1.36390E-04 ± 4.92%										
step	T (C)	t (min.)		^{36}Ar	%err	^{37}Ar	%err	^{38}Ar	%err	^{39}Ar	%err	^{40}Ar	%err	$\chi^{20}\text{Ar}$	% $^{40}\text{Ar}^*$	$^{40}\text{Ar}/^{39}\text{ArK}$	Age (Ma)	1s.d.
1	500	12	1.84E-06 ± 2.67	1.19E-05 ± 3.88	3.88E-07 ± 6.74	4.26E-06 ± 1.87	8.71E-04 ± 0.52	0.025	37.49	75.577	18.82	0.80						
2	600	12	1.35E-06 ± 3.23	6.90E-06 ± 6.08	2.61E-07 ± 11.07	3.91E-06 ± 1.63	6.12E-04 ± 0.23	0.048	34.82	53.690	13.42	0.47						
3	700	12	1.56E-06 ± 1.77	4.83E-05 ± 10.15														

Appendix 2.3 $^{40}\text{Ar}/^{39}\text{Ar}$ Data Tables - Paleocene igneous rocks

PNG03-188 Panapom pom Is. metabasalt whole rock				97.72 mg						J=	1.26226E-04	\pm	2.76%						
step	T (C)	t (min.)		^{36}Ar	%err	^{37}Ar	%err	^{38}Ar	%err	^{39}Ar	%err	^{40}Ar	%err	$\Sigma^{39}\text{Ar}$	$\%^{40}\text{Ar}^*$	$^{40}\text{Ar}/^{39}\text{ArK}$	Age (Ma)	1s.d.	
1	500	12	8.84E-05 \pm 0.21	3.17E-04 \pm 1.79	1.65E-05 \pm 0.59	6.65E-06 \pm 1.51	2.63E-02 \pm 0.03	0.044	0.62	-*	7.4828	9.3							
2	600	12	1.21E-05 \pm 0.96	2.13E-04 \pm 2.56	2.12E-06 \pm 2.15	7.70E-06 \pm 1.32	4.05E-03 \pm 0.09	0.095	11.62	58.3924	14.3408	0.9							
3	700	12	9.97E-06 \pm 0.52	1.08E-04 \pm 2.13	1.85E-06 \pm 2.79	9.53E-06 \pm 1.75	3.53E-03 \pm 0.09	0.158	16.62	59.4760	14.2172	1.1							
4	800	12	1.58E-05 \pm 0.48	2.91E-04 \pm 1.32	3.07E-06 \pm 2.47	1.34E-05 \pm 1.25	5.21E-03 \pm 0.08	0.247	10.41	38.2315	9.5016	0.5							
5	900	12	1.98E-05 \pm 0.44	2.17E-03 \pm 0.67	4.20E-06 \pm 1.49	2.69E-05 \pm 1.17	7.05E-03 \pm 0.07	0.425	17.22	46.6992	11.1144	0.2							
6	1000	12	1.54E-05 \pm 0.38	2.25E-03 \pm 0.55	3.52E-06 \pm 1.17	2.75E-05 \pm 1.14	5.67E-03 \pm 0.07	0.608	19.67	42.4601	10.0314	0.1							
7	1100	12	2.87E-05 \pm 0.50	1.39E-03 \pm 1.30	5.61E-06 \pm 0.84	1.41E-05 \pm 1.26	9.37E-03 \pm 0.06	0.701	9.44	61.8467	15.4551	0.9							
8	1200	12	7.10E-05 \pm 0.26	5.68E-03 \pm 0.45	1.42E-05 \pm 0.57	4.04E-05 \pm 1.22	2.58E-02 \pm 0.03	0.969	18.82	123.7941	29.1991	0.7							
9	1300	12	1.45E-05 \pm 0.48	8.13E-04 \pm 0.59	2.90E-06 \pm 1.35	4.29E-06 \pm 2.30	4.57E-03 \pm 0.07	0.998	6.62	70.7330	18.4372	5.1							
10	1500	12	3.59E-06 \pm 3.31	1.39E-04 \pm 2.22	3.15E-07 \pm 12.76	3.55E-07 \pm 7.78	5.10E-04 \pm 0.61	1.000	-*	-*	-*	-*							
													Total Gas Age =	16.41	0.33				

PNG10-017 Woodlark Island metabasalt whole rock				128.9 mg						J=	1.30810E-04	\pm	3.24%						
step	T (C)	t (min.)		^{36}Ar	%err	^{37}Ar	%err	^{38}Ar	%err	^{39}Ar	%err	^{40}Ar	%err	$\Sigma^{39}\text{Ar}$	$\%^{40}\text{Ar}^*$	$^{40}\text{Ar}/^{39}\text{ArK}$	Age (Ma)	1s.d.	
1	500	12	1.44E-05 \pm 0.45	1.63E-04 \pm 1.68	2.66E-06 \pm 1.63	2.07E-06 \pm 2.40	4.50E-03 \pm 0.06	0.024	5.35	102.3802	29.01	11.0							
2	600	12	1.09E-05 \pm 1.02	4.51E-04 \pm 1.05	1.97E-06 \pm 1.52	4.87E-06 \pm 2.42	3.29E-03 \pm 0.08	0.081	2.49	14.3260	5.01	3.5							
3	700	12	1.13E-05 \pm 0.65	6.44E-04 \pm 1.42	2.10E-06 \pm 1.17	6.13E-06 \pm 1.52	3.61E-03 \pm 0.08	0.153	7.35	42.7416	11.40	1.5							
4	800	12	2.00E-05 \pm 0.68	9.59E-04 \pm 0.93	3.69E-06 \pm 1.91	1.01E-05 \pm 1.27	6.40E-03 \pm 0.08	0.271	7.88	48.9507	12.95	1.0							
5	900	12	9.90E-06 \pm 0.73	6.47E-04 \pm 0.90	1.82E-06 \pm 4.46	9.35E-06 \pm 1.72	3.31E-03 \pm 0.10	0.380	11.60	41.1454	10.45	1.1							
6	1100	12	4.93E-05 \pm 0.45	4.69E-03 \pm 0.47	9.31E-06 \pm 0.87	2.78E-05 \pm 1.32	1.71E-02 \pm 0.03	0.706	15.13	97.3873	24.13	1.3							
7	1200	12	3.12E-05 \pm 0.55	1.01E-02 \pm 0.44	5.84E-06 \pm 0.99	2.41E-05 \pm 1.32	1.19E-02 \pm 0.04	0.989	22.78	133.6090	32.22	1.3							
8	1300	12	2.52E-06 \pm 2.24	2.90E-04 \pm 2.14	3.65E-07 \pm 7.67	5.87E-07 \pm 4.04	4.32E-04 \pm 0.35	0.996	1.30	25.7600	10.88	17.0							
9	1550	12	2.63E-06 \pm 3.08	2.18E-04 \pm 1.90	2.76E-07 \pm 11.57	3.49E-07 \pm 6.95	4.11E-04 \pm 0.58	1.000	-*	-*	-*	-*							
													Total Gas Age =	21.52	0.61				

Appendix 3.1 Whole rock geochemical concentrations. (major element in wt%, trace elements in ppm)

Table 3.1									
Sample ID	PNG03-075a	PNG03-075b	PNG03-075c	PNG03-084	PNG03-117	PNG08-004a	PNG08-005a	PNG08-005b	PNG08-055a
Location	Dawson Strait	Dawson Strait	Dawson Strait	Dawson Strait	Moresby Strait	Moresby Strait	Moresby Strait	Moresby Strait	Dawson Strait
Dobu ls.	Dobu ls.	Dobu ls.	Dobu ls.	Fergusson ls.	Goodenough ls.	Goodenough ls.	Goodenough ls.	Goodenough ls.	Fergusson ls.
SiO ₂	62.24	70.9	70.3	64.91	48.34	62.34	53.43	52.8	67.38
Al ₂ O ₃	13.23	12.12	11.69	14.48	14.78	18.14	18.33	18.46	15.87
Fe ₂ O ₃	3.6	4.61	6.15	4.75	9.43	4.22	8.44	8.93	3.46
CaO	1.16	0.19	0.21	0.44	10.38	0.88	4.01	4.3	0.29
MgO	3.24	0.15	0.26	0.84	8.34	2.16	8.08	8.21	0.29
Na ₂ O	4.43	5.79	5.2	2.85	2.78	4.91	3.62	3.56	6.52
K ₂ O	3.9	4.83	4.95	4.51	1.38	3.57	1.41	1.24	3.81
MnO	0.38	0.3	0.43	0.29	1.57	0.84	1.11	1.09	0.5
TiO ₂	0.06	0.02	0.02	0.05	0.6	0.36	0.32	0.28	0.03
P ₂ O ₅	0.09	0.14	0.15	0.1	0.15	0.1	0.14	0.14	0.09
Cr ₂ O ₃	0.009	<0.002	<0.002	<0.002	0.073	<0.002	<0.002	<0.002	<0.002
Ba	187	15	12	615	577	1005	531	489	595
LOI	7.5	0.7	0.4	6.6	1.8	2.2	0.8	0.7	1.6
Total	99.97	99.97	99.98	99.99	99.79	99.98	99.91	99.89	100
Li	30	49	30	10	10	14	6	7	23
Be	3.5	6.0	5.2	3.3	0.9	1.5	0.7	0.7	3.8
Sc	4.4	3.0	4.6	3.5	17.3	4.1	14.8	17.6	6.2
V	10	0	0	3	189	44	222	167	6
Cr	56	6	1	4	432	3	4	8	2
Co	3.2	0.7	0.6	2.3	34.0	4.3	20.1	62.1	1.1
Ni	26.8	3.1	2.1	27.9	207.0	7.2	7.1	29.9	3.3
Cu	5.1	3.5	4.7	4.4	42.2	5.0	50.0	40.3	1.9
Zn	68	140	106	88	75	65	88	87	102
Ga	19	24	25	18	13	17	17	17	22
As	5.4	3.5	8.4	2.6	1.1	0.9	1.2	0.7	1.8
Rb	79	127	110	92	24	67	16	15	84
Sr	192	5	6	60	546	262	801	802	25
Y	51	58	88	47	20	32	20	18	36
Zr	658	1178	1093	504	150	276	147	146	754
Nb	19	33	31	15	7	9	3	3	23
Mo	2.9	1.0	2.1	2.7	0.6	2.7	0.7	5.3	1.4
Sn	4.4	8.1	7.1	3.9	1.2	1.4	0.9	0.9	5.5
Sb	0.30	0.33	0.28	0.25	0.06	0.11	0.02	0.04	0.18
Cs	3.0	2.8	0.3	3.8	0.5	0.5	0.2	0.2	1.2
Ba	124	10	10	412	394	644	363	334	528
La	32	37	54	27	19	33	14	13	22
Ce	67	108	119	58	41	65	30	27	46
Pr	8.0	9.7	14.1	7.1	5.6	7.9	4.1	3.7	5.2
Nd	29	35	52	27	24	30	18	16	19
Sm	6.7	8.7	12.0	6.6	5.3	6.3	4.2	24.0	3.9
Eu	0.55	0.43	0.80	0.88	1.60	1.62	1.26	1.14	1.07
Gd	6.1	7.4	10.9	6.2	4.5	5.0	3.7	3.4	3.7
Tb	1.08	1.44	2.03	1.06	0.61	0.76	0.53	0.50	0.72
Dy	7.2	9.8	13.8	7.0	3.4	4.6	3.1	2.9	5.1
Ho	1.6	2.1	3.0	1.5	0.6	0.9	0.6	0.6	1.2
Er	4.7	6.6	9.3	4.4	1.6	2.6	1.6	1.5	3.9
Tm	0.77	1.13	1.52	0.71	0.22	0.39	0.24	0.22	0.68
Yb	5.2	8.0	10.3	4.7	1.3	2.6	1.5	1.4	4.9
Lu	0.81	1.29	1.66	0.73	0.20	0.41	0.23	0.21	0.79
Hf	12.5	23.7	20.8	10.2	3.0	5.5	3.3	3.3	16.7
Ta	1.0	1.9	1.7	0.8	0.3	0.6	0.1	0.1	1.4
Pb	17.1	24.7	22.8	16.4	4.6	14.5	5.6	5.6	20.6
Th	10.3	16.5	14.8	8.9	2.5	9.5	2.2	2.2	15.2
U	2.9	4.1	4.0	2.3	0.7	2.6	0.5	0.4	3.9
La _N /Yb _N	7.55	5.64	6.34	7.02	17.12	15.66	11.63	11.09	5.41
Eu/Eu*	0.26	0.16	0.21	0.41	0.97	0.85	0.94	0.82	0.85
Ce/Ce*	0.95	1.30	0.99	0.95	0.93	0.90	0.90	0.92	0.97
Nb*/Nb	2.29	1.08	2.17	2.32	3.56	4.99	5.55	5.02	1.23
Ta*/Ta	3.34	1.07	3.00	3.27	5.48	7.19	9.99	8.75	1.61

Table 3.1 cont.									
Sample ID	PNG08-058a	PNG08-059a	PNG08-059b	PNG08-060a	PNG08-061a	PNG08-061b	PNG08-063a	PNG08-064a	PNG08-065a
Location	Dawson Strait								
Sanaroa Is.	Fergusson Is.	Fergusson Is.	Fergusson Is.	Fergusson Is.	Fergusson Is.	Fergusson Is.	Fergusson Is.	Fergusson Is.	Oiau Is.
SiO ₂	68.88	66.77	68.51	69.53	69.97	69.77	70.26	54.53	69.77
Al ₂ O ₃	16.15	13.26	14.22	14.28	14.25	14.23	12.67	11.39	12.91
Fe ₂ O ₃	2.51	5.74	4.41	3.08	3.47	3.46	4.27	2.87	4.41
CaO	0.07	0.21	0.16	0.19	0.26	0.21	0.13	1.16	0.24
MgO	0.64	0.28	0.35	0.35	0.38	0.31	0.23	1.15	0.28
Na ₂ O	5.49	5.4	6.33	6.13	6.46	6.42	6.03	9.6	5.97
K ₂ O	4.46	4.59	4.83	5.07	4.15	4.18	4.69	3.95	4.84
MnO	0.29	0.31	0.29	0.28	0.33	0.33	0.26	0.25	0.32
TiO ₂	0.04	0.04	0.04	0.03	0.05	0.1	0.02	0.03	0.02
P ₂ O ₅	0.04	0.08	0.1	0.09	0.1	0.09	0.09	0.08	0.12
Cr ₂ O ₃	<0.002	0.002	0.003	<0.002	<0.002	<0.002	<0.002	<0.002	<0.002
Ba	733	107	94	38	388	382	11	90	24
LOI	1.3	3.1	0.6	0.8	0.4	0.7	1.1	14.8	0.9
Total	100	99.98	99.99	99.99	100	99.99	99.99	99.98	99.98
Li	19	38	40	51	36	33	39	37	50
Be	2.8	4.7	4.3	5.4	3.9	5.2	5.9	4.3	7.0
Sc	3.4	5.2	4.5	4.1	6.8	6.6	3.5	4.7	5.6
V	4	2	1	1	2	2	4	2	1
Cr	1	13	17	0	0	0	0	2	0
Co	0.7	0.6	0.7	0.5	0.6	0.5	0.4	0.6	0.4
Ni	0.1	3.0	59.8	0.3	0.6	0.2	1.2	1.5	0.0
Cu	2.7	4.4	13.2	4.4	4.3	2.4	7.9	3.6	4.4
Zn	67	117	97	110	100	61	94	74	128
Ga	18	24	21	24	23	23	28	20	29
As	1.9	8.5	3.0	5.1	0.8	3.3	2.9	4.7	1.7
Rb	113	101	93	114	97	95	140	89	133
Sr	64	10	3	6	8	12	4	84	5
Y	41	68	61	72	44	58	35	59	117
Zr	406	930	827	939	879	868	1602	805	1370
Nb	13	26	23	28	24	24	41	22	36
Mo	2.1	4.7	15.6	4.3	1.3	1.0	1.1	3.5	1.5
Sn	3.4	7.8	5.6	7.7	8.3	7.2	14.0	6.9	12.9
Sb	0.16	0.50	0.30	0.36	0.16	0.17	0.32	0.43	0.18
Cs	2.2	3.8	3.1	4.6	0.9	0.8	1.0	3.9	1.0
Ba	521	105	67	35	396	353	11	97	27
La	46	48	39	53	35	44	36	49	88
Ce	55	102	82	112	75	95	125	102	172
Pr	11.8	11.8	9.6	12.9	9.2	11.4	11.1	12.1	21.3
Nd	41	43	35	47	34	42	40	44	78
Sm	8.3	9.3	7.9	9.9	7.3	8.9	8.4	9.1	16.1
Eu	1.20	0.64	0.47	0.47	0.90	1.03	0.31	0.60	0.92
Gd	6.3	8.8	7.2	8.8	6.5	7.9	6.4	8.4	15.5
Tb	1.03	1.65	1.32	1.64	1.19	1.41	1.20	1.53	2.81
Dy	6.3	11.2	8.8	11.1	7.8	9.2	7.9	10.2	19.0
Ho	1.3	2.5	1.9	2.4	1.7	2.0	1.7	2.2	4.2
Er	3.7	7.6	5.9	7.4	5.2	5.9	5.2	6.8	12.8
Tm	0.58	1.23	0.96	1.22	0.90	0.98	0.97	1.11	2.05
Yb	4.0	8.5	6.6	8.5	6.6	6.8	7.8	7.6	13.9
Lu	0.62	1.34	1.04	1.33	1.09	1.08	1.36	1.19	2.21
Hf	8.8	20.9	16.2	20.6	19.9	18.8	37.0	18.7	32.3
Ta	0.8	1.7	1.3	1.7	1.6	1.5	2.7	1.5	2.4
Pb	18.6	38.6	20.2	27.4	28.4	19.0	41.6	23.8	33.9
Th	12.1	16.5	12.8	17.4	19.4	18.0	26.2	15.2	22.8
U	3.5	4.6	3.6	4.9	1.3	3.7	1.4	4.3	2.6
La _N /Yb _N	14.29	6.96	7.22	7.63	6.44	7.87	5.60	7.81	7.68
Eu/Eu*	0.48	0.21	0.18	0.15	0.39	0.36	0.12	0.20	0.17
Ce/Ce*	0.53	0.96	0.95	0.96	0.95	0.97	1.48	0.95	0.90
Nb*/Nb	8.51	2.43	2.22	2.48	1.88	2.33	0.69	2.89	3.43
Ta*/Ta	19.28	3.09	3.24	3.26	2.20	2.91	0.49	3.52	4.49

Table 3.1 cont.									
Sample ID	PNG08-069b	PNG10-063a	PNG10-064a	PNG10-065a	PNG10-067a	PNG03-001	PNG03-004	PNG03-005b	PNG03-006
Location	Dawson Strait	Dawson Strait	Dawson Strait	Dawson Strait	Dawson Strait	Sewa Bay	Sewa Bay	Sewa Bay	Sewa Bay
	Dobu Is.	Goodenough Is.	Goodenough Is.	Goodenough Is.	Fergusson Is.	Normanby Is.	Normanby Is.	Normanby Is.	Normanby Is.
SiO ₂	70.34	-	52.49	52.65	70.19	57.22	58.77	57.61	56.57
Al ₂ O ₃	12.22	-	15.76	15.69	15.6	16.17	16.42	17.37	16.07
Fe ₂ O ₃	4.63	-	7.63	7.99	1.57	6.02	5.93	5.67	7
CaO	0.12	-	8.12	8.17	0.23	3.73	2.85	2.64	3.79
MgO	0.25	-	7.86	8.11	0.57	4.89	4.5	4.96	5.38
Na ₂ O	6.17	-	3.57	3.51	4.85	4.09	4.11	3.98	3.78
K ₂ O	4.82	-	1.54	1.54	4.64	3.52	3.14	2.66	2.83
MnO	0.3	-	1.14	1.17	0.28	1.23	1.3	1.08	1.13
TiO ₂	0.02	-	0.37	0.37	0.03	0.47	0.48	0.34	0.41
P ₂ O ₅	0.12	-	0.12	0.13	0.02	0.09	0.09	0.09	0.07
Cr ₂ O ₃	<0.002	-	0.046	0.05	<0.002	0.026	0.008	0.003	0.052
Ba	10	-	517	510	831	1039	924	736	802
LOI	0.7	-	1	0.3	1.9	2.2	2.1	3.3	2.6
Total	99.97	-	99.84	99.84	100.02	99.91	99.94	99.94	99.91
Li	71	14.24	15.98	15.10	18.74	16	29	20	10.79
Be	7.7	1.05	1.05	1.04	1.79	1.7	1.5	1.2	1.40
Sc	4.9	18.95	20.8	21.1	2.3	10.7	10.8	8.8	17.23
V	1	170.22	205.01	216.85	3.92	81	118	91	85.2
Cr	1	367.46	417.41	464.57	25.93	163	50	19	334.17
Co	0.4	26.51	34.98	35.98	4.65	18.9	14.6	11.9	23.82
Ni	1.4	84.88	1518.68	1394.65	1379.65	130.6	44.4	10.6	147.95
Cu	4.9	25.89	30.87	27.48	1.74	46.1	29.1	11.2	31.10
Zn	142	60.76	-	-	-	60	61	47	-
Ga	30	14.77	17.44	17.29	17.56	20	20	16	20.01
As	6.9	-	2.8	1.9	0.5	2.2	1.9	2.4	4.2
Rb	156	39.38	35.786	33.997	120.155	71	87	61	65.51
Sr	2	599.28	649.76	628.93	80.01	696	634	563	699.59
Y	115	22.88	23.184	22.741	13.802	25	28	21	24.23
Zr	1539	182.84	180.642	176.115	342.016	310	289	163	274.05
Nb	42	7.54	7.70	7.92	10.37	12	12	8	10.92
Mo	6.3	0.80	0.88	0.85	1.88	0.4	0.6	0.5	0.54
Sn	12.9	1.64	1.73	1.56	2.63	2.1	2.1	1.1	2.1
Sb	0.58	0.10	0.21	0.19	0.24	0.20	0.20	0.26	0.16
Cs	7.2	1.78	1.51	1.44	2.07	0.3	1.4	1.2	0.91
Ba	11	524.29	507.63	511.99	781.29	882	833	470	825.40
La	83	25.36	24.79	24.81	24.66	37	32	17	36.99
Ce	178	53.38	52.78	52.83	43.40	74	69	36	75.48
Pr	21.1	6.69	6.51	6.53	4.65	9.2	8.5	4.4	9.37
Nd	76	27.62	26.88	26.90	16.11	36	34	18	37.96
Sm	16.0	1.67	5.55	5.42	2.80	7.2	7.2	4.2	7.16
Eu	0.76	5.71	1.59	1.57	0.79	1.76	1.86	1.17	1.89
Gd	15.2	5.20	4.90	4.81	2.08	5.5	5.9	3.6	5.93
Tb	2.86	0.73	0.71	0.71	0.35	0.76	0.84	0.53	0.81
Dy	19.0	4.26	4.15	4.14	2.20	4.2	4.8	3.1	4.43
Ho	4.2	0.85	0.81	0.81	0.46	0.8	0.9	0.6	0.84
Er	12.9	2.26	2.18	2.16	1.37	2.1	2.5	1.7	2.22
Tm	2.10	0.32	0.32	0.32	0.22	0.30	0.36	0.25	0.31
Yb	14.5	2.10	2.05	2.02	1.53	1.9	2.3	1.6	2.00
Lu	2.24	0.32	0.31	0.31	0.23	0.28	0.34	0.24	0.30
Hf	34.6	4.51	4.57	4.46	8.92	7.2	6.6	3.6	6.65
Ta	2.7	0.44	0.45	0.47	0.76	0.7	0.7	0.4	0.68
Pb	44.6	10.45	10.67	10.29	22.50	16.3	14.0	9.4	15.93
Th	27.5	6.10	6.25	6.10	12.52	11.1	8.4	5.3	9.32
U	7.9	1.61	1.71	1.57	2.71	1.6	1.9	1.4	1.60
La _N /Yb _N	7.04	50.90	47.73	50.39	19.61	24.58	17.41	13.48	22.58
Eu/Eu*	0.15	0.98	0.91	0.91	0.95	0.82	0.84	0.89	0.86
Ce/Ce*	0.96	0.90	0.97	0.96	0.86	0.90	0.95	0.94	0.92
Nb*/Nb	2.59	16.55	13.54	13.81	3.78	4.33	3.51	2.94	4.64
Ta*/Ta	3.16	16.55	13.54	13.81	4.89	6.56	4.96	4.17	6.12

Table 3.1 cont.									
Sample ID	PNG03-058a	PNG03-065	PNG06-043a	PNG06-043b	PNG10-057a	PNG10-058a	PNG10-059a	PNG10-060a	PNG10-061a
Location	Near Sewa Bay Normanby Is.	Sewa Bay Normanby Is.	Woodlark Rise Nuamata Is.						
SiO ₂	47.33	55.17	61.21	50.36	65.15	61.64	62.2		
Al ₂ O ₃	13.55	15.93	15.2	14.59	14.79	15.54	15.43		
Fe ₂ O ₃	13.7	6.31	4.63	9.13	3.65	4.53	4.58		
CaO	6.75	4.31	4.56	8.91	1.08	3.97	4.7		
MgO	9.69	6.06	4.1	9.92	2.21	4.21	4.01		
Na ₂ O	2.49	3.74	4.67	2.92	2.55	4.5	4.23		
K ₂ O	0.07	2.25	2.72	1.08	7.71	2.65	2.6		
MnO	1.26	1.21	0.58	0.45	1.03	0.64	0.62		
TiO ₂	0.13	0.4	0.19	0.09	0.42	0.23	0.2		
P ₂ O ₅	0.21	0.09	0.06	0.13	0.04	0.06	0.09		
Cr ₂ O ₃	0.009	0.023	0.037	0.058	0.01	0.037	0.039		
Ba	30	787	733	266	2200	711	700		
LOI	4.6	4.2	1.7	2	0.8	1.7	1		
Total	99.82	99.9	99.92	99.82	99.92	99.93	99.92		
Li	13.89	11.41	13	30	23.86	19.61	12.07	15.54	14.55
Be	0.40	1.59	1.3	0.8	1.86	1.80	1.24	1.65	1.47
Sc	44.55	15.90	7.4	27.8	10.2	10.38	12.0	9.76	9.99
V	332.5	115.2	64	186	86.60	46.6	110.02	70.49	77.57
Cr	48.07	142.72	185	360	320.53	278.42	388.19	303.82	274.68
Co	48.52	22.18	14.6	30.8	20.67	20.83	24.78	18.69	15.76
Ni	38.29	96.63	107.5	164.3	1532.51	155.31	1607.43	136.40	119.75
Cu	170.51	30.76	16.4	30.7	21.96	26.23	28.34	18.27	28.51
Zn	-	-	66	79	19.05	18.97	18.04	53.13	49.77
Ga	16.95	18.97	16	13	-	-	-	16.98	16.21
As	4.1	3.2	2.5	1.8	2.4	3.7	4.8	-	-
Rb	0.82	51.13	56	19	67.168	69.64	52.200	66.45	65.51
Sr	144.09	570.44	583	356	723.56	664.07	948.53	688.76	742.15
Y	31.72	28.13	9	9	14.561	14.42	15.791	12.94	14.51
Zr	79.73	278.52	124	52	186.613	179.86	155.234	164.21	152.81
Nb	5.51	14.60	4	2	5.53	5.52	4.83	4.51	4.50
Mo	0.30	0.78	3.5	9.0	0.63	0.59	0.70	0.52	0.49
Sn	0.8	2.2	0.9	0.9	1.29	2.0	1.07	1.21	1.09
Sb	0.24	0.09	0.25	0.20	0.30	0.21	0.39	0.28	0.20
Cs	0.14	3.85	1.2	1.2	1.30	2.45	1.52	1.59	2.61
Ba	31.54	766.80	488	180	706.77	700.61	837.61	719.87	686.55
La	6.43	32.99	14	9	23.12	23.32	27.83	24.77	20.63
Ce	14.44	68.42	30	18	48.20	48.60	56.11	49.21	42.01
Pr	1.99	8.64	3.6	2.2	5.81	5.80	6.95	6.17	5.27
Nd	9.77	35.04	14	9	23.34	22.96	28.52	24.15	21.18
Sm	3.04	6.94	3.0	2.0	4.50	4.49	5.38	1.23	1.17
Eu	1.10	1.86	0.80	0.57	1.20	1.20	1.43	4.74	4.37
Gd	4.32	6.19	2.2	1.6	3.51	3.61	4.14	3.68	3.61
Tb	0.79	0.89	0.28	0.22	0.47	0.48	0.56	0.46	0.48
Dy	5.32	5.08	1.5	1.3	2.62	2.60	2.99	2.48	2.58
Ho	1.17	0.98	0.3	0.3	0.49	0.48	0.56	0.45	0.50
Er	3.41	2.71	0.7	0.7	1.24	1.29	1.43	1.21	1.32
Tm	0.51	0.39	0.10	0.10	0.18	0.18	0.21	0.17	0.19
Yb	3.39	2.50	0.6	0.7	1.14	1.15	1.33	1.02	1.21
Lu	0.54	0.39	0.09	0.10	0.17	0.18	0.20	0.15	0.19
Hf	2.37	6.82	2.9	1.3	5.04	4.81	4.23	4.40	4.27
Ta	0.37	0.93	0.2	0.1	0.35	0.38	0.30	0.27	0.29
Pb	1.88	13.38	15.3	7.9	18.92	18.85	19.97	22.58	22.39
Th	0.52	8.34	4.3	2.1	6.85	6.86	7.75	6.41	6.61
U	0.46	1.74	1.1	0.6	1.94	1.89	2.04	1.72	1.84
La _N /Yb _N	2.31	16.10	28.06	15.91	24.79	24.80	25.46	29.49	20.77
Eu/Eu*	0.93	0.85	0.91	0.94	0.89	0.88	0.89	6.33	6.01
Ce/Ce*	0.94	0.92	0.93	0.93	0.94	0.94	0.91	0.90	0.91
Nb ⁺ /Nb	1.45	3.05	5.59	5.59	5.60	5.67	7.99	7.72	6.30
Ta ⁷ /Ta	1.62	3.85	8.53	9.09	7.13	6.62	10.52	10.68	7.98

Table 3.1 cont.									
Sample ID	PNG08-042	PNG10-046a	PNG10-046b	PNG10-047c	PNG10-048a	PNG10-048b	PNG10-048c	PNG10-048d	PNG10-048e
Location	Amphlett ls.								
Yabwiwa ls.	Apuo ls.	Apuo ls.	Wawiwa ls.	Yabwiwa ls.	Yabwiwa ls.	Yabwiwa ls.	Yabwiwa ls.	Yabwiwa ls.	Yabwiwa ls.
SiO ₂	58.96		54.82	60.02	63.01	61.76	62.71	62.45	62.92
Al ₂ O ₃	15.32		14.69	15.17	16.24	14.88	15.4	15.22	15.18
Fe ₂ O ₃	5.6		6.36	4.46	3.78	4.43	3.88	4	3.82
CaO	4.21		8.09	4.38	2.24	3.04	3.71	4	3.68
MgO	5.04		6.16	4.41	3.27	2.5	3.88	3.88	3.72
Na ₂ O	4.02		3.5	3.72	4.84	3.92	3.9	4.07	3.81
K ₂ O	3.16		2.03	3.27	2.97	2.9	3.41	3.48	3.72
MnO	0.9		0.93	0.64	0.61	0.66	0.66	0.66	0.62
TiO ₂	0.35		0.35	0.23	0.23	0.22	0.25	0.26	0.23
P ₂ O ₅	0.08		0.09	0.07	0.06	0.04	0.06	0.06	0.06
Cr ₂ O ₃	0.039		0.052	0.041	0.022	0.028	0.024	0.029	0.022
Ba	985		737	928	940	827	915	958	999
LOI	2		2.5	3.3	2.4	5.3	1.8	1.6	1.9
Total	99.91		99.85	99.92	99.95	99.94	99.93	99.94	99.94
Li	13	14.51	9.62	12.28	15.98	15.94	14.30	14.23	15.68
Be	1.8	2.25	1.18	2.48	2.01	2.29	1.98	2.03	2.20
Sc	11.6	3.7	15.33	10.47	8.32	9.43	9.0	9.1	8.36
V	89	28.30	102.9	68.5	52.9	59.2	67.22	70.84	55.1
Cr	242	50.17	354.30	292.40	163.97	194.91	192.99	234.83	154.54
Co	24.8	5.80	31.75	17.58	17.81	12.03	19.56	20.35	14.78
Ni	146.7	30.59	215.86	120.79	94.95	131.29	1588.14	1641.42	87.49
Cu	19.6	3.02	30.83	25.89	24.18	18.81	12.68	12.24	10.11
Zn	93	-	-	-	-	-	-	-	-
Ga	18	40.46	17.08	19.07	19.67	18.88	19.63	20.02	19.16
As	2.4	18.9	3.0	5.1	2.9	5.4	6.6	6.9	6.2
Rb	72	115.208	40.42	86.76	78.77	81.16	90.591	94.800	116.58
Sr	883	770.41	782.61	768.86	981.65	832.88	886.05	904.72	832.05
Y	16	7.690	17.74	13.79	11.71	13.71	12.991	13.183	12.84
Zr	193	193.376	200.55	196.43	186.98	207.04	189.751	198.462	181.94
Nb	8	4.76	8.56	5.71	5.77	6.55	6.07	6.61	6.58
Mo	0.8	0.10	0.70	0.81	0.49	0.56	1.09	1.15	0.86
Sn	1.4	1.96	1.4	2.0	3.0	1.5	1.51	1.55	1.7
Sb	0.20	0.29	0.07	0.22	0.14	0.35	0.51	0.52	0.23
Cs	2.1	2.97	1.68	5.34	4.49	5.67	5.22	5.44	7.03
Ba	767	1166.76	739.87	917.86	899.20	826.19	889.83	925.50	958.22
La	30	32.43	28.12	34.83	30.59	35.71	29.25	31.97	30.66
Ce	58	63.03	58.27	65.16	60.52	67.57	58.20	63.37	59.94
Pr	7.3	7.56	7.10	7.61	6.96	8.13	6.76	7.28	6.89
Nd	28	28.01	28.04	28.87	26.42	30.70	26.31	27.78	26.32
Sm	5.7	1.23	5.27	5.19	4.80	5.39	4.96	5.18	4.85
Eu	1.51	4.96	1.49	1.31	1.28	1.39	1.27	1.30	1.25
Gd	4.2	3.39	4.33	3.96	3.52	3.96	3.61	3.74	3.66
Tb	0.54	0.35	0.60	0.51	0.46	0.49	0.48	0.49	0.47
Dy	2.8	1.60	3.30	2.67	2.34	2.61	2.54	2.56	2.46
Ho	0.5	0.26	0.62	0.49	0.42	0.48	0.47	0.47	0.45
Er	1.3	0.60	1.64	1.26	1.09	1.24	1.20	1.19	1.17
Tm	0.18	0.08	0.24	0.18	0.16	0.17	0.17	0.17	0.16
Yb	1.1	0.48	1.51	1.13	0.96	1.11	1.09	1.05	1.05
Lu	0.16	0.06	0.23	0.17	0.15	0.17	0.16	0.16	0.16
Hf	4.6	5.29	4.94	5.34	4.88	5.37	4.94	5.16	4.93
Ta	0.4	0.31	0.52	0.42	0.42	0.46	0.42	0.46	0.50
Pb	24.8	43.16	13.61	34.95	31.77	34.26	33.76	33.24	37.25
Th	10.2	14.91	5.86	13.75	11.90	14.01	11.72	13.49	13.89
U	2.7	4.51	1.27	3.74	3.38	3.68	3.38	3.86	4.04
La _n /Yb _n	32.02	82.27	22.77	37.72	38.84	39.17	32.71	37.31	35.77
Eu/Eu [*]	0.89	1.01	0.92	0.84	0.90	0.87	0.87	0.85	0.86
Ce/Ce [*]	0.90	0.90	0.93	0.88	0.92	0.88	0.92	0.92	0.91
Nb ⁺ /Nb	5.56	9.79	4.43	9.11	7.49	8.06	6.77	6.83	6.67
Ta ⁺ /Ta	8.13	13.03	5.93	11.13	8.70	10.05	8.14	8.25	7.57

Table 3.1 cont.

Sample ID	PNG10-049a	PNG10-049b	PNG10-050a	PNG10-051a	PNG10-052a	PNG10-039	PNG10-041C	PNG10-042f	PNG10-044d
Location	Amphlett Is.	Egum Atoll	Egum Atoll	Egum Atoll	Egum Atoll				
	Yamea Is.	Yamea Is.	Yamea Is.	Urasi Is.	Urasi Is.	Center Ids.	Center Ids.	Center Ids.	Center Ids.
SiO ₂	63.59	62.03	60.39	63.47				54.99	57.83
Al ₂ O ₃	15.73	15.43	15.2	16.33				14.04	15.74
Fe ₂ O ₃	3.71	4.06	4.65	3.87				5.6	5.53
CaO	2.97	3.15	4.82	2.27				7.48	3.48
MgO	3.57	4.16	4.7	2.99				7.38	6.38
Na ₂ O	4.36	3.8	3.99	4.47				3.8	4.55
K ₂ O	3.46	3.43	3.3	3.68				2.07	2.15
MnO	0.63	0.74	0.71	0.7				0.61	0.71
TiO ₂	0.2	0.27	0.28	0.25				0.28	0.31
P ₂ O ₅	0.06	0.06	0.06	0.06				0.07	0.09
Cr ₂ O ₃	0.018	0.018	0.028	0.017				0.07	0.053
Ba	1009	938	951	1083				784	879
LOI	1.4	2.5	1.5	1.6				3.2	2.8
Total	99.94	99.94	99.91	99.97				99.85	99.93
Li	16.37	6.02	13.36	15.62	12.58	9.39	11.81	9.70	11.64
Be	1.83	1.88	2.07	2.96	2.07	1.85	1.32	1.06	1.35
Sc	7.8	9.04	10.22	8.3	11.6	14.12	13.57	14.0	16.3
V	65.15	61.6	76.5	35.72	83.93	0.55	0.54	0.55	0.68
Cr	160.64	131.88	213.20	176.78	362.31	544.59	393.23	517.26	433.96
Co	21.68	15.59	17.24	16.90	20.97	29.72	27.62	33.06	27.96
Ni	1555.31	63.84	102.06	1431.80	146.28	362.26	203.91	1693.98	1629.80
Cu	18.38	22.91	20.38	17.08	23.88	34.41	53.16	52.39	34.45
Zn	-	-	-	-	57.65	47.90	-	-	-
Ga	19.95	19.90	18.25	22.02	17.0	14.93	48.05	16.11	17.74
As	3.1	4.4	3.9	2.9	-	-	16.39	1.5	3.1
Rb	97.760	78.80	68.51	95.851	84.526	40.50	45.40	39.153	45.209
Sr	907.72	798.09	857.28	861.87	844.07	1065.15	1202.71	1086.70	1086.56
Y	13.483	13.84	15.52	14.724	18.442	22.06	14.58	11.498	16.061
Zr	194.178	211.32	200.01	220.416	203.029	128.87	147.00	121.503	152.935
Nb	5.99	7.00	6.48	6.44	6.88	4.95	5.40	4.74	5.04
Mo	0.65	0.71	0.50	0.49	0.98	0.47	0.32	0.48	0.70
Sn	1.83	59.9	1.4	2.00	1.65	0.66	0.72	0.62	0.95
Sb	0.41	0.15	0.21	0.54	0.33	0.05	0.19	0.13	0.38
Cs	3.16	3.81	3.08	3.19	4.11	0.55	0.67	0.61	0.87
Ba	961.97	918.97	925.43	1043.16	900.70	814.42	932.48	780.86	874.30
La	39.06	31.40	36.88	36.20	36.97	30.59	29.89	23.25	23.53
Ce	85.76	62.30	69.04	68.89	68.84	52.07	56.90	47.39	47.03
Pr	8.97	7.50	8.39	8.15	8.65	6.84	6.94	5.68	5.88
Nd	33.54	29.24	32.06	31.26	33.44	27.84	27.31	22.59	23.94
Sm	5.93	5.37	5.61	5.78	1.63	1.41	1.35	4.19	4.54
Eu	1.42	1.38	1.38	1.47	6.53	5.06	4.87	1.15	1.26
Gd	3.98	4.04	4.41	4.07	5.05	4.50	3.93	3.08	3.63
Tb	0.52	0.51	0.56	0.52	0.64	0.55	0.49	0.41	0.49
Dy	2.73	2.64	2.97	2.72	3.35	3.01	2.69	2.12	2.79
Ho	0.48	0.48	0.55	0.49	0.62	0.60	0.51	0.40	0.54
Er	1.22	1.24	1.43	1.27	1.61	1.61	1.34	1.03	1.42
Tm	0.17	0.17	0.20	0.18	0.23	0.22	0.19	0.15	0.21
Yb	1.08	1.09	1.31	1.14	1.42	1.36	1.23	0.96	1.31
Lu	0.16	0.16	0.19	0.17	0.21	0.22	0.19	0.15	0.21
Hf	5.19	5.38	5.35	5.78	5.36	3.31	3.74	3.25	4.03
Ta	0.42	0.46	0.46	0.43	0.44	0.27	0.29	0.26	0.29
Pb	32.85	24.98	35.32	35.52	30.90	8.33	11.84	10.55	20.61
Th	13.07	10.53	13.36	14.94	13.59	7.18	8.58	7.13	6.37
U	3.74	3.07	3.82	3.35	3.56	1.87	1.97	1.83	1.74
La _n /Nb _n	44.14	35.08	34.44	38.70	31.80	27.42	29.61	29.40	21.89
Eu/Eu [*]	0.84	0.86	0.81	0.87	0.88	0.85	0.93	0.93	0.91
Ce/Ce [*]	1.02	0.91	0.87	0.89	0.86	0.80	0.88	0.93	0.90
Nb ^{+/} Nb _n	8.30	6.32	8.50	8.25	8.07	10.16	8.13	6.73	6.54
Ta ⁺ /Ta _n	9.11	8.05	10.81	10.90	11.25	18.57	13.46	10.08	9.38

Table 3.1 cont.

Sample ID	PNG03-188	PNG03-191	PNG03-199	PNG10-053a	PNG10-053c	PNG10-053e	PNG10-054a	PNG10-055a	PNG10-056a
Location	Lousiade Arch. Panapompom Is.	Lousiade Arch. Panapompom Is.	Lousiade Arch. Panapompom Is.	Lusancay Is. Wagalasu Is.	Lusancay Is. Wagalasu Is.	Lusancay Is. Wagalasu Is.	Lusancay Is. Simsim Is.	Lusancay Is. Kawa Is.	Lusancay Is. Nauria Is.
SiO ₂				52.75	63.37	63.96	64.08		63.01
Al ₂ O ₃				15.99	14.75	13.87	14.91		15.11
Fe ₂ O ₃				6.87	3.8	3.67	3.92		2.94
CaO				5.49	1.37	2.08	1.22		1.8
MgO				4.76	1.59	3.2	1.5		5.38
Na ₂ O				2.72	2.89	2.38	2.64		3.04
K ₂ O				1.29	8	7.68	8.09		5.41
MnO				0.93	1.07	1.03	1.08		0.92
TiO ₂				0.2	0.44	0.43	0.44		0.39
P ₂ O ₅				0.09	0.04	0.04	0.03		0.04
Cr ₂ O ₃				0.08	0.009	0.013	0.013		0.004
Ba				1419	2505	2400	2450		1654
LOI				8.4	2	1	1.4		1.3
Total				99.87	99.93	99.91	99.93		99.93
Li	5.06	5.48	6.42	6.81	4.91	4.80	4.73	8.01	9.14
Be	0.21	0.24	1.01	2.35	2.40	1.93	1.67	1.61	1.89
Sc	38.93	45.24	10.38	9.2	8.20	9.3	6.43	6.57	8.79
V	248.94	354.98	90.91	70.61	143.7	135.35	117.7	103.38	185.7
Cr	100.60	185.59	148.91	96.53	101.00	122.64	31.88	29.21	90.18
Co	37.42	50.03	13.20	17.37	11.86	17.15	10.43	9.01	16.88
Ni	88.72	80.42	79.52	1449.77	39.74	1381.26	26.04	20.99	44.72
Cu	185.93	50.51	10.79	261.27	260.54	263.67	177.31	41.74	326.86
Zn	57.10	94.72	28.59	-	-	-	-	43.27	-
Ga	14.03	14.28	19.72	27.25	24.85	27.52	24.86	21.55	28.14
As	-	-	-	0.8	1.3	0.4	2.1	-	2.3
Rb	6.08	10.67	48.45	155.369	155.07	160.440	76.63	92.07	167.99
Sr	168.40	148.30	940.00	1500.59	1441.94	1497.07	2600.65	1763.10	1805.29
Y	18.32	28.42	8.84	9.620	9.68	13.544	7.85	9.32	8.95
Zr	42.29	81.26	100.73	704.926	690.98	699.299	441.41	396.52	712.52
Nb	2.86	6.24	2.48	5.03	4.89	5.15	5.71	4.21	5.44
Mo	0.08	0.05	0.25	0.89	0.64	0.81	0.54	0.53	0.82
Sn	0.41	0.67	0.66	2.40	2.8	2.26	1.2	1.49	2.3
Sb	0.76	0.10	0.21	0.22	0.05	0.20	0.05	0.11	0.08
Cs	0.50	0.92	2.41	0.63	0.90	0.84	0.54	0.64	1.00
Ba	37.19	81.87	544.38	2411.72	2622.51	2354.50	1868.00	2056.15	2723.19
La	2.57	4.58	13.82	57.06	56.64	60.43	53.38	51.88	66.81
Ce	6.64	11.97	29.59	111.84	109.64	119.43	108.24	101.66	127.31
Pr	1.01	1.75	3.84	13.07	13.09	15.10	12.86	12.56	14.81
Nd	5.32	8.78	15.80	47.96	47.19	57.62	48.15	46.33	52.76
Sm	0.74	1.08	0.93	7.25	6.78	8.83	6.74	1.88	7.24
Eu	1.79	2.93	3.23	1.74	1.63	2.06	1.78	7.34	1.78
Gd	2.49	3.96	2.50	3.91	4.16	5.31	4.04	4.79	4.35
Tb	0.44	0.71	0.32	0.46	0.46	0.62	0.42	0.50	0.47
Dy	2.94	4.74	1.66	2.15	2.04	2.86	1.82	2.21	2.11
Ho	0.63	1.02	0.31	0.34	0.33	0.48	0.28	0.34	0.34
Er	1.82	2.90	0.80	0.79	0.79	1.13	0.61	0.77	0.82
Tm	0.27	0.44	0.11	0.10	0.10	0.15	0.07	0.09	0.11
Yb	1.76	2.85	0.73	0.64	0.64	0.92	0.46	0.56	0.69
Lu	0.28	0.45	0.11	0.06	0.06	0.10	0.04	0.06	0.06
Hf	1.21	2.24	2.82	19.72	19.23	19.63	11.72	11.76	19.83
Ta	0.17	0.35	0.13	0.29	0.29	0.29	0.32	0.24	0.32
Pb	1.45	1.17	6.61	25.06	23.61	25.12	22.84	29.85	30.33
Th	0.22	0.48	3.62	27.19	25.78	26.73	16.41	18.05	27.07
U	0.09	0.16	1.06	4.69	3.74	4.18	2.02	2.57	3.73
La _N /Yb _N	1.78	1.96	23.20	108.09	107.21	79.96	141.67	112.95	117.46
Eu/Eu*	1.00	1.00	1.06	0.89	0.86	0.84	0.96	0.89	0.89
Ce/Ce*	0.99	1.01	0.93	0.91	0.90	0.89	0.93	0.90	0.89
Nb*/Nb	0.97	0.78	7.29	16.19	16.74	16.59	12.89	17.59	18.02
Ta*/Ta	1.05	0.89	10.68	23.86	24.47	24.57	19.22	26.44	26.98

Table 3.1 cont.

Sample ID	PNG10-001	PNG10-005a	PNG10-005b	PNG10-005c	PNG10-006a	PNG10-008a	PNG10-009a	PNG10-010a	PNG10-010c
Location	Kulamadau Woodlark Is.	Manau Hill Woodlark Is.	Manau Hill Woodlark Is.	Manau Hill Woodlark Is.	NW Loluai Woodlark Is.	Loluai Woodlark Is.	Loluai Woodlark Is.	Loluai Woodlark Is.	Loluai Woodlark Is.
SiO ₂	58.6	50.38	58.17	63.52	48.9	43.09	48.87	48.6	60.83
Al ₂ O ₃	14.63	20.04	16.21	15.13	14.83	13.34	16.29	13.76	15
Fe ₂ O ₃	4.02	7.17	5.77	5.17	11.16	17.72	10.28	14.59	4.75
CaO	2.91	3.25	3.05	2.68	7.21	7.88	7.16	8.31	5.32
MgO	6.45	5.45	5.35	3.99	11.26	7.05	12.57	8.66	5.43
Na ₂ O	3.09	3.65	4.2	3.86	3.02	2.01	2.24	2.36	4.17
K ₂ O	2.54	1.07	1.99	2.26	0.21	1.89	0.22	0.28	2.3
MnO	0.44	0.79	0.61	0.55	1.29	2.8	1.31	2	0.55
TiO ₂	0.15	0.17	0.17	0.15	0.11	0.32	0.11	0.17	0.19
P ₂ O ₅	0.16	0.12	0.12	0.09	0.17	0.34	0.18	0.25	0.07
Cr ₂ O ₃	0.007	0.013	0.011	0.008	0.053	0.002	0.036	0.01	0.034
Ba	767	510	1162	1522	38	300	38	80	902
LOI	6.7	7.6	4	2.2	1.6	3.2	0.5	0.7	1
Total	99.95	99.92	99.94	99.95	99.84	99.74	99.83	99.77	99.9
Li	12.5	24.74	16.18	30.82	4.72	24.77	2.98	5.24	7.54
Be	0.6	0.89	0.86	0.74	0.27	0.40	0.27	0.41	1.42
Sc	11.2	18.59	15.69	14.1	40.22	32.67	42.1	47.8	13.2
TiO ₂	0.4	0.72	0.59	0.54	1.23	2.65	1.26	1.98	0.54
V	92.2	121.9	110.6	108.75	256.3	410.6	282.47	438.24	100.26
Cr	46.3	69.48	57.82	54.92	345.89	3.34	259.09	75.89	287.86
Co	11.1	17.48	17.22	15.88	39.79	80.59	44.94	48.93	24.44
Ni	17.5	28.57	20.06	19.84	72.87	31.79	82.08	58.46	1654.91
Cu	29.7	46.16	17.56	44.04	112.81	452.69	132.78	175.02	92.85
Zn	67.1	-	-	-	-	-	-	-	-
Ga	15.5	22.26	15.70	15.62	15.65	22.50	17.91	21.60	18.25
As	3.0	1.8	4.6	0.6	1.8	2.8	0.6	0.7	1.0
Rb	77.0	19.33	35.87	43.839	3.80	46.85	5.373	5.905	51.869
Sr	1017.6	634.57	1040.47	941.73	161.99	154.44	154.90	274.93	871.88
Y	14.5	23.01	15.52	24.875	21.75	51.43	25.672	39.012	12.686
Zr	99.7	120.08	107.63	97.751	65.42	201.89	71.395	114.739	159.280
Nb	4.1	5.33	4.71	4.19	3.50	13.13	4.04	7.35	4.12
Mo	0.3	0.15	0.13	0.36	0.18	0.54	0.36	0.35	0.42
Sn	0.9	1.4	1.2	2.22	0.7	1.0	0.58	1.00	0.92
Sb	0.7	0.07	0.30	0.17	0.04	0.43	0.06	0.22	0.28
Cs	7.3	3.83	2.92	1.42	0.82	4.81	0.48	0.50	0.45
Ba	751.6	497.74	1288.70	1562.95	39.14	302.74	40.69	88.57	929.21
La	10.9	15.81	12.55	18.37	3.75	12.28	4.13	6.88	22.69
Ce	21.6	29.56	27.07	26.11	9.98	31.10	10.91	17.90	44.81
Pr	2.7	3.71	3.05	4.48	1.54	4.52	1.67	2.66	5.34
Nd	11.3	16.10	12.60	19.49	8.15	22.23	8.61	13.82	21.37
Sm	2.6	3.59	2.66	4.25	2.54	6.55	2.72	4.23	4.05
Eu	0.9	1.15	0.84	1.38	1.02	1.90	1.08	1.59	1.11
Gd	2.6	3.76	2.72	4.40	3.39	8.03	3.72	5.80	3.08
Tb	0.4	0.57	0.41	0.65	0.57	1.37	0.64	0.99	0.42
Dy	2.4	3.56	2.60	3.97	3.70	8.83	4.14	6.51	2.27
Ho	0.5	0.76	0.54	0.81	0.79	1.87	0.88	1.38	0.43
Er	1.4	2.18	1.54	2.21	2.19	5.28	2.42	3.84	1.17
Tm	0.2	0.32	0.24	0.34	0.33	0.79	0.36	0.56	0.17
Yb	1.5	2.13	1.59	2.16	2.09	5.10	2.29	3.59	1.15
Lu	0.2	0.35	0.26	0.34	0.33	0.78	0.36	0.57	0.18
Hf	2.7	3.28	2.97	2.60	1.89	5.43	2.00	3.21	4.32
Ta	0.3	0.37	0.30	0.30	0.24	0.83	0.27	0.45	0.28
Pb	6.6	21.21	25.61	18.19	1.40	2.58	1.12	2.34	13.63
Th	2.6	3.73	3.21	2.87	0.32	1.05	0.32	0.56	9.27
U	0.94	1.36	1.02	0.90	0.10	0.47	0.10	0.17	2.69
La _N /Yb _N	9.17	9.06	9.64	10.36	2.18	2.94	2.20	2.34	24.08
Eu/Eu*	1.02	0.94	0.95	0.96	1.06	0.80	1.04	0.98	0.92
Ce/Ce*	0.90	0.86	0.98	0.65	1.00	0.99	1.00	1.00	0.91
Nb ^{*/Nb}	3.80	4.43	3.46	8.62	1.12	1.03	1.08	1.01	7.79
Ta/Ta	5.15	5.72	4.17	14.41	1.02	1.08	1.02	1.06	9.67

Table 3.1 cont.									
Sample ID	PNG10-011a		PNG10-012a		PNG10-013a		PNG10-014a		PNG10-018
Location	Loluai	Loluai	Loluai	Granite Pt.	Loluai	Loluai	Loluai	Suloga Pt.	Kulamadau
	Woodlark Is.								
SiO ₂	57.15	49.37	48.5		60.28	63.51	48.26	48.9	50.42
Al ₂ O ₃	14.05	13.45	15.35		18.31	16.3	14.43	14.58	16.89
Fe ₂ O ₃	4.87	14.3	10.12		4.66	4.46	10.18	11.61	8.91
CaO	7.52	6.51	8.52		1.77	1.96	9.51	7.48	3.94
MgO	7.37	10.32	10.87		4.89	2.61	11.89	11.84	7.62
Na ₂ O	3.89	2.85	3.03		4.5	3.67	2.64	2.43	3.2
K ₂ O	2.76	0.18	0.09		3.3	4.44	0.25	0.08	2.64
MnO	0.63	1.91	1.07		0.81	0.67	1.02	1.39	1.03
TiO ₂	0.22	0.17	0.08		0.3	0.18	0.09	0.11	0.43
P ₂ O ₅	0.08	0.19	0.16		0.07	0.06	0.16	0.16	0.57
Cr ₂ O ₃	0.061	0.011	0.08		0.003	0.007	0.139	0.047	0.002
Ba	1075	51	35		1021	930	58	14	1145
LOI	1	0.5	1.9		0.8	1.9	1.2	1.1	4
Total	99.87	99.81	99.81		99.94	99.96	99.81	99.82	99.87
Li	3.13	2.60	9.46	38.41	10.03	19.40	12.75	12.84	13.15
Be	1.34	0.40	0.20	2.56	1.84	2.31	0.21	0.28	0.74
Sc	15.7	46.5	40.0	4.5	8.9	10.1	42.8	43.4	19.05
TiO ₂	0.60	1.88	1.04	0.29	0.79	0.63	0.99	1.30	1.01
V	114.71	442.53	255.48	30.60	120.48	88.88	254.39	357.98	230.0
Cr	486.79	114.21	562.68	16.59	39.12	75.87	1058.00	370.19	6.68
Co	26.90	55.02	49.74	4.99	14.57	15.73	46.84	51.60	24.77
Ni	1708.06	1587.90	1564.76	6.04	1414.34	1500.68	1516.54	1475.15	13.06
Cu	7.46	198.31	116.87	41.24	95.48	47.67	81.01	145.96	216.71
Zn	-	-	-	-	-	-	-	-	-
Ga	17.50	19.60	14.94	20.51	21.46	20.19	15.10	16.98	19.28
As	1.6	-0.3	-0.4	16.3	1.4	1.1	87.7	0.8	10.1
Rb	38.991	2.803	1.047	129.265	117.566	145.083	5.708	1.099	50.59
Sr	927.66	173.63	236.30	462.56	877.23	463.91	196.03	132.28	952.94
Y	15.204	37.017	33.464	10.980	18.525	19.312	18.536	26.118	25.76
Zr	153.748	110.522	50.514	231.017	209.467	290.576	55.586	73.157	78.18
Nb	4.02	6.92	2.76	6.66	6.74	8.99	2.92	4.31	4.22
Mo	0.58	0.63	0.37	0.39	0.47	0.96	0.51	0.37	0.39
Sn	1.14	1.06	0.37	1.73	1.45	2.17	0.65	0.69	1.0
Sb	0.63	0.13	0.12	0.13	0.31	0.25	1.51	0.16	0.62
Cs	0.57	0.35	0.32	5.01	8.40	5.84	1.06	0.15	4.58
Ba	1094.46	54.67	34.68	1140.08	1019.89	932.58	58.49	14.44	1147.75
La	24.68	6.67	3.21	31.90	31.22	32.19	3.20	4.08	19.74
Ce	50.50	16.86	8.07	59.22	62.99	65.46	8.54	10.81	40.65
Pr	6.19	2.53	1.36	6.25	7.40	7.86	1.31	1.71	5.30
Nd	25.55	13.19	7.37	21.35	29.22	30.57	6.94	8.97	22.86
Sm	5.03	4.20	2.48	0.75	5.31	5.85	2.16	2.81	5.18
Eu	1.23	1.54	1.04	3.51	1.34	1.14	0.87	1.08	1.59
Gd	3.82	5.63	3.91	2.46	4.08	4.35	2.85	3.84	4.97
Tb	0.51	0.95	0.72	0.34	0.55	0.63	0.48	0.66	0.73
Dy	2.73	6.22	4.90	1.94	3.13	3.59	3.16	4.37	4.37
Ho	0.52	1.33	1.08	0.39	0.62	0.69	0.66	0.93	0.91
Er	1.37	3.70	2.98	1.15	1.71	1.91	1.82	2.63	2.51
Tm	0.19	0.54	0.43	0.19	0.25	0.30	0.27	0.39	0.37
Yb	1.27	3.51	2.51	1.37	1.66	1.95	1.71	2.51	2.39
Lu	0.19	0.55	0.40	0.21	0.26	0.29	0.27	0.40	0.37
Hf	4.22	3.09	1.46	6.49	5.62	8.12	1.56	2.14	2.13
Ta	0.25	0.42	0.17	0.58	0.41	0.59	0.20	0.27	0.26
Pb	9.37	2.16	2.95	25.16	33.41	34.49	9.17	0.71	17.03
Th	8.90	0.54	0.21	22.93	11.82	19.41	0.24	0.35	2.85
U	2.58	0.16	0.09	4.41	3.64	5.33	0.08	0.28	0.77
La _N /Yb _N	23.67	2.32	1.56	28.31	22.99	20.13	2.28	1.98	10.06
Eu/Eu*	0.82	0.97	1.02	1.01	0.84	0.66	1.07	1.00	0.94
Ce/Ce*	0.92	0.98	0.93	0.90	0.93	0.93	1.00	0.99	0.91
Nb*/Nb	8.38	1.07	1.29	7.22	6.42	4.92	1.15	1.00	6.35
Ta/Ta	10.86	1.16	1.37	7.51	8.81	6.18	1.07	1.00	8.40

Table 3.1 cont.

Sample ID	PNG10-023	PNG10-024	PNG10-025	PNG10-026	PNG10-027	PNG10-028	PNG10-029	PNG10-030	PNG10-031
Location	Kulamadau Woodlark Is.	Busai Woodlark Is.	Busai Woodlark Is.	Busai Woodlark Is.					
SiO ₂	49.9	50.4	50.27	56.48	50.14	57.99	51.36	52.07	
Al ₂ O ₃	16.24	17.01	16.75	15.22	16.96	16.74	17.14	16.79	
Fe ₂ O ₃	10.04	9.8	9.6	4.18	9.98	6.11	8.68	8.73	
CaO	5.19	4.66	4.79	2.42	4.67	3.05	3.84	3.26	
MgO	9.18	8.94	7.92	5.34	9.08	4.97	6.33	5.82	
Na ₂ O	3.38	3.63	3.46	1.96	3.5	3.1	3.88	3.8	
K ₂ O	2.21	2.12	2.6	3.74	2.01	1.94	2.21	2.73	
MnO	1.13	1.13	1.12	0.48	1.15	0.57	1.08	1.04	
TiO ₂	0.24	0.35	0.34	0.17	0.35	0.2	0.36	0.35	
P ₂ O ₅	0.21	0.18	0.17	0.09	0.19	0.21	0.17	0.14	
Cr ₂ O ₃	0.019	<0.002	<0.002	0.005	<0.002	0.006	0.003	0.003	
Ba	663	888	789	704	870	1079	1101	1085	
LOI	1.9	1.4	2.6	9.8	1.6	4.8	4.6	4.9	
Total	99.84	99.87	99.86	99.95	99.86	99.93	99.89	99.9	
Li	12.09	11.35	17.68	23.79	9.38	21.39	25.91	27.43	39.53
Be	0.89	0.86	0.84	1.03	0.87	0.81	0.92	1.07	1.18
Sc	28.50	24.56	25.18	9.66	26.76	13.29	25.6	25.2	21.47
TiO ₂	1.08	1.08	1.10	0.44	1.16	0.55	1.05	1.03	0.87
V	233.2	245.5	247.4	72.8	263.7	111.9	274.53	230.52	222.33
Cr	125.77	11.94	9.69	34.25	10.45	46.87	59.59	51.51	29.65
Co	34.51	27.96	28.07	10.36	29.63	16.67	29.07	28.16	20.83
Ni	45.02	16.75	16.64	12.45	17.88	19.63	1819.31	1665.99	24.11
Cu	307.96	109.28	134.04	41.50	127.96	63.81	86.57	104.89	45.88
Zn	-	-	-	-	-	-	-	-	72.00
Ga	17.47	18.26	18.15	15.34	19.47	17.99	19.34	18.11	16.92
As	16.0	3.9	7.3	4.8	4.7	7.6	15.0	19.4	-
Rb	40.35	38.33	58.11	123.08	37.37	48.70	44.791	58.245	113.62
Sr	680.16	932.40	885.82	188.83	1015.69	764.14	776.10	792.59	483.25
Y	23.68	24.13	23.45	11.68	25.57	14.55	24.162	24.047	24.11
Zr	105.17	101.48	100.77	130.16	104.84	116.63	137.018	134.174	141.30
Nb	5.41	5.19	4.99	4.88	5.42	4.89	5.33	5.23	5.71
Mo	4.01	0.70	0.45	0.12	0.99	1.53	0.51	0.70	0.34
Sn	1.3	1.3	1.1	0.9	1.1	1.2	1.06	1.04	1.16
Sb	0.32	0.18	0.17	0.83	0.17	0.39	1.74	2.20	2.23
Cs	3.56	4.21	17.57	7.92	3.76	5.12	3.40	3.13	6.74
Ba	666.93	881.40	795.14	686.51	873.70	1054.07	1057.71	1045.42	770.15
La	13.64	16.46	15.30	15.19	16.97	12.67	20.28	20.54	20.54
Ce	28.96	35.02	32.97	29.55	35.80	25.17	43.36	42.50	45.25
Pr	3.80	4.62	4.32	3.34	4.74	3.10	5.45	5.43	5.82
Nd	16.65	20.52	19.36	13.28	21.01	12.73	23.82	23.69	25.14
Sm	4.08	4.72	4.58	2.66	4.97	2.70	5.34	5.32	1.83
Eu	1.30	1.48	1.43	0.80	1.54	0.87	1.56	1.63	5.88
Gd	4.24	4.73	4.59	2.34	4.93	2.59	4.85	4.86	5.22
Tb	0.66	0.70	0.68	0.33	0.74	0.39	0.71	0.71	0.74
Dy	4.07	4.19	4.10	2.00	4.46	2.42	4.21	4.16	4.27
Ho	0.85	0.86	0.84	0.41	0.91	0.52	0.86	0.85	0.87
Er	2.36	2.38	2.32	1.16	2.51	1.51	2.36	2.29	2.38
Tm	0.35	0.35	0.34	0.18	0.37	0.23	0.35	0.35	0.35
Yb	2.32	2.31	2.24	1.24	2.39	1.58	2.26	2.26	2.29
Lu	0.37	0.37	0.36	0.21	0.39	0.26	0.36	0.36	0.36
Hf	3.00	2.91	2.80	3.46	2.94	3.16	3.68	3.58	3.78
Ta	0.34	0.32	0.31	0.34	0.34	0.30	0.31	0.32	0.31
Pb	24.38	15.10	18.28	11.41	15.12	19.50	9.95	13.32	8.05
Th	3.77	3.64	3.39	5.52	3.49	3.57	5.05	4.96	5.36
U	1.06	1.02	0.96	1.59	0.98	1.19	1.47	1.37	1.38
La _N /Yb _N	7.17	8.71	8.32	14.90	8.67	9.76	10.93	11.10	10.93
Eu/Eu*	0.94	0.95	0.94	0.95	0.94	0.99	0.92	0.96	1.03
Ce/Ce*	0.93	0.93	0.94	0.92	0.92	0.91	0.94	0.92	0.96
Nb*/Nb	3.32	4.17	3.98	4.48	4.15	3.64	4.98	5.31	4.57
Ta*/Ta	4.10	5.32	5.05	5.50	5.19	4.97	6.67	6.98	6.31

Table 3.1 cont.

Sample ID	PNG10-032	PNG10-033	PNG10-034	PNG10-037	PNG10-038	08P-001	08P-002	08P-003	08P-004
Location	Busai	Busai	Busai	Busai	Busai	Papuan Peninsula	Papuan Peninsula	Papuan Peninsula	Papuan Peninsula
	Woodlark Is.								
SiO ₂						46.17	47.88	53.72	49.12
Al ₂ O ₃						13.25	13.19	11.18	9.69
Fe ₂ O ₃						12.03	12.75	18.72	18.84
CaO						7.58	7.06	1.66	3.48
MgO						12.37	10.77	7.05	9.21
Na ₂ O						2.29	2.93	3.09	3.47
K ₂ O						0.15	0.14	0.17	0.55
MnO						1.31	1.31	2.21	4.15
TiO ₂						0.11	0.1	0.4	0.19
P ₂ O ₅						0.19	0.2	0.31	0.38
Cr ₂ O ₃						0.025	0.024	<0.002	<0.002
Ba						66	24	36	40
LOI						4.3	3.4	1.4	0.8
Total						99.81	99.82	99.95	99.93
Li	29.00	33.10	20.34	32.33	37.70	3.1	3.8	3.6	5.7
Be	0.86	0.63	0.97	2.33	1.29	0.3	0.3	0.9	0.5
Sc	20.95	13.69	19.81	25.17	25.40	45.7	48.6	34.4	58.8
TiO ₂	0.84	0.55	0.83	1.59	1.95	1.3	1.4	2.2	4.1
V	207.38	134.43	212.62	200.59	141.11	345.9	359.6	5.4	35.0
Cr	28.93	18.77	38.27	759.02	1196.43	160.8	62.5	0.3	0.1
Co	18.69	12.72	20.71	44.53	48.42	46.9	49.0	26.4	42.0
Ni	20.52	13.08	31.03	196.77	335.63	88.3	77.0	2.4	2.2
Cu	100.20	21.27	112.42	103.24	49.69	163.8	172.8	9.0	2.1
Zn	75.49	48.64	71.51	84.17	84.14	84.5	84.6	140.9	91.9
Ga	16.32	10.66	15.78	13.81	12.85	17.0	15.9	24.3	17.0
As	-	-	-	-	-	1.4	6.1	1.6	1.6
Rb	81.70	89.90	144.23	85.61	161.65	1.5	2.8	2.6	11.8
Sr	212.36	205.03	292.16	246.44	254.32	150.3	134.9	116.4	106.4
Y	24.05	22.89	22.52	23.34	27.17	26.2	27.6	87.0	45.6
Zr	138.15	84.92	133.89	527.71	566.06	72.2	69.8	260.5	114.5
Nb	5.41	3.32	5.42	20.63	22.38	6.1	5.2	18.7	10.8
Mo	0.27	39.39	0.79	0.16	0.53	0.2	0.1	0.2	0.0
Sn	1.06	0.65	1.03	4.20	4.08	1.7	1.2	5.7	1.5
Sb	1.42	12.08	1.45	4.93	8.59	0.0	0.0	0.0	0.0
Cs	4.52	4.21	7.29	5.46	2.41	0.7	0.1	0.3	0.0
Ba	653.57	4226.41	1118.22	884.33	185.93	70.0	26.0	38.1	42.8
La	20.82	22.65	19.91	49.59	55.80	4.7	4.2	14.7	6.6
Ce	43.64	43.45	41.65	110.29	121.78	11.7	10.6	37.4	17.4
Pr	5.60	5.42	5.39	14.16	16.07	1.7	1.6	5.6	2.7
Nd	23.90	23.18	22.87	58.22	66.49	8.6	8.3	28.5	13.7
Sm	1.76	1.45	1.65	2.91	4.12	2.8	2.7	9.1	4.6
Eu	5.62	5.47	5.33	11.29	13.03	1.0	1.0	3.2	2.1
Gd	5.21	5.21	4.99	8.64	10.28	3.7	3.7	12.2	6.3
Tb	0.75	0.70	0.72	1.03	1.20	0.7	0.7	2.1	1.1
Dy	4.37	3.87	4.14	5.06	5.55	4.3	4.4	14.1	7.5
Ho	0.89	0.73	0.83	0.84	0.91	0.9	1.0	3.1	1.6
Er	2.42	1.90	2.30	2.03	2.13	2.6	2.7	8.8	4.5
Tm	0.35	0.27	0.34	0.27	0.27	0.4	0.4	1.3	0.7
Yb	2.26	1.73	2.26	1.67	1.64	2.5	2.7	8.7	4.5
Lu	0.36	0.27	0.36	0.22	0.21	0.4	0.4	1.4	0.7
Hf	3.73	2.30	3.62	15.11	15.94	2.0	2.0	7.2	3.1
Ta	0.31	0.19	0.30	1.18	1.19	0.4	0.3	1.1	0.6
Pb	13.72	81.67	15.72	10.05	22.36	0.5	0.4	0.3	0.2
Th	5.19	3.12	4.98	14.35	15.20	0.5	0.4	1.5	0.5
U	1.43	0.86	1.46	3.29	3.51	0.2	0.1	0.4	0.2
La/Yb _N	11.25	15.96	10.76	36.27	41.40	2.26	1.89	2.07	1.79
Eu/Eu ⁺	1.03	1.03	1.05	1.08	1.03	1.00	0.97	0.91	1.20
Ce/Ce ⁺	0.93	0.88	0.92	0.96	0.94	0.98	0.97	0.98	1.00
Nb/Nb	5.13	9.93	4.91	3.02	3.19	0.87	0.89	0.86	0.65
Ta ⁺ /Ta	7.26	15.27	7.21	3.97	4.61	0.96	1.02	1.00	0.70

Table 3.1 cont.										
Sample ID	08P-006	08P-007	08P-008A	08P-008B	08P-010	08P-011	08P-012	08P-013	08P-014	08P-016
Location	Papuan Peninsula									
SiO ₂	57.89	45.17	47.25	45.66		47.83	48.4	45.82	45.88	47.96
Al ₂ O ₃	20.47	13.5	12.78	14.72		13.39	13.71	13.27	13.37	13.04
Fe ₂ O ₃	3.64	10.83	13.32	7.65		11.32	12.35	11.88	11.8	14.65
CaO	0.48	7.08	7.06	6.15		7.71	7.73	7.85	7.45	6.44
MgO	5.03	9.8	9.7	14.6		9.52	9.69	10.05	9.93	9
Na ₂ O	4.42	1.9	2.23	0.23		2.96	3.22	2.5	2.29	3.34
K ₂ O	5.82	0.19	0.33	0.04		0.56	0.19	0.08	0.04	0.18
MnO	0.32	1.36	1.45	0.64		1.18	1.28	1.26	1.26	1.73
TiO ₂	0.1	0.11	0.12	0.04		0.09	0.11	0.1	0.1	0.13
P ₂ O ₅	0.08	0.2	0.22	0.11		0.16	0.18	0.2	0.18	0.23
Cr ₂ O ₃	<0.002	0.051	0.016	0.011		0.033	0.03	0.029	0.026	0.003
Ba	2392	26	46	<5		50	44	14	9	34
LOI	1.1	9.6	5.3	10		5	2.9	6.7	7.4	3
Total	99.98	99.83	99.81	99.85		99.82	99.8	99.81	99.81	99.81
Li	4.3	5.6	4.5	2.4	8.5	6.5	5.0	5.0	3.3	2.4
Be	4.1	0.3	0.3	0.1	2.6	0.2	0.3	0.2	0.3	0.4
Sc	4.6	44.0	46.1	41.5	3.5	46.4	48.0	47.5	45.2	45.7
TiO ₂	0.3	1.4	1.5	0.7	0.2	1.2	1.3	1.3	1.3	1.7
V	88.2	314.6	396.2	236.6	8.7	376.5	398.3	397.2	377.8	469.5
Cr	2.0	361.2	113.4	77.4	4.1	232.5	210.4	200.0	189.0	17.2
Co	3.0	46.7	47.8	32.7	1.9	45.8	47.5	46.2	45.6	49.3
Ni	2.4	99.7	74.7	84.6	1.7	92.8	91.0	86.8	85.8	56.1
Cu	48.0	125.9	191.7	186.7	3.5	142.4	159.7	152.8	156.4	159.4
Zn	39.3	79.1	99.7	42.1	35.8	72.6	93.1	82.9	81.0	88.7
Ga	21.0	14.6	14.3	15.2	16.1	12.5	13.9	10.8	14.0	16.1
As	2.4	1.1	1.2	1.1	-	1.1	1.1	1.0	1.1	0.5
Rb	132.5	2.0	3.9	0.3	80.4	4.0	2.3	1.0	0.5	3.2
Sr	2587.3	165.9	71.2	12.8	126.1	154.1	166.0	198.7	178.1	171.2
Y	17.7	23.6	29.9	14.4	17.7	23.5	25.9	25.3	25.1	32.9
Zr	167.5	69.7	78.4	31.5	146.3	62.4	70.1	66.9	68.0	94.5
Nb	6.3	6.8	5.5	2.2	11.7	5.0	5.7	5.4	5.4	7.8
Mo	0.0	-0.1	-0.1	-0.1	1.1	0.0	-0.1	-0.2	-0.2	0.3
Sn	1.4	0.7	1.1	-0.1	2.6	0.4	0.6	1.0	0.2	1.2
Sb	0.2	0.0	0.0	0.0	0.2	0.0	0.0	0.0	0.0	0.0
Cs	3.2	0.2	0.0	0.0	2.7	0.1	0.1	0.0	0.0	0.0
Ba	2400.7	27.5	48.4	1.0	546.1	51.6	44.9	15.9	10.1	34.8
La	23.5	5.2	4.4	1.7	33.5	3.8	4.2	4.1	4.1	5.5
Ce	46.9	12.9	11.4	4.6	66.8	9.7	10.9	10.4	10.5	14.0
Pr	5.6	1.9	1.8	0.7	7.3	1.5	1.6	1.6	1.6	2.1
Nd	22.2	9.2	9.0	3.8	25.1	7.4	8.3	8.0	7.9	10.9
Sm	4.8	2.7	3.0	1.3	0.5	2.4	2.7	2.5	2.6	3.5
Eu	1.5	1.0	1.1	0.5	4.5	0.9	1.0	1.0	1.0	1.3
Gd	4.2	3.6	4.1	1.9	3.5	3.4	3.6	3.5	3.6	4.7
Tb	0.6	0.6	0.7	0.3	0.5	0.6	0.6	0.6	0.6	0.8
Dy	3.0	3.9	4.8	2.3	3.1	3.9	4.2	4.0	4.1	5.5
Ho	0.6	0.8	1.0	0.5	0.6	0.8	0.9	0.9	0.9	1.2
Er	1.6	2.3	3.0	1.4	1.7	2.4	2.5	2.5	2.5	3.3
Tm	0.2	0.3	0.5	0.2	0.3	0.4	0.4	0.4	0.4	0.5
Yb	1.6	2.1	2.9	1.4	1.9	2.3	2.5	2.4	2.4	3.3
Lu	0.3	0.3	0.5	0.2	0.3	0.4	0.4	0.4	0.4	0.5
Hf	3.9	2.0	2.1	0.9	4.8	1.8	1.9	1.8	1.9	2.7
Ta	0.2	0.4	0.3	0.1	0.9	0.3	0.3	0.3	0.3	0.4
Pb	27.4	0.4	0.5	0.1	23.6	0.4	0.3	0.3	0.3	0.2
Th	8.6	0.5	0.4	0.2	12.1	0.4	0.4	0.4	0.4	0.6
U	3.2	0.1	0.1	0.0	2.0	0.1	0.1	0.1	0.1	0.2
La/Yb _N	18.27	3.01	1.83	1.55	21.79	2.05	2.05	2.11	2.06	2.04
Eu/Eu*	0.96	0.99	0.96	1.07	0.98	1.01	0.99	1.00	1.00	0.99
Ce/Ce*	0.92	0.97	0.98	0.99	0.94	0.98	1.01	0.98	0.99	0.99
Nb*/Nb	5.18	0.88	0.86	0.82	4.01	0.84	0.80	0.83	0.83	0.77
Ta*/Ta	11.98	1.03	0.98	0.89	4.56	0.99	0.92	0.99	0.95	0.87

Table 3.1 cont.

Sample ID	08P-017	08P-018	08P-019	08P-020	08P-021	08P-022	08P-023	08P-024	08P-025	08P-026
Location	Papuan Peninsula									
SiO ₂	48.36	48.65	47.99	48.23	51.31	47.92	50.08	52.62	51.41	47.95
Al ₂ O ₃	13.17	13.77	13.65	13.43	13.99	13.58	13.54	9.08	14.06	14.61
Fe ₂ O ₃	14.21	12.24	12.8	12.62	8.73	10.71	9.16	9.31	11.26	11.28
CaO	6.05	7.62	7.57	7.56	5.24	6.66	6.62	12.07	5.94	7.21
MgO	9.06	10.68	10.95	10.44	5.25	8.49	8.78	6.18	7.42	12.34
Na ₂ O	3.07	2.93	2.63	2.76	5.34	3.47	2.45	0.44	2.43	2.12
K ₂ O	0.18	0.14	0.06	0.13	0.84	0.53	0.33	0.89	0.35	0.06
MnO	1.67	1.31	1.33	1.29	0.7	0.67	0.67	0.28	0.82	1.37
TiO ₂	0.13	0.11	0.1	0.1	0.09	0.07	0.08	0.05	0.08	0.12
P ₂ O ₅	0.2	0.19	0.18	0.19	0.11	0.17	0.14	0.14	0.14	0.19
Cr ₂ O ₃	0.003	0.024	0.023	0.023	0.018	0.019	0.012	0.145	0.004	0.049
Ba	32	33	14	22	28	50	33	54	20	17
LOI	3.7	2.1	2.4	3	8.2	7.5	7.9	8.5	5.9	2.5
Total	99.82	99.8	99.8	99.8	99.88	99.84	99.83	99.77	99.86	99.83
Li	3.0	3.1	4.7	3.6	2.8	4.5	2.9	2.1	48.3	3.5
Be	0.4	0.3	0.3	0.3	0.3	0.2	0.2	0.2	0.2	0.3
Sc	43.0	44.7	47.1	45.1	33.5	39.4	38.4	29.9	38.9	42.4
TiO ₂	1.6	1.3	1.3	1.3	0.7	0.7	0.7	0.3	0.8	1.3
V	454.3	397.3	443.0	430.5	336.4	389.4	391.0	221.6	469.2	416.4
Cr	19.3	163.9	168.4	163.0	120.1	107.2	89.1	1308.0	17.4	387.8
Co	46.5	46.0	47.7	46.4	33.0	39.5	34.6	48.2	40.9	46.9
Ni	50.1	81.4	84.7	80.0	65.6	59.7	59.8	237.7	28.6	93.0
Cu	179.7	166.8	177.7	173.1	60.6	127.2	121.5	114.9	19.8	139.2
Zn	84.2	81.4	90.0	85.1	62.5	70.4	70.2	64.6	73.9	82.9
Ga	16.7	15.0	16.5	15.1	12.6	13.9	10.3	8.5	16.1	17.1
As	0.6	0.5	0.4	0.4	2.4	2.6	1.5	0.9	2.2	0.3
Rb	2.8	1.9	0.7	1.1	30.3	8.6	6.9	15.1	9.0	0.4
Sr	144.7	192.0	181.8	264.6	94.0	123.1	535.4	223.0	99.1	160.0
Y	31.5	25.5	27.5	26.4	13.0	15.5	13.2	6.0	18.0	25.4
Zr	87.4	71.1	71.8	69.1	65.2	43.3	48.4	48.5	47.1	81.0
Nb	7.3	5.8	5.3	5.0	4.5	3.0	4.0	2.6	1.2	4.6
Mo	0.2	0.2	0.1	0.1	0.1	0.1	0.1	0.1	0.1	0.1
Sn	1.5	1.5	1.1	1.2	1.0	0.7	0.7	0.9	0.5	1.5
Sb	0.0	0.0	0.0	0.0	0.0	0.1	0.0	0.2	0.1	0.0
Cs	0.0	0.0	0.0	0.0	0.3	0.2	0.0	0.3	0.3	0.0
Ba	33.3	35.5	14.5	22.9	29.5	51.2	33.0	57.5	20.2	18.2
La	5.7	4.5	4.3	4.2	4.8	3.3	3.9	3.8	2.2	4.4
Ce	14.3	11.6	11.0	11.0	10.8	7.6	8.9	7.5	5.8	12.0
Pr	2.2	1.7	1.7	1.6	1.5	1.0	1.2	0.9	0.9	1.8
Nd	10.8	8.8	8.6	8.5	6.9	5.0	5.6	3.8	5.1	9.5
Sm	3.3	2.7	2.8	2.7	1.8	1.5	1.5	0.9	1.7	2.9
Eu	1.2	1.0	1.1	1.0	0.6	0.6	0.5	0.3	0.7	1.1
Gd	4.4	3.6	3.9	3.6	2.1	2.0	1.9	1.0	2.4	3.8
Tb	0.8	0.6	0.7	0.7	0.3	0.4	0.3	0.2	0.4	0.7
Dy	5.3	4.3	4.6	4.4	2.2	2.5	2.2	1.0	3.0	4.3
Ho	1.1	0.9	1.0	0.9	0.5	0.6	0.5	0.2	0.6	0.9
Er	3.2	2.6	2.8	2.7	1.3	1.7	1.4	0.6	1.8	2.5
Tm	0.5	0.4	0.4	0.4	0.2	0.3	0.2	0.1	0.3	0.4
Yb	3.1	2.5	2.8	2.7	1.3	1.8	1.5	0.6	1.8	2.4
Lu	0.5	0.4	0.4	0.4	0.2	0.3	0.3	0.1	0.3	0.4
Hf	2.5	2.0	2.1	2.0	1.7	1.2	1.3	1.1	1.4	2.3
Ta	0.4	0.3	0.3	0.3	0.3	0.2	0.2	0.2	0.1	0.3
Pb	0.2	0.4	0.3	0.4	0.7	0.4	1.0	0.7	0.3	0.3
Th	0.6	0.5	0.4	0.4	0.6	0.4	0.5	0.7	0.3	0.4
U	0.2	0.1	0.1	0.1	0.2	0.1	0.1	0.2	0.1	0.1
La _N /Yb _N	2.25	2.18	1.89	1.94	4.51	2.27	3.14	7.73	1.47	2.25
Eu/Eu*	0.98	1.00	0.98	1.00	0.95	0.98	0.98	1.02	1.04	1.01
Ce/Ce*	0.98	1.00	0.97	1.00	0.95	0.96	0.97	0.92	0.99	1.01
Nb*/Nb	0.86	0.85	0.90	0.91	1.29	1.36	1.19	2.09	1.93	0.97
Ta*/Ta	0.97	0.95	1.00	0.99	1.58	1.66	1.48	2.56	2.11	1.01

Appendix 3.2 Electron Microprobe Data Tables

Sample:	PNG10-044D						
Analysis:	10044D_1	10044D_2	10044D_3	10044D_4	10044D_5	10044D_6	10044D_7
Mineral:	pyrope	diopside	diopside	bytownite	anorthite	anorthite	diopside
SiO ₂	35.14	53.45	51.28	45.57	43.86	42.08	51.74
TiO ₂	0.52	0.10	0.21	0.02	0.01	0.00	0.19
Al ₂ O ₃	5.04	1.10	2.20	34.47	33.97	36.73	1.93
Cr ₂ O ₃	11.19	0.29	0.85	-	0.01	0.03	0.69
Fe ₂ O ₃	-	1.15	1.78	-	0.00	0.00	0.81
FeO	18.41	2.62	2.34	0.28	0.37	0.12	3.00
MnO	0.31	0.11	0.11	0.03	0.00	0.02	0.16
MgO	13.27	16.27	15.52	0.00	0.75	0.00	15.71
CaO	15.11	24.58	23.63	17.63	19.53	20.24	24.04
Na ₂ O	0.00	0.17	0.24	1.60	0.74	0.02	0.02
K ₂ O	-	-	-	0.02	0.02	0.01	-
Total	98.99	99.84	98.16	99.60	99.26	99.24	98.28
Xalmandine	29.82	-	-	-	-	-	-
Xpyrope	38.31	-	-	-	-	-	-
Xgrossular	31.35	-	-	-	-	-	-
Xspessartine	0.51	-	-	-	-	-	-
Xwollastonite	-	49.09	48.92	-	-	-	49.26
XEnstatite	-	45.22	44.71	-	-	-	44.78
XFerrosilite	-	5.69	6.37	-	-	-	5.95
Xanorthite	-	-	-	85.81	93.46	99.80	-
Xalbite	-	-	-	14.09	6.44	0.14	-
Xorthoclase	-	-	-	0.10	0.10	0.06	-

Sample:	PNG10-0431						
Analysis:	100431_1.1	100431_1.2	100431_3	100431_4	100431_5	100431_6	100431_7
Mineral:	cummingtonite (rim)	enstatite (core)	enstatite	diopside	diopside	biotite	biotite
SiO ₂	58.14	56.47	56.54	53.79	53.13	45.58	48.07
TiO ₂	0.32	0.33	0.38	0.17	0.13	0.76	0.69
Al ₂ O ₃	3.96	1.06	1.13	1.74	1.28	9.93	10.28
Cr ₂ O ₃	0.09	0.04	0.09	0.20	0.39	0.05	0.07
NiO	0.12	0.13	0.10	0.06	0.02	0.05	0.05
Fe ₂ O ₃	-	-	-	-	0.18	-	-
FeO	6.54	8.59	8.44	3.59	3.55	2.05	2.67
MnO	0.15	0.12	0.21	0.12	0.16	0.05	0.03
MgO	19.87	31.84	31.77	16.79	16.06	26.26	22.24
CaO	1.03	1.15	1.17	22.15	23.17	0.32	0.42
Na ₂ O	0.12	0.03	0.03	0.34	0.35	0.53	0.57
K ₂ O	0.04	-	-	-	-	8.98	7.49
Total	90.36	99.76	99.86	98.96	98.41	187.12	85.08
Xwollastonite	-	2.21	2.25	45.85	47.86	-	-
XEnstatite	-	84.94	85.07	48.35	46.14	-	-
XFerrosilite	-	12.85	12.68	5.80	5.99	-	-

Sample:	PNG10-064					
Analysis:	10064b_1	10064b_2	10064b_3	10064b_4.1	10064b_4.2	10064b_5
Mineral:	diopside	diopside	diopside	olivine (core)	olivine (rim)	labradorite
SiO ₂	49.54	51.01	48.57	38.51	36.93	51.20
TiO ₂	1.05	0.75	1.31	-	0.03	0.07
Al ₂ O ₃	4.14	3.17	5.65	0.03	-	30.24
Cr ₂ O ₃	0.67	0.66	0.30	0.01	-	-
Fe ₂ O ₃	4.25	2.33	3.04	0.73	0.03	-
FeO	3.02	3.73	4.54	18.93	28.86	0.60
MnO	0.18	0.14	0.15	0.30	0.53	-
MgO	14.93	15.70	14.84	40.93	32.92	0.11
CaO	22.25	22.05	20.52	0.18	0.23	13.45
Na ₂ O	0.40	0.33	0.39	-	-	4.08
K ₂ O	-	-	-	-	-	0.22
Total	100.44	99.88	99.31	99.62	99.52	99.95
Xwollastonite	46.00	45.51	43.81	-	-	-
XEnstatite	42.95	45.10	44.07	-	-	-
XFerrosilite	11.05	9.40	12.13	-	-	-
Xforsterite	-	-	-	78.38	66.38	-
Xfayalite	-	-	-	21.04	32.68	-
Xanorthite	-	-	-	-	-	63.80
Xalbite	-	-	-	-	-	34.99
Xorthoclase	-	-	-	-	-	1.21

Sample:	PNG10-064				
Analysis:	10064b_6	10064b_7	10064c_1	10064c_2	10064c_3
Mineral:	olivine	anorthoclase	labradorite	diopside	bytownite
SiO ₂	38.95	63.04	51.10	50.88	49.23
TiO ₂	0.02	0.49	0.04	0.67	0.04
Al ₂ O ₃	0.04	20.83	31.37	3.12	31.87
Cr ₂ O ₃	0.02	-	0.00	0.25	-
Fe ₂ O ₃	0.11	-	0.00	2.73	-
FeO	18.02	1.01	0.52	3.35	0.49
MnO	0.30	0.00	0.01	0.18	0.00
MgO	41.93	0.09	0.09	16.06	0.07
CaO	0.16	2.73	13.95	21.76	14.29
Na ₂ O	-	7.42	3.77	0.30	2.87
K ₂ O	-	3.56	0.19	-	0.15
Total	99.54	99.17	101.05	99.30	99.00
Xwollastonite	-	-	-	44.74	-
XEnstatite	-	-	-	45.94	-
XFerrosilite	-	-	-	9.32	-
Xforsterite	80.06	-	-	-	-
Xfayalite	19.41	-	-	-	-
Xanorthite	-	13.38	66.44	-	72.71
Xalbite	-	65.83	32.49	-	26.39
Xorthoclase	-	20.79	1.08	-	0.91

Sample:	PNG10-043k						
Analysis:	10043k_1	10043k_2	10043k_3	10043k_4	10043k_5	10043k_6	10043k_7
Mineral:	aerinite	sanidine	sanidine	diopside	diopside	aerinite	diopside
SiO ₂	46.40	63.97	62.62	54.12	52.62	48.99	53.87
TiO ₂	0.05	0.20	0.14	0.06	0.52	0.00	0.28
Al ₂ O ₃	8.65	18.70	20.47	0.66	2.72	2.23	0.64
Cr ₂ O ₃	-	0.00	0.01	0.09	0.97	0.00	0.01
NiO	0.36	0.00	0.00	-	-	0.49	-
Fe ₂ O ₃	-	0.31	0.41	-	-	-	1.39
FeO	4.64	0.01	0.03	4.10	4.02	2.25	3.56
MnO	0.10	0.01	0.00	0.23	0.07	0.01	0.17
MgO	15.75	0.31	2.27	16.00	15.22	20.47	16.70
CaO	0.75	0.00	0.00	23.34	23.02	0.49	21.17
Na ₂ O	0.10	1.44	1.84	0.35	0.45	0.08	0.87
K ₂ O	0.13	13.26	10.60	-	-	0.17	-
Total	76.92	98.21	98.39	98.94	99.61	75.18	98.66
Xanorthite	-	1.66	12.48	-	-	-	-
Xalbite	-	13.97	18.27	-	-	-	-
Xorthoclase	-	84.37	69.25	-	-	-	-
Xwollastonite	-	-	-	47.83	48.64	-	43.95
XEnstatite	-	-	-	45.62	44.74	-	48.25
XFerrosilite	-	-	-	6.55	6.63	-	7.80

References

- Abers, G.A., Ferris, A., Craig, M., Davies, H., Lerner-Lam, A.L., Mutter, J.C., and Taylor, B., 2002, Mantle compensation of active metamorphic core complexes at Woodlark rift in Papua New Guinea: Nature, v. 418, p. 862-865.
- Adshead, N.D., and Appleby, A.K., 1996, The Umina Au-Ag deposit, Misima Island, Papua New Guinea: spatially but not genetically associated with porphyry, Porphyry related copper and gold deposits of the Asia Pacific region: Australian Mineral Foundation, Glenside, South Aust., Australia, p. 10.
- Ashley, P.M., and Flood, R.H., 1981, Low-K tholeiites and high-K igneous rocks from Woodlark Island, Papua New Guinea: Journal of the Geological Society of Australia, v. 28, p. 227 - 240.
- Baldwin, S.L., Fitzgerald, P.G., and Webb, L.E., 2012, Tectonics of the New Guinea Region: Annual Review of Earth and Planetary Sciences, v. 40, p. null.
- Baldwin, S.L., Lister, G.S., Hill, E.J., Foster, D.A., and McDougall, I., 1993, Thermochronologic constraints on the tectonic evolution of active metamorphic core complexes, D'Entrecasteaux Islands, Papua New Guinea: Tectonics, v. 12, p. 611-628.
- Baldwin, S.L., Monteleone, B.B., Webb, L.E., Fitzgerald, P.G., Grove, M., and Hill, E.J., 2004, Pliocene eclogite exhumation at plate tectonic rates in eastern Papua New Guinea: Nature, v. 431, p. 263-267.
- Baldwin, S.L., Webb, L.E., and Monteleone, B.D., 2008, Late Miocene coesite-eclogite exhumed in the Woodlark Rift: Geology, v. 36, p. 735-738.

- Beiersdorf, H., Bach, W., Duncan, R., Erzinger, J., and Weiss, W., 1995, New evidence for the production of EM-type ocean island basalts and large volumes of volcaniclastites during the early history of the Manihiki Plateau: *Marine Geology*, v. 122, p. 181-205.
- Castillo, P.R., 2006, An overview of adakite petrogenesis: *Chinese Science Bulletin*, v. 51, p. 257-268.
- Catalano, J.P., Baldwin, S.L., Fitzgerald, P.G., and Webb, L.E., 2011, The extent of eclogite in the Woodlark Rift, Papua New Guinea: Insights from xenoliths from the Woodlark Rise, 9th International Eclogite Conference: Mariánské Lázně, Czech Republic.
- Chadwick, J., Perfit, M., McInnes, B., Kamenov, G., Plank, T., Jonasson, I., and Chadwick, C., 2009, Arc lavas on both sides of a trench: Slab window effects at the Solomon Islands triple junction, SW Pacific: *Earth and Planetary Science Letters*, v. 279, p. 293-302.
- Chung, S.-L., Chu, M.-F., Zhang, Y., Xie, Y., Lo, C.-H., Lee, T.-Y., Lan, C.-Y., Li, X., Zhang, Q., and Wang, Y., 2005, Tibetan tectonic evolution inferred from spatial and temporal variations in post-collisional magmatism: *Earth-Science Reviews*, v. 68, p. 173-196.
- Cloos, M., 2005, Collisional delamination in New Guinea: The geotectonics of subducting slab breakoff, Geological Society of America, 51 p.
- Dallwitz, W.B., Green, D.H., and Thompson, J.E., 1966, Clinoenstatite in a volcanic rock from the cape vogel area, papua: *Journal of Petrology*, v. 7, p. 375-403.
- Davies, H., 1971, Peridotite-gabbro-basalt complex in eastern Papua: an overthrust plate of oceanic mantle and crust: *Australian Bur: Mineral Resources Bull*, v. 128, p. 48.
- Davies, H., 1980, CRUSTAL STRUCTURE AND EMPLACEMENT OF OPHIOLITE IN SOUTHEASTERN PAPUA, NEW GUINEA, *Colloques Internationaux du Centre*

National de la Recherche Scientifique, Volume 5: Grenoble, France, Centre National de la Recherche Scientifique, p. 17 - 33.

Davies, H., and Jaques, A., 1984, Emplacement of ophiolite in Papua New Guinea: Geological Society, London, Special Publications, v. 13, p. 341.

Davies, H.L., and Ives, D.J., 1965, The Geology of Fergusson and Goodenough Islands, Papua, Bureau of Mineral Resources, Geology and Geophysics, p. 64.

De Keyser, F., 1961, Misima Island: geology and gold mineralization, Bureau of Mineral Resources, Geology, and Geophysics, p. 35.

Ellis, S.M., Little, T.A., Wallace, L.M., Hacker, B.R., and Buit, S.J.H., 2011, Feedback between rifting and diapirism can exhume ultrahigh-pressure rocks: Earth and Planetary Science Letters, v. 311, p. 427-438.

Ewart, A., 1982, The mineralogy and petrology of Tertiary-Recent orogenic volcanic rocks: with special reference to the andesitic-basaltic compositional range: Andesites: Orogenic Andesites and Related Rocks, p. 25-95.

Ferris, A., Abers, G.A., Zelt, B., Taylor, B., and Roecker, S., 2006, Crustal structure across the transition from rifting to spreading: The Woodlark rift system of Papua New Guinea: Geophysical Journal International, v. 166, p. 622-634.

Francis, G., Rogerson, R., and Queen, L., 1991, The Distribution, Petrology, Syngenetic Mineralisation and Origin of Mid Cretaceous to Palaeogene Marine Volcanics in Papua New Guinea, PNG Geology, Mining, and Exploration Conference, Geological Survey of Papua New Guinea, p. 17 - 25.

Gaina, C., Müller, R.D., Royer, J.Y., and Symonds, P., 1999, Evolution of the Louisiade triple junction: Journal of Geophysical Research, v. 104, p. 12,927-12,939.

Gibson, S.A., 2009, Head-to-tail transition of the Afar mantle plume: Geochemical evidence from a Miocene bimodal basalt–rhyolite succession in the Ethiopian Large Igneous Province: *Lithos*, v. 112, p. 461-476.

Gill, J., Morris, J., and Johnson, R., 1993, Timescale for producing the geochemical signature of island arc magmas: U-Th-Po and Be-B systematics in recent Papua New Guinea lavas: *Geochimica et cosmochimica acta*, v. 57, p. 4269-4283.

Green, T.H., Sie, S.H., Ryan, C.G., and Cousens, D.R., 1989, Proton microprobe-determined partitioning of Nb, Ta, Zr, Sr and Y between garnet, clinopyroxene and basaltic magma at high pressure and temperature: *Chemical geology*, v. 74, p. 201-216.

Grove, T.L., Till, C.B., and Krawczynski, M.J., 2012, The role of H₂O in subduction zone magmatism: *Annual Review of Earth and Planetary Sciences*, p. 413 - 439.

Harrison, M.T., 1982, Diffusion of 40 Ar in hornblende: Contributions to Mineralogy and Petrology, v. 78, p. 324-331.

Haschke, M., and Ben-Avraham, Z., 2005, Adakites from collision-modified lithosphere: *Geophysical Research Letters*, v. 32.

Hegner, E., and Smith, I.E.M., 1992, Isotopic compositions of late Cenozoic volcanics from southeast Papua New Guinea: evidence for multi-component sources in arc and rift environments: *Chemical geology*, v. 97, p. 233-249.

Hill, E.J., and Baldwin, S.L., 1993, Exhumation of high-pressure metamorphic rocks during crustal extension in the D'Entrecasteaux region, Papua New Guinea: *Journal of Metamorphic Geology*, v. 11, p. 261-277.

Hill, K., and Hall, R., 2003, Mesozoic-Cenozoic evolution of Australia's New Guinea margin in a west Pacific context: Evolution and dynamics of the Australian plate, v. 22, p. 265-290.

- Hill, K.C., and Raza, A., 1999, Arc-continent collision in Papua Guinea: Constraints from fission track thermochronology: *Tectonics*, v. 18, p. 950-966.
- Honza, E., Davies, H., Keene, J., and Tiffin, D., 1987, Plate boundaries and evolution of the Solomon Sea region: *Geo-Marine Letters*, v. 7, p. 161-168.
- Jakeš, P., and Smith, I.E., 1970, High potassium calc-alkaline rocks from Cape Nelson, eastern Papua: *Contributions to Mineralogy and Petrology*, v. 28, p. 259-271.
- Jaques, A., 1976, High-K₂O island-arc volcanic rocks from the Finisterre and Adelbert Ranges, northern Papua New Guinea: *Bulletin of the Geological Society of America*, v. 87, p. 861.
- Johnson, R.W., Mackenzie, D.E., and Smith, I.E., 1971, Seismicity and late cenozoic volcanism in parts of Papua-New Guinea: *Tectonophysics*, v. 12, p. 15-22.
- Johnson, R.W., Mackenzie, D.E., and Smith, I.E.M., 1978, Delayed partial melting of subduction-modified mantle in papua new guinea: *Tectonophysics*, v. 46, p. 197-216.
- Johnson, T., and Molnar, P., 1972, Focal Mechanisms and Plate Tectonics of the Southwest Pacific: *J. Geophys. Res.*, v. 77, p. 5000-5032.
- Joshima, M., Okuda, Y., Murakami, F., Kishimoto, K., and Honza, E., 1986, Age of the Solomon Sea Basin from magnetic lineations: *Geo-Marine Letters*, v. 6, p. 229-234.
- Kay, R.W., 1978, Aleutian magnesian andesites: Melts from subducted Pacific ocean crust: *Journal of Volcanology and Geothermal Research*, v. 4, p. 117-132.
- Komatsu, M., 1980, Clinoenstatite in volcanic rocks from the Bonin Islands: *Contributions to Mineralogy and Petrology*, v. 74, p. 329-338.
- Little, T.A., Hacker, B.R., Gordon, S.M., Baldwin, S.L., Fitzgerald, P.G., Ellis, S., and Korchinski, M., 2011, Diapiric exhumation of Earth's youngest (UHP) eclogites in the

gneiss domes of the D'Entrecasteaux Islands, Papua New Guinea: Tectonophysics, v. 510, p. 39-68.

Lus, W.Y., McDougall, I., and Davies, H.L., 2004, Age of the metamorphic sole of the Papuan Ultramafic Belt ophiolite, Papua New Guinea: Tectonophysics, v. 392, p. 85-101.

Martinez, F., Goodliffe, A.M., and Taylor, B., 2001, Metamorphic core complex formation by density inversion and lower-crust extrusion: Nature, v. 411, p. 930-934.

Martinez, F., and Taylor, B., 2002, Mantle wedge control on back-arc crustal accretion: Nature, v. 416, p. 417-420.

Mason, B., and Nelen, J., 1968, The weatherford meteorite: Geochimica et cosmochimica acta, v. 32, p. 661-664.

McDonough, W.F., and Sun, S.s., 1995, The composition of the Earth: Chemical geology, v. 120, p. 223-253.

McDougall, I., and Harrison, M.T., 1988, Geochronology and Thermochronology by the $^{40}\text{Ar}/^{39}\text{Ar}$ Method, Oxford University Press, 212 p.

McMillan, N.J., Dickin, A.P., and Haag, D., 2000, Evolution of magma source regions in the Rio Grande rift, southern New Mexico: Geological Society of America Bulletin, v. 112, p. 1582.

Miller, C., Schuster, R., Klötzli, U., Frank, W., and Purtscheller, F., 1999, Post-Collisional Potassic and Ultrapotassic Magmatism in SW Tibet: Geochemical and Sr–Nd–Pb–O Isotopic Constraints for Mantle Source Characteristics and Petrogenesis: Journal of Petrology, v. 40, p. 1399-1424.

Monteleone, B., 2007, Timing and conditions of formation of the D'Entrecasteaux Islands, Papua New Guinea: Syracuse, NY, Syracuse University.

Monteleone, B.D., Baldwin, S.L., Ireland, T.R., and Fitzgerald, P.G., 2001, Thermochronologic constraints for the tectonic evolution of the Moresby Seamount, Woodlark Basin, Papua New Guinea, Proceeding of the oceanic drilling program, scientific results, Volume 180, p. 35.

Page, R.W., 1976, Geochronology of igneous and metamorphic rocks in the New Guinea Highlands: Canberra, Australian Govt. Publ. Service.

Rogerson, R., 1991, New stratigraphic and whole-rock geochemical data from the Waria River area, northern Papuan Peninsula, Geological Survey of Papua New Guinea.

Rogerson, R., and Hilyard, D.B., 1989, Scrapland: a suspect composite terrane in Papua New Guinea, Geological Survey of Papua New Guinea.

Ruxton, B., 1999, The Managalase Volcanic Field and Associated Mineral Occurrences, Papua New Guinea, Australasian Institute of Mining and Metallurgy, p. 335.

Ryerson, F.J., and Watson, E.B., 1987, Rutile saturation in magmas: implications for TiNbTa depletion in island-arc basalts: Earth and Planetary Science Letters, v. 86, p. 225-239.

Shiraki, K., Kuroda, N., Urano, H., and Manuyama, S., 1980, Clinoenstatite in boninites from the Bonin Islands, Japan: Nature, v. 285, p. 31-32.

Silver, E.A., Abbott, L.D., Kirchoff-Stein, K.S., Reed, D.L., Bernstein-Taylor, B., and Hilyard, D., 1991, Collision propagation in Papua New Guinea and the Solomon Sea: Tectonics, v. 10, p. 863-874.

Smith, I.E., 1972, High-potassium intrusives from southeastern Papua: Contributions to Mineralogy and Petrology, v. 34, p. 167-176.

Smith, I.E., 1976a, Geology of the southeast Papuan mainland, Australian Bureau of Mineral Resources.

Smith, I.E.M., 1976b, Volcanic rocks from southeastern Papua: The evolution of volcanism at a plate boundary., Australian National University.

Smith, I.E.M., 1981, Young volcanoes in eastern Papua: Cooke-Ravian volume of volcanological papers, p. 257-265.

Smith, I.E.M., 1982, Volcanic evolution in eastern Papua: Tectonophysics, v. 87, p. 315-333.

Smith, I.E.M., Chappell, B.W., Ward, G.K., and Freeman, R.S., 1977, Peralkaline rhyolites associated with andesitic arcs of the southwest Pacific: Earth and Planetary Science Letters, v. 37, p. 230-236.

Smith, I.E.M., and Clarke, D.S., 1991, Intrusive rocks associated with gold mineralisation in southeastern Papua New Guinea, p. 34-39.

Smith, I.E.M., Taylor, S.R., and Johnson, R.W., 1979, REE-fractionated trachytes and dacites from Papua New Guinea and their relationship to andesite petrogenesis: Contributions to Mineralogy and Petrology, v. 69, p. 227-233.

Stoltz, A.J., Davies, G.R., Crawford, A.J., and Smith, I.E.M., 1992, Sr, Nd and Pb isotopic compositions of calc-alkaline and peralkaline silicic volcanics from the D'Entrecasteaux Islands, Papua New Guinea, and their tectonic significance: Mineralogy and Petrology, v. 47, p. 103-126.

Taylor, B., 2006, The single largest oceanic plateau: Ontong Java-Manihiki-Hikurangi: Earth and Planetary Science Letters, v. 241, p. 372-380.

Taylor, B., Goodliffe, A., Martinez, F., and Hey, R., 1995, Continental rifting and initial sea-floor spreading in the Woodlark basin: Nature, v. 374, p. 534-537.

Tomioka, N., and Fujino, K., 1997, Natural (Mg,Fe)SiO₃-Ilmenite and -Perovskite in the Tenham Meteorite: Science, v. 277, p. 1084-1086.

Trail, D.S., 1967, Geology of Woodlark Island, Papua, by D. S. Trail: (Canberra), Bureau of Mineral Resources, Geology and Geophysics.

van Ufford, A.Q., and Cloos, M., 2005, Cenozoic tectonics of New Guinea: AAPG bulletin, v. 89, p. 119.

Walker, D.A., and McDougall, I., 1982, ^{40}Ar ^{39}Ar and KAr dating of altered glassy volcanic rocks: the Dabi Volcanics, P.N.G: Geochimica et cosmochimica acta, v. 46, p. 2181-2190.

Wallace, L.M., Stevens, C., Silver, E., McCaffrey, R., Loratung, W., Hasiata, S., Stanaway, R., Curley, R., Rosa, R., and Taugaloidi, J., 2004, GPS and seismological constraints on active tectonics and arc-continent collision in Papua New Guinea: Implications for mechanics of microplate rotations in a plate boundary zone: J. geophys. Res, v. 109.

Webb, L.E., Baldwin, S.L., Fitzgerald, P.G., Castellani, L., and Zirakparvar, N.A., 2009, Structural Analysis of the Louisiade Archipelago, Southeastern Papua New Guinea, American Geophysical Union, Fall Meeting.

Webb, L.E., Baldwin, S.L., Little, T.A., and Fitzgerald, P.G., 2008, Can microplate rotation drive subduction inversion?: Geology, v. 36, p. 823-826.

Weiland, R.J., 1999, Emplacement of the Irian ophiolite and unroofing of the Ruffaer metamorphic belt of Irian Jaya, Indonesia, University of Texas at Austin.

Weissel, J.K., and Watts, A.B., 1979, Tectonic evolution of the Coral Sea basin: Journal of Geophysical Research, v. 84, p. 4572-4582.

Worthing, M.A., 1988, Petrology and tectonic setting of blueschist facies metabasites from the Emo Metamorphics of Papua New Guinea: Australian Journal of Earth Sciences, v. 35, p. 159-168.

Worthing, M.A., and Crawford, A.J., 1996, The igneous geochemistry and tectonic setting of metabasites from the emo metamorphics, Papua New Guinea; A record of the evolution and destruction of a backarc basin: *Mineralogy and Petrology*, v. 58, p. 79-100.

Yan, C., and Kroenke, L., 1993, A plate tectonic reconstruction of the Southwest Pacific, 0–100 Ma, Volume 130, College Station Texas, p. 697-709.

Zirakparvar, N., Baldwin, S., and Vervoort, J., 2011, Lu-Hf garnet geochronology applied to plate boundary zones: Insights from the (U) HP terrane exhumed within the Woodlark Rift: *Earth and Planetary Science Letters*.

Zirakparvar, N.A., 2012, Geochemical and Geochronological Constraints on the Origin and Evolution of Rocks in the Active Woodlark Rift of Papua New Guinea: Syracuse, Syracuse University.

VITA

NAME OF AUTHOR: Joseph Paul Catalano

PLACE OF BIRTH: Albany, New York

DATE OF BIRTH: March 31, 1987

UNDERGRADUATE SCHOOL ATTENDED:

Bachelor of Science, 2009, Union College

PROFESSIONAL EXPERIENCE:

Teaching Assistant, Syracuse University, 2009-2010

Research Assistant, Syracuse University, 2010-2012